National Academy of Sciences of Ukraine,
Ministry of Education and Science of Ukraine

Institute of Ionosphere

O.V. Bogomaz
L.F. Chernogor
V.V. Barabash
S.V. Katsko

APERIODIC AND WAVE DISTURBANCES IN THE IONOSPHERE: THE RESULTS OF VERTICAL SOUNDING

Monograph

KHARKIV – 2021

National Academy of Sciences of Ukraine,
Ministry of Education and Science of Ukraine

Institute of Ionosphere

O. V. Bogomaz
L. F. Chernogor
V. V. Barabash
S. V. Katsko

APERIODIC AND WAVE DISTURBANCES IN THE IONOSPHERE: THE RESULTS OF VERTICAL SOUNDING

Monograph

KHARKIV – 2021

UDC 621.396:654.147
B 71

https://doi.org/10.36074/iion.monograph-2021

Reviewers:

Feliks Kivva,
D.Sc., Prof., Head of the Department of Radiowave Propagation in Natural Media,
O.Ya. Usikov Institute for Radiophysics and Electronics
of the National Academy of Sciences of Ukraine
Volodymyr Dolzhykov,
D.Sc., Full Prof., Professor of the Department of Computer Radio Engineering
and Technical Information Security Systems,
Kharkiv National University of Radio Electronics
Yuriy Sumaruk,
D.Sc., Senior Scientist, Leading Researcher of the Department of Geomagnetism,
Institute of Geophysics by S.I. Subbotin name
of National Academy of Sciences of Ukraine

Recommended for printing by the Scientific Council of Institute of Ionosphere
(Protocol № 4 of June 4, 2021)

Bogomaz O.V.

B 71 Aperiodic and wave disturbances in the ionosphere: the results of vertical sounding» : monograph. / O.V. Bogomaz, L.F. Chernogor, V.V. Barabash, S.V. Katsko. – Dallas: Primedia eLaunch LLC. – 160 p.

ISBN 978-1-63944-406-9
DOI 10.36074/iion.monograph-2021

The monograph presents the study results of aperiodic and quasi-periodic wave perturbations in the ionosphere during unique phenomena in geospace: partial solar eclipses, the fall of the Chelyabinsk cosmic body and during the operation of a powerful radio source – the heating stand «Sura». Experimental data obtained by the method of remote sensing are analyzed.

Designed for scientists in the field of ionosphere physics, radio physics, radar, as well as for lecturers, graduate and Ph.D. students.

UDC 621.396:654.147

© Bogomaz O.V., Chernogor L.F., Barabash V.V., Katsko S.V, 2021
ISBN 978-1-63944-406-9
© Primedia eLaunch LLC, 2021

PREFACE

The monograph is dedicated to the study of wave-likel variations in the electron density in the ionospheric F region as well as aperiodic and quasi-periodic disturbances in the ionosphere caused by solar eclipses, by flight and explosion of the Chelyabinsk meteoroid, by influence of powerful radio transmission, spaced by thousands kilometers from a powerful radio system.

The goal is investigation of the ionosphere reaction (mainly F region) to the impact of high-energy source, as well as diurnal and seasonal variations of electron density during growing and declining phases of solar by ionosondes.

To achieve the goal, the following numerous studies were conducted. Namely, study of the reaction of the electron density in the ionospheric F region to the solar eclipses on January 4, 2011 and March 20, 2015 over Kharkiv and over Europe; study of the reaction of the electron density of the ionospheric F region to the explosion of the Chelyabinsk meteoroid on February 15, 2013: study of the ionosphere reaction to the powerful radio transmission of the radio engineering system spaced from the observation site at a distance of about 1000 km; study of diurnal and seasonal variations of the electron density at the ionospheric F2-peak during periods of growth and decline of solar activity.

The subject of the study is regular and irregular variations of the electron density in the lower and middle ionosphere during natural and disturbed conditions. In order to observe the state of the ionosphere the radiophysical method of vertical sounding of the ionosphere was used. For the analysis of the results of the observations, methods of mathematical statistics and statistical radio physics were used, as well as system spectral analysis, based on the windowed Fourier transform, adaptive Fourier transform, and also wavelet transform.

Investigated natural disturbances for four seasons during the periods of growth and decline of solar activity are the background for the disturbations of another nature development. Investigation of the ionosphere reaction to two solar eclipses, including the ionospheric response over Europe, enables to model the influence of ionospheric

disturbances on the conditions of the propag+ation of radio waves transmitted by radio engineering systems of various applications. Research of the ionosphere reaction and, first of all, wave disturbances caused by the fall of the Chelyabinsk cosmic body, allowed determining the propagation range and the amplitude of disturbances of the electron density during such a unique event and thus to obtain the initial data for the modeling of disturbed ionospheric radio channel. Detecting of the magnitude of the reaction and determining range of the ionosphere reaction during the ionosphere heating by powerful radio transmission is of practical importance. The initial data obtained will enable predicting the effect of the onset of disturbances on the ionospheric channels of telecommunications and radionavigation. The quasi-periodic and aperiodic disturbances investigated in the work ultimately limit the potential characteristics of telecommunication radio systems, radionavigation, etc.

CONTENTS

ABBREVIATIONS

AFT – adaptive Fourier transform

EAIM – Earth – atmosphere – ionosphere – magnetosphere

IGW – internal gravity waves

IMF – interplanetary magnetic field

MHD –magnetohydrodynamic

NIS – negative ionospheric storms

PIS – positive ionospheric storms

RRD – radio receiving device

RTD – radio transmitting device

SE – solar eclipse

SIMMIAE – Sun – interplanetary medium – magnetosphere – ionosphere – atmosphere – Earth

UT – universal time

VS – vertical sounding

WFT – windowed Fourier transform

WT – wavelet transform

INTRODUCTION

Geospace is a combination of the upper atmosphere, the ionosphere, and the magnetosphere. At present, thousands of artificial Earth satellites operate in geospace, and they provide peoples with data on space weather, atmospheric weather, processes under the Earth, on the Earth's surface and in space using radio signals. The geospace environment is the main radio channel for radio- and telecommunication, radio navigation and monitoring of processes in various environments. In addition to regular variations in the parameters of the ionosphere, aperiodic and quasi periodic disturbances exist in the ionosphere limiting the potential capabilities of telecommunication and radio navigation due to their random time of occurrence, considerable amplitudes and durations. Therefore, the study of geospace and, in particular, the ionosphere, as well as variations in the characteristics of radio waves caused by the influence of powerful sources of energy on the ionosphere, is an *important radio physics problem*.

It is known that the ionosphere can be considered as a "mirror" which reflects the processes occurring underground, on Earth's surface, and in space. In other words, the ionosphere is a subsystem of Sun – interplanetary medium – magnetosphere – ionosphere – atmosphere – Earth system. The ionosphere is also responsible for the interaction of subsystems inside this system. Since the processes of the interaction are superimposed on each other, there is a need for their separation.

Solving the problem of separation of ionosphere disturbances caused by a particular source of energy (earthquakes, tsunamis, volcanic eruptions, thunderstorms, falls of large space bodies, solar flares, coronal mass ejections, solar terminator, solar eclipses, gusts and flights, powerful radio transmission, emissions of chemical reagents, etc.) requires continuous observations on a global scale. Such observations are conducted over the world. An example of such a project is the GIRO (Global Ionospheric Radio Observatory) project. Also, maps of total electronic content provided by different research teams reflect global variations of this parameter. So far, researchers are limited in studying the response of the geospace

environment to the source of energy of a given nature. Therefore, the study of the geospace and, in particular, the ionosphere, as well as variations in the characteristics of radio waves is an important radio physical problem.

Despite the existing strong achievements in the field of investigation of aperiodic and quasi-periodic processes in the ionosphere, there are a number of gaps. Thus, aperiodic and quasi-periodic perturbations during such a unique event as the explosion of the Chelyabinsk meteoroid, during rare phenomena such as solar eclipses, during the action of a powerful radio transmitter 1,000 km away, etc. have been poor studied.

A significant amount of works have been devoted to the study of the ionosphere response to solar eclipses. However, the study of the ionosphere reaction remains an important problem. The fact is that the ionosphere response depends on the state of atmospheric and space weather, place and time of day, as well as on the magnitude of the solar eclipse (SE).

Numerous of works are also devoted to the study of modifying the ionospheric plasma by intense radio waves. Usually, the perturbations that occur within the antenna pattern are studied, and only the monograph [1] is devoted to the study of large-scale (about 1000 km) perturbations.

The unique effects in the ionosphere that accompanied the fall of the Chelyabinsk cosmic body have a special novelty. Since such events occur once in about a hundred years, such studies are of great importance. This monograph presents studies of the ionosphere response to two solar eclipses, the fall of the Chelyabinsk cosmic body, and the effect of powerful radio transmission from a system distant about 1,000 km away from the source.

In addition, natural (background) disturbances in the ionosphere were observed for four seasons (vernal and fall equinoxes, winter and summer solstices) during the growing and declining phases of the 24^{th} solar activity cycle.

Chapter 1
IONOSPHERE: BASIC MORPHOLOGY AND METHODS OF DIAGNOSTIC

The ionosphere is one of the main channels of radio wave propagation. It significantly affects the characteristics of radio waves with a wavelength of centimeters to thousands of kilometers (see, for example, [2–6]). Non-stationary processes in the ionosphere play a special role. They limit the potential characteristics of radar, radio navigation and telecommunications systems (see, for example, [3]).

Quasi-periodic (wave) processes occupy an important place among non-stationary processes in the ionosphere. Many experimental and theoretical works are devoted to their research. Despite this, the systematic study of such processes is just beginning (see, for example, [7–28]). Radio physical methods play a leading role in the study of wave processes and include methods of incoherent scatter technique, Doppler method, partial reflection technique, remote sensing, etc.

Creation of a model of wave processes in the ionosphere requires continuous observations on a global scale. So far this is impossible. Therefore, researchers are limited to measurements for specific periods like. Vernal and fall equinoxes, as well as the summer and winter solstices.

1.1. Remote Sensing

Experimental study of the ionosphere is carried out mainly using radio physical methods, i.e. by studying the conditions of propagation, reflection and scattering of radio waves in the ionosphere.

The method of vertical sounding (VS) of the ionosphere is one of the methods being employed to obtain operational information about the ionosphere.

The method is based on the reflection of a radio wave from an inhomogeneous plasma, including a random inhomogenities, which is the altitude structure of the Earth's ionosphere. The radio receiving equipment allows measuring and analyzing

the delay time (or the effective height) of the radio pulses reflected from the ionosphere as a function of the gradually changing carrier frequency.

The dependence of the reflections' height on the frequency is called the altitude-frequency characteristic (a digital ionogram) (Fig. 1.1).

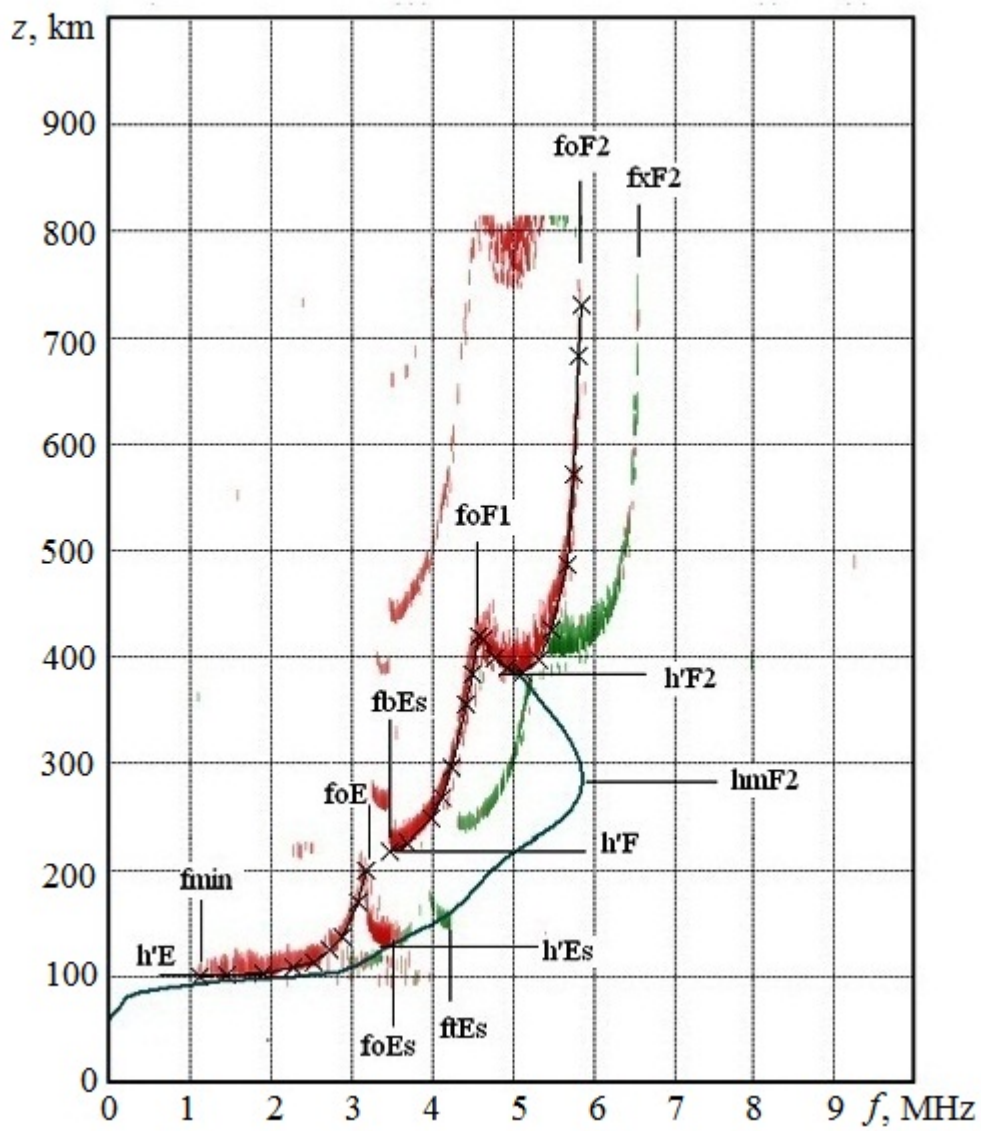

Fig. 1.1. A digital ionogram processed with automatic scaling technique

Ionograms allow retrieving the following parameters in real time: effective height of each layer (denoted as *h*'E, *h*'F1 and *h*'F2, etc.) and the frequency at which the effective height becomes infinitely large because of the wave reaches the level of the maximum electron density in this layer (denoted as f_oE, f_oF1 and f_oF2, etc.) [10].

The refractive height is always greater than the actual one. This is because of the signal propagates at a group speed v which is lower than the speed of light in vacuum c. It takes time for the signal to propagate over a certain distance:

$$\Delta t = \int_s \frac{ds}{v}.$$

If the signal propagates upward to the height of reflection z, then we obtain

$$\Delta t = \frac{1}{c}\int_0^z \frac{dz}{n} = \frac{h'}{c},$$

where $h' = \int_0^z \frac{dz}{n}$ – a refractive height, n – a refractive index. Since in isotropic plasma $v = cn = c\sqrt{1-\omega_p^2/\omega^2}$ will always be less than the velocity of the electromagnetic wave in vacuum c, then Δt is always larger than the propagation time of the signal in vacuum, hence that $h' \geq z$.

The method allows obtaining profiles of electron density $N(z)$ at altitudes from about 100 to 350–400 km.

In the F region of ionosphere, there is a splitting of the waves reflected from the F2-layer. This is caused by the fact that two types of waves can propagate along the external magnetic field line. The dielectric permittivity for these waves by definition is equal to

$$\varepsilon_{o,x} = \varepsilon_{xx} \mp i\varepsilon_{xy},$$

where $\varepsilon_{xx} = 1 - \omega_p^2 / \left(\omega^2 - \omega_B^2\right)$ and $\varepsilon_{xy} = i\left(\omega_p^2 \omega_B / \omega \cdot (\omega^2 - \omega_B^2)\right)$ – components of the dielectric permittivity, ω_p – the plasma frequency, ω_B – the electron gyrofrequiency. Substituting ε_{xx} and ε_{xy} and making the transformation, we obtain:

$$\varepsilon_{o,x} = 1 - \frac{\omega_p^2}{\omega\left(\omega \pm \omega_B\right)}.$$

Waves corresponding to the indices “o” and “x” are called ordinary and extraordinary, respectively. The term of “extraordinary wave” arose from a feature in the denominator at $\omega \to \omega_B$. Physically, the angular velocity of rotation of the vector of the electric or magnetic field coincides in magnitude and direction with the angular

velocity of electron rotation (gyrofrequency). This phenomenon is called gyroresonance.

The above expression is accurate for the longitudinal propagation of fairly high-frequency waves in cold plasma without collisions.

1.2. Ionosondes

The largest amount of experimental data on the ionosphere were obtained using the radio facilities. The ionospheric stations (ionosondes) are the most widespread facilities for ionospheric investigation.

The basic parts of the ionosonde are the radio transmitting device (RTD), the receiving and transmitting antennas, the radio receiving device (RRD), the recorder. Ionospheric station is aimed to obtain altitude-frequency characteristics.

RTD emits radio waves as short pulses, their duration is τ = 10–100 μs, and the pulse repetition frequency F = 50–100 Hz. Since $\tau F \ll 1$, there is enough time for the emitted pulse to be reflected from a given ionospheric region and to return. The reflected pulse is received by the RRD located next to the transmitter.

The receiving and transmitting antenna of the ionosonde are arranged so that the transmission propagates upward. RTD emits short sequences of radio pulses through the antenna, and RRD in the mode of receiving (using the receiving antenna) catches radio wave, which were reflected by the ionosphere. Therefore, knowing the time of the start of the transmission and the time of the signal returning to the receiver, it is possible to estimate the reflective hight.

The ionosonde emits not at a single fixed frequency, but in some frequency range. The frequency inside the frequency range can change continuously or discretely. In a time of approximately one minute, the frequency range can vary from 0.5 to 20 MHz. Signals with low frequencies are reflected from the lower ionosphere layers (0.5 MHz corresponds to electron density N about $2.5 \cdot 10^9$ m^{-3} and a reflection height of about 100 km), and signals with high frequencies are reflected from the upper layers, where $N \approx (5–15) \cdot 10^{11}$ m^{-3}.

Changes in the frequency and height of the reflective layer are recorded using different types of equipment.

When working with ionograms, the international instruction on processing and interpretation (the International Unionof Radio Science (URSI) standard) is used [29]. The study of altitude-frequency characteristics allows obtaining various parameters of the ionospheric layers.

The location of the ionosonde on the Earth's surface imposes some restrictions on the received information about the ionosphere. It is possible to study only bottomside ionosphere located below the main maximum, i.e. up to an altitude of 200–350 km.

Currently, there is an international network of 164 ionosondes of different types (models), which allows large-scale monitoring of the ionosphere.

The types of ionosondes, the data of which are used in this work, and their geographical position are presented in Table 1.1.

Table 1.1. Types of ionosondes and their geographical location

Ionosonde	Latitude	Longitude	Types of ionosondes
Tromsö	69.6°N	19.2°E	DPS-4
Fairford	51.7°N	1.5°W	DISS
Dourbes	50.1°N	4.6°E	DGS-256
Juliusruh	54.6°N	13.4°E	DPS-1
Pruhonice	50.0°N	14.6°E	DPS-4
Rocuetes	40.8°N	0.5°E	DGS-256
El Arinosillo	37.1°N	6.7°W	DGS-256
Moscow	55.5°N	37.3°E	DPS-4
San Vito	40.6°N	17.8°E	DISS
Kharkiv	49.6°N	36.3°E	NDI
Athens	38.0°N	23.5°E	DGS-128

1.3. Morphology of Quiet Ionosphere at Mid-latitudes

For the first time in 1878, Stewart generated hypothese on the existence of a conductive layer in the upper atmosphere to explain the peculiarities of perturbations of the geomagnetic field. Appleton, Bright, Barnet, and Tue [4] were the first to experimentally prove the presence of radio-reflecting layers. They also became the founders of the systematic study of ionospheric regions.

The ionosphere is an ionized region of the Earth's atmosphere located from altitudes of about 60 km to more than 1,000 km. The ionosphere is a weakly ionized plasma which motion is controlled by the Earth's magnetic field. The ionosphere exists because of influence of electromagnetic and corpuscular radiation of the Sun on the atmosphere of Earth.

It is known that the electron density in the ionosphere is irregularly distributed over altitude. There are regions where the density reaches a maximum (Fig. 1.2).

D region of the ionosphere is located below 90 km. It almost absent disappears in the mid-latitudes at night. At high latitudes D region is present almost all the time. The reason os that ionization at altitudes less than 100 km in the high-latitude ionosphere is maintained by the penetration of corpuscles into the atmosphere. This process is called particle precipitation. At these altitudes, the role of the magnetic field is increased and there is a strong plasma turbulence.

The E region is located in the altitude range of 90–140 km. At these altitudes, sporadic layer E_s occurs occasionally. Ionization is mainly provided by ultraviolet radiation. In this layer, the influence of the geomagnetic field is relatively weak and the strongest currents exist. The E region of the ionosphere is the most stable.

The F region of ionosphere is located above the E region. At night, the F region extends to altitudes of 250–400 km, and during the day (mainly in summer) it splits into layer F1, located at altitudes of 150–200 km, and layer F2 which is located at altitudes of 200–1000 km. The main ionization maximum is observed at altitudes of 200–400 km. Shortwave solar radiation is the main source of the ionization there. In this region, the magnetic field influence enhances, the charged particle diffusion and

other electrodynamic processes are more pronounced. The ionospheric F region is unstable in contradistinction to the E region.

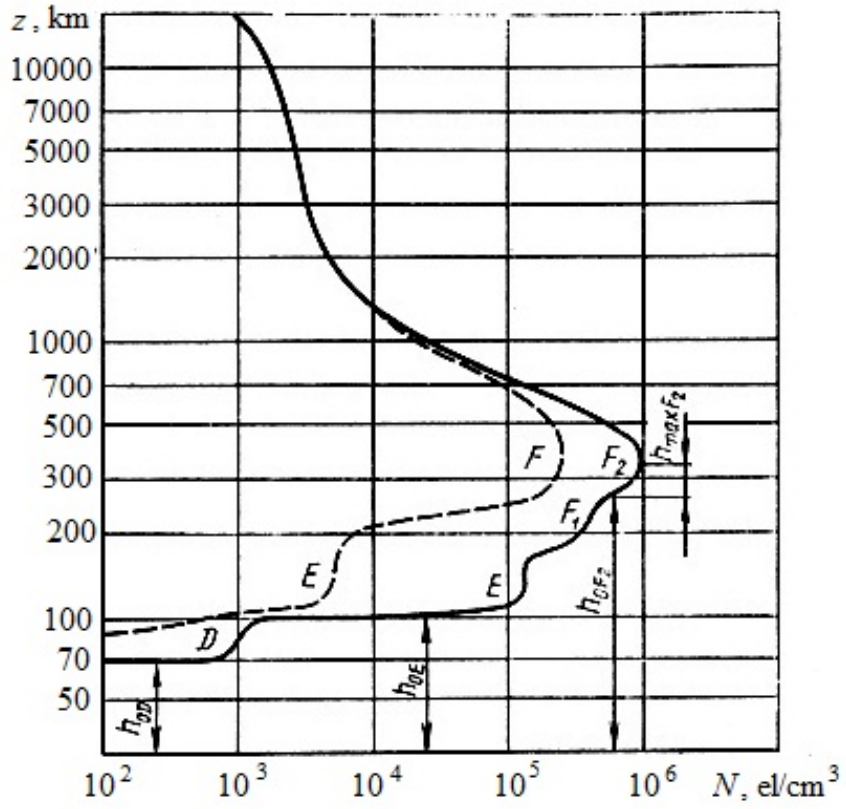

Fig. 1.2. Typical vertical distribution of the electron density N in the ionosphere: solid line – day-time variations, dashed line – night-time variations. The positions of different layers are marked with letters

Altitude stratification of ionospheric layers is due to changes in the conditions of the layers formation at different altitudes. Up to the maximum of ionization, electron T_e and ion T_i temperatures as well as the electron density N increase rapidly. In the upper part of the ionosphere (at the altirudes of F region) the increase of temperatures T_e, T_i and density N slows down. Above the F region, the density N decreases first gradually to altitudes of 15–20 thousand km (so-called plasma knee) and then N moves to low densities more sharply and transits to the the interplanetary medium. Ionosphere characteristics change with latitude. It's distinguished the mid-latitude,

equatorial, auroral and polar ionospheres. The mid-latitude ionosphere is more regular.

The structure of the quiet ionosphere changes regularly over time: during the day, season, and 11-year solar cycle. From the minimum to the maximum of the solar cycle, the electron density changes from $N_{\min}$ to $N_{\max}$, the electrons and ions temperature increases, the altitude range of ionosphere layers increases too, the recombination coefficient α decreases. The average values of ionospheric parameters are given in the Table 1.2 [30]. The ionosphere is a system which is controlled by chemical and dynamic processes. Free electrons are produced in the ionosphere under the action of electromagnetic and corpuscular radiation. The speed of electron production q_e is ~$(10^7–10^{11})$ $m^{-3}s^{-1}$. Simultaneously with the electron production, the electron disappearance with the speed q_r takes place. The change in density N over time is described by the equation of electron density balance (continuity equation) which takes into account the vertical plasma transfer velocity v_z:

$$\frac{dN}{dt} = \frac{\partial N}{\partial t} + \frac{\partial}{\partial z}\left(N v_z\right) = q_e - q_r . \qquad (1.1)$$

Table 1.2. Values of ionospheric region parameters for mid-latitudes [30]

Region (layer) of the ionosphere	Layer peak altitudes, km	T_i, K	Day-time		Night-time N, m^{-3}	α, m^3s^{-1}
			$N_{\min}$, m^{-3}	$N_{\max}$, m^{-3}		
D	70	220	10^8	$2\cdot10^8$	10^7	10^{-12}
E	110	270	$1.5\cdot10^{11}$	$3\cdot10^{11}$	$3\cdot10^{10}$	10^{-13}
F1 (summer)	180	800–1500	$3\cdot10^{11}$	$5\cdot10^{11}$	–	$3\cdot10^{-14}$
F2 (winter)	220–280	1000–2000	$6\cdot10^{11}$	$25\cdot10^{11}$	$\sim10^{11}$	$2\cdot10^{-16}$
F2 (summer)	250–320		$2\cdot10^{11}$	$8\cdot10^{11}$	$\sim3\cdot10^{11}$	10^{-16}

The transport of plasma should be taken into account only at altitudes higher than 250–300 km.

Similarly, the balance equations for positive N^+ and negative N^- ions are

introduced, and the law of charge conservation is preserved, i.e. $N+N^- = N^+$.

At low altitudes, electrons disappear in the reaction of radiative recombination with heavy molecular ions. In this case, the following equation is valid:

$$q_r \approx \alpha N^2 .$$

In the F region, electrons disappear in the reaction of radiative recombination with heavy molecular ions too. However, at this altitudes, the recombination rate directly depends on the density of neutral molecules and the following equation is valid:

$$q_r = \beta N.$$

Dynamic processes also take place in the ionosphere. The reasons for their occurrence are the same as in the neutral atmosphere. At $z \leq 400–500$ km, the ionized component, which is a small constituent, is dragged by the neutral medium.

Also, at altitudes of more than 100 km electrodynamic processes begin to have a significant effect.

In the ionosphere, diffusion, thermodiffusion and thermal conductivity take place. Dynamic processes are primarily related to moving electrons, but they moves together with ions because of Coulomb forces. Therefore, we can talk about ambipolar diffusion and ambipolar thermodiffusion.

Electrodynamic forces lead to the currents and drift of charged particles. Electrodynamic processes can exist because of the presense of the Earth's magnetic field and the electric fields of ionospheric-magnetospheric origin.

1.4. Sources of Disturbed Ionosphere

Sources of ionospheric perturbations can be classified by source, energy, way of impact on the ionosphere, etc. The most important and most "influential" source is the Sun, other sources have less effect on the ionosphere. The parameters of the perturbations sources are described in more detail in [31].

1.5. The Results of the Study of Disturbances in the Middle Ionosphere

The vertical sounding method is successfully used to observe processes not only in the quiet ionosphere, but also in the ionosphere disturbed by solar flares, coronal mass ejections, solar eclipses, falling large space bodies, rocket launches, powerful radio radiation, etc.

1.5.1. Effects of Ionospferic Storms

Ionospheric storm is one of the components of geospace storm [31]. It represents rather fast and essential deviations of ionospheric parameters from their undisturbed values typical for a quiet ionosphere.

Ionospheric storm is an irregular phenomenon. The rise time of the storm can vary from a few minutes to several hours, its duration is 1–7 days. Approximate characteristics of magnetic disturbances and classification of magnetic storms are given in Tables 1.3, 1.4.

Decreasing of the critical frequency value of the F2-layer is one of the main effects manifested in the ionosphere during a storm. A decrease in the critical frequency value for the F1-layer is less frequent effect.

The phenomenon of electron density decreasing is called the negative phase of the ionospheric storm, and the electron density increase is called the positive phase of the storm [31].

In some cases, the development of storms lead to the appearance of the layer with strong radio waves absorption below the E region. Frequently, such a layer shields the reflection of radio waves from the ionosphere.

Occasionally, there may be a “powerful” sporadic E_s-layer during weak magnetic storms. This effect predominates at high latitudes.

There is an increase in the minimum height of the F2-layer in the course of further evolution of the storm.

Table 1.3. Classification of negative ionospheric storms (NIS) and their main parameters [55]

Kind of ionospheric storm	Name of NIS	$\frac{N_{m0}}{N_{m\min}}$	I_{st}, dB	$\frac{T_e}{T_{e0}}$	$\frac{T_i}{T_{i0}}$	Duration of ionospheric storm, hours	Number of ionospheric storms per cycle of solar activity
NIS5	Extreme	>10	>10	3–4	2–2.5	70–100	2–4
NIS4	Severe	4–10	6–10	2–3	1.5–2	50–70	50–150
NIS3	Strong	2–4	3–6	1.5–2	1.3–1.5	30–50	150–300
NIS2	Moderate	1.4–2	1.5–3.0	1.2–1.5	1.1–1.3	20–30	400–800
NIS1	Minor	1–1.4	0–1.5	1–1.2	1–1.1	5–20	1000–2000

Observed storms have different morphology [32]. The results of observations of the same storm at different stations may differ significantly. The differences are caused by the differences in geographical location of the stations, the differences in local time, moments at sunrise or sunset, etc.

An ionospheric storm, which is a response to a geomagnetic storm, has a set of distinguishing characteristics. There is a classification of ionospheric storms by the intensity [31].

1.5.2. Effects of Solar Eclipses

Solar eclipse (SE) provides to researchers a unique opportunity to study the dynamics of the Earth – atmosphere – ionosphere – magnetosphere system over a period of several hours [33]. Disturbances in this system caused by different SE differ

significantly. The parameters of those perturbations depend on the time of the SE, on the space weather conditions, season, phase of the cycle of solar activity, geographical coordinates and on the magnitude of the coverage of the Sun's disk [33].

Table 1.4. Characteristics of positive ionospheric storms (PIS) in the F and E regions of the ionosphere

Kind of ionospheric storm	Name of PIS	Effects of PIS	Index of PIS, dB	Number of ionospheric storms per cycle of solar activity
PIS5	Extreme	Total electron content may increase up to 2–3 times, the frequency capacity of the decameter radio channel increases, the absorption coefficient of hectometer, decameter and meter radio waves may increase up to 1.5–2 times	>4.8	1–3
PIS4	Severe	The same	4.0	~100
PIS3	Strong	The same	3.2	~200
PIS2	Moderate	The same	2.3	~600
PIS1	Minor	Total electron content, the frequency capacity of decameter radio channel, the absorption coefficient of hectometer, decameter and meter radio waves may increase by tens of percent	1.0	1000–2000

The study of the effects of SE in the ionosphere has a century-long history. The first radio physical observations of SE effects were made in 1912 [34]. Initially, the effect of eclipses on the propagation of radio waves in the ionosphere was studied.

Since the SE on August 31, 1932, the dynamic processes in the ionosphere accompanied eclipses have been studing. The most common method of observation is the method of vertical sounding which uses ionospheric stations (ionosonde) [35–40].

The arsenal of methods espaned considerably in the 1960s. Satellite and rocket methods [41–45], incoherent scattering technique [46–54], and a number of other methods (see, for example, [55–67]) are widely used. The mentioned works describe the decrease in electron density in all layers of the ionosphere, decrease in electron and ion temperatures, change in plasma drift velocity, plasma and heat fluxes, generation of wave-like perturbations in the upper ionosphere and other effects accompanying SE with different phases in different regions of the globe.

The results of ionosonde observations during the previous years are presented in [35–40]. Recent studies are analyzed in [49–53].

Ionosonde observations shown that SEs are accompanied by a number of stable effects: a decrease in the electron density N, an increase in the effective reflection height, a delay in the N decreases relative to the moment of the maximum eclipse phase, and the generation of quasi periodic (wave) disturbances in the ionosphere. At the same time, it should be borne in mind that each eclipse has its own, individual, features.

1.5.3. Effects of the Chelyabinsk Meteor

The explosion of the Chelyabinsk space body over the settlements, accompanied by a bright flash and roar, found a resonant response in the minds of many people. Buildings and mainly windows, doors, walls and ceilings were partially damaged. In Chelyabinsk, the explosion knocked out about 20 000 m^2 of windows. More than 1.6 thousand people suffered from minor injuries in Chelyabinsk Region. Fortunately, there were no casualties. The damage exceeded 30 million US dollars.

The initial data on the Chelyabinsk space body effects are presented on the website [68].

The meteoroid entered the Earth's atmosphere on February 15, 2012 at 03:20:26 UT. The cosmic body moved approximately from east to west (azimuth was about 270°) at an angle to the horizon of about 20°. The initial body mass $m_0 \approx 11$ kt, the initial velocity $v_0 \approx 18.5$ km/s, and the initial body diameter $d_0 \approx 18$ m (see, for example, [68]). Found fragments of the meteorite indicate that it was a stone, or rather, the cosmic body was a chondrite type LL5, which consisted of metallic iron, olivine and sulfites. The remains of the body fell into Lake Chebarkul and near it.

The physics of meteor phenomena is discussed in a large number of studies (see, for example, [69–71]).

Features of the fall of large cosmic bodies are described in a number of works (see, for example, [70–75]). A fundamental feature is the generation of a strong shock wave by large bodies.

The main physical effects, that accompanied the fall of the Chelyabinsk meteoroid, were theoretically estimated in works [76–79]. This used the theory presented in the books [69, 70, 72, 75, 76, 78]. In books [76, 78], it was shown that the main energy release of about 0.2 Mt TNT (trinitrotoluene) took place near an altitude of 25 km, where the rate of mass loss was of the order of 10 kt/s, the energy of optical radiation reached several hundred TJ. In works [76, 78] it was substantiated that the fall of the body should have led to the disturbance of not only the lower but also the upper atmosphere, as well as the ionosphere at a distance of at least several thousand kilometers from the place of falling.

The results of the first observations of a number of effects, that accompanied the fall of the Chelyabinsk meteoroid, in the ionosphere and geomagnetic field are described in papers [77, 80, 81].

The search for perturbations in the atmosphere and ionosphere at considerable distances from the place of the Chelyabinsk meteorite falling has an absolute interest. It is known that its invasion of the Earth's atmosphere came as a surprise. Therefore, purposeful measurements of the whole complex of the physical effects of the space body fall in all environments (in all geospheres) turned out to be impossible. Some effects are registered by "regular" instruments. These include a network of

ionosondes, which allows almost continuous monitoring of the ionosphere on an almost global scale.

The fall of the Chelyabinsk space body caused a response in the ionosphere. The magnitude of the effects, recorded by various radio physical means of observation, depended on the place of registration.

The closest source of information about the impact of the flight and explosion of a meteoroid is the radar YeKB (Yekaterinburg) of Institute of Solar-Earth Physics (Siberian Branch of the Russian Academy of Sciences (ISEF SB of RAS)) and ionosonde “Sail” of Institute of Geophysics (Ural Branch of the Russian Academy of Sciences (IGF UB of RAS)). The radar and ionosonde are approximately 200 km from the place where the meteoroid fell [82–90]. The perturbations had a high amplitude and dynamics, but in the first hours it did not cause changes in the average ionosphere parameters above the center of perturbation.

The main effects were recorded at distances from 200 to 1500 km. The fall and explosion of the meteoroid caused a surge of electron density at altitudes of 80–120 km. The time of irregularity formation roughly coincided with the moment of the meteoroid falling [90].

In the F region, the experimentally estimated velocities of the disturbances were 250, 400 and 800 m/s. The increase in electron density was about 15%. The scale of the disturbed area was about 200 km. The radial nature of the disturbances was observed for 80–100 min.

Large-scale observations taken at stations far from the falling place of large space bodies allow determining the degree of impact of their flight and explosion on the Earth’s atmosphere on the ionosphere. The fall of the Chelyabinsk meteoroid, observed at stations approximately 200, 1400, 1700 and 1900 km away, caused a response in the ionosphere. It was concluded in the change of the electron density and the height of the maximum of the F2-layer h_mF2. Disturbances were recorded at ionospheric altitudes from 100 to 250 km [90–108]. The first response of the ionosphere was recorded in Sverdlovsk (200 km) and had the appearance of a powerful sporadic E_s-layer about an hour after the meteoroid falling. At a distance of

about 1400 and 1700 km, the E_s-layer appeared after 4.5 and 6 h, respectively. There are no data on the presence of a sporadic layer over St. Petersburg.

In the F region, the response of the ionosphere was expressed in the change of the critical frequency f_oF2. It consisted of superimposing of critical frequency's oscillations from 1.2 to 3.9 MHz with the regular variation of the frequency. There was a sharp increase in the values of f_oF2 to the maximum level, a deep reducing after that, and following return to the initial frequencies.

The change in the electron density at the maximum of the F2-layer reached 2.7 times within 1–1.5 h. Given the fact that the ionosphere response to the fall of the meteoroid was recorded at a station located in St. Petersburg (1900 km), it can be argued that the disturbances spread over a distance of at least 2000 km [90–108].

The most complete information about the Chelyabinsk meteoroid is given in the works [85–91].

1.5.4. Effects of Powerful Radio Transmission

Many articles and scientific works are devoted to the study of the influence of powerful radio transmission on the ionosphere, for example [107–121]. There is a single monograph that describes large-scale (~1000 km) disturbances in the ionosphere [1].

Plasma disturbances caused by the influence of powerful radio transmission within the irradiated region are called localized [1]. The horizontal size of such disturbances is 10–100 km. The main determining factors are the width of the antenna pattern and the processes of particle and heat transfer. Localized disturbances are caused by heating, striction and ionization mechanisms of nonlinearity. In addition, the influence of powerful radio transmission in geospace causes effects associated with the interaction of subsystems in the system Earth – atmosphere – ionosphere – magnetosphere (EAIM), with the transfer of disturbances over long distances. Such disturbances are called large-scale [1]. They are characterized by a

horizontal size of about 1–3 thousand km. Powerful radio transmission acts as a stimulator of natural processes.

The effects stimulated by powerful radio transmission of the hectometer range were first discovered in September 1972 (see, for example, [1]).

In 1983, a heating stand of the decimeter range “Sura” was put into operation at the landfill of the Science and Research Radio Physical Institute (SRRPhI) (Vasilsursk, Russia). This allowed the author [1] conducting systematic experimental studies of large-scale disturbances near Kharkiv. Diagnostic of large-scale disturbances was carried out using the equipment of the Radio Physical Observatory (RPhO) of V.N. Karazin Kharkiv National University (the distance between the SRRPhI test site and the observatory is about 960 km).

In the course of research it was established that the influence of powerful radio transmission on the ionosphere leads to the emergence of a whole complex of geophysical and radio physical effects in the near-Earth environment (geospace) [1].

The identified manifestations of geophysical effects include the following:

– formation of ionization layers at altitudes $z \approx 70$–100 km with horizontal scale of at least 1000 km;

– generation or amplification of the sporadic E_s-layer ($z \geq 100$ km);

– strengthening of the irregularity structure in the lower, middle and upper ionosphere ($L_\perp \approx 1000$ km);

– generation and propagation of wave disturbances of plasma density in the middle ionosphere ($z \approx 150$–300 km) with a speed of 0.3–0.6 km/s and a period of 10–60 min ($L_\perp \approx 1000$ km);

– increase in electron temperature by 200–500 K in the outer ionosphere with $L_\perp \approx 1000$–2000 km;

– increase in electron temperature and density by approximately 200 K and 10%, respectively, in the magnetically coupled region for the heating stand;

– increase by 1–4 nT of the level of the geomagnetic field registered on the Earth’s surface ($L_\perp$ not less than 500 km).

Examples of stimulated radio physical effects are:

– variations in the level of electromagnetic noises in the frequency range not less than 1−20 MHz, recorded on the Earth's surface;

– amplification of the level of extremely low-frequency (ELF) and very low-frequency (VLF) radiation in the outer ionosphere ($L_{\perp} \approx$ 500–700 km);

– generation of quasi-constant electric fields with a voltage of about 30 mV/m in the outer ionosphere ($L_{\perp} \approx$ 1000 km);

– an increase the frequency of whistling in approximately three times.

From the listed complex of effects it is necessary to highlight the phenomena in the magnetic flux tube and in the magnetically conjugate region, and also wave disturbances with $v \approx$ 0.3–0.6 km/s [1]. The first phenomenon is related to the transfer of heat and energy of low-frequency radiation (whistles, etc.) along the flux tube. The second phenomenon is related to the propagation of density waves (along the ionosphere) from the location of the source of the perturbation. The remaining effects belong to the group stimulated by powerful radio transmission. The mechanism of their generation and transfer is not so obvious and still requires detailed study.

In favor of the fact that these effects are stimulated processes, the following arguments exist [1]. The disturbances developed 1–10 min after the powerful radio transmission was switched on. After cessation of exposure, the perturbation could disappear or continue (even intensify), i.e. the effect of exhaustion was observed. Disturbances could not occur during the first cycle of periodic plasma heating, i.e. there was an effect of accumulation or the effect of inertia of the system. Switching off the source could lead to effects similar to those that occurred when it was turned on, i.e. there was a switching effect. Disturbances were observed at distances up to $R \approx$ 1000–2000 km from a powerful radio system. The magnitude of disturbances and the frequency of their occurrence significantly depended on the geophysical conditions (space weather conditions). These facts indicate that powerful non-stationary radio transmission acts as a stimulator of natural processes.

Based on observations for the period from 1972 to 2012, the author [1] experimentally established and theoretically explained the previously unknown phenomenon of large-scale (about 1000 km) disturbances in the lower ionosphere, accompanied by variations in geomagnetic field and quasi-periodic processes in the middle ionosphere, which were stimulated by the influence of powerful non-stationary radio transmission of the decameter and hectometer ranges on the ionosphere.

1.5.5. Effects of Rockets Launches and Flights

The effects that occur in the ionosphere during the launches and flights of powerful rockets, have been studied for about 60 years. The observed effects depend on the space weather conditions, distance from the launch site, type of rocket, etc. Thus, the response of the ionosphere to the launch of two identical rockets will be different. A special place in these studies is devoted to investigation of large-scale and global disturbances. They are characterized by horizontal dimensions of about 1000 and 10000 km, respectively.

The ionosonde method is actively used to study the effects of rocket launches [122–128]. These works show that powerful rockets launch can cause not only localized (~10–100 km), but also large-scale (~1000 km) and even global disturbances in the ionosphere. Ionosonde [129–132] and Doppler [129] methods, as well as the method of incoherent scattering [129, 133–135] were used for their study.

The main effects of rocket launch are summarized in monographs [129, 136–138].

On the example of the study of the responses to the “Proton” and “Soyuz” rockets launches, the main effects can be identified, which are expressed in the generation of disturbances of different nature [130, 131, 135]. They are characterized by a velocity of disturbance propagation of 1.5–3.5 km/s and 375–440 m/s. Such velocities are inherent to slow magnetohydrodynamic (MHD) and internal gravity waves (IGW), respectively. The period, wavelength, and relative amplitude of the

wave perturbations of the electron density associated with IGW were 90 min, 2000–2400 km, and 2.5–5%, respectively. During the launch of the “Soyuz” rocket, two groups of disturbances were detected, with velocities of about 2 km/s and 600 m/s. Such velocities, which have been repeatedly observed before, are characteristic of slow MHD waves and IGW, respectively. The relative amplitude of electron density disturbances reached 5–7%, and the value of the quasi-period was about 2–3 h.

1.6. Investigation of Aperiodic and Wave Disturbances in the Ionosphere: Instruments and Methods

1.6.1. Ionosonde

In this work, observations of the ionosphere were carried out using a modified ionosonde “Basis” with digital registration of the reflected signal parameters. The ionosonde is located in Ionospheric Observatory of Institute of Ionosphere (49.63ºN, 36.33ºE) near Kharkiv.

The “Basis” ionosonde transmitter operates in frequency range of 0.3–20 MHz. The output power is 10 kW, the duration of the emitted pulse is 100 μs. The pulse repetition frequency can vary from 3.125 to 25 Hz.

The receiving equipment of ionosonde “Basis” is based on a superheterodyne with frequency conversion: in the frequency range from 0.3 to 2.3 MHz with double conversion, from 2.3 to 40 MHz with triple conversion.

The receiving and transmitting ionosonde antennas are identical and orthogonally arranged. Each of the antennas consists of two broadband vertical rhombuses. The small rhombus operates in the frequency range 6–20 MHz, and the large rhombus operates in the frequency range 0.3–6 MHz.

Ionogram registration rate is one ionogram every 15 min. Frequency estimation error is 25 kHz.

1.6.2. Methods of Analysis

For the spectral analysis of quasi-periodic variations in the electron density, the windowed Fourier transform (WFT), the adaptive Fourier transform (AFT), and the wavelet transform (WT) were used [139–142]. In addition to spectrograms, energy diagrams (distribution of energy of oscillation by periods) were also analyzed. The format of data analysis is the same as in [142].

Before spectral analysis, the trend was first determined using a moving average in the range of 120 or 180 min. The sliding step was equal to 1, 5 or 15 min depending on the rate of ionograms' recording. Since we were interested in the periods of more than 10–30 min, the distortion of the spectrum due to the use of a rectangular window was insignificant.

After eliminating the trend, spectral analysis was performed using window and adaptive Fourier transforms, as well as wavelet transforms [142]. The purpose of spectral analysis was to obtain spectrograms and energy diagrams. Hereinafter, the spectrogram means the dependence of the intensity of the spectral components on the period and time, and the energy diagram means the dependence of the normalized energy of the spectral components on the period.

The limitations of spectral analysis are as follows. The minimum period according to Nyquist's theorem is determined by two ionosonde samples (2, 10 or 30 min in different measurement campaigns). The maximum period is determined by the sliding average window of 120–180 min.

The following expressions are used for WFT and AFT, respectively [142]:

$$Sf(T,\tau)=\sqrt{\frac{2}{t_{ws}}}\int_{-\infty}^{\infty} f(t)g\left(\frac{t-\tau}{t_{ws}/2}\right)\exp\left(i\frac{2\pi t}{T}\right)dt,,$$

$$A_{\nu}f\left(T_{\nu},\tau\right)=\sqrt{\frac{2}{\nu T_{\nu}}}\int_{-\infty}^{\infty} f\left(t\right)g\left(\frac{t-\tau}{\nu T_{\nu}/2}\right)\exp\left(-i\frac{2\pi}{T_{\nu}}\left(t-\tau\right)\right)dt\,,$$

where t_{wS} is window width for WFT; $T=2\pi/\omega$ and $T_{\nu}=2a/\nu$ are quantities that have the physical meaning of period of oscillation.

In this work Hamming window $g(t)$ is used for WFT and AFT:

$$g_H(t) = \gamma[0.54 + 0.46\cos\pi t],$$

where $\gamma \approx 1.12$ – normalizing multiplier, t – dimensionless time.

Continuous WT functions $f(t)$ were created out on the basis of the expression:

$$Wf(a,b) = \frac{1}{a^{1/2}} \int_{-\infty}^{\infty} f(t)\Psi^*\left(\frac{t-b}{a}\right)dt,$$

where the symbol * denotes a complex combination, and the decomposition is based on wavelets

$$\Psi_{a,b}(t) = \frac{1}{a^{1/2}}\Psi\left(\frac{t-b}{a}\right),$$

where a is a scaling pameter ($a > 0$), b is a shift parameter.

Morle's wavelet was used as $\psi(t)$ for WT.

In addition to functions $P_S(\tilde{T},\tau)$, $P_A(\tilde{T},\tau)$ i $P_W(\tilde{T},\tau)$, energy diagrams were also used in the work [173]:

$$E_S(\tilde{T}) = \int_{-\infty}^{\infty} P_S(\tilde{T},\tau)d\tau, E_A(\tilde{T}) = \int_{-\infty}^{\infty} P_A(\tilde{T},\tau)d\tau, E_W(\tilde{T}) = \int_{-\infty}^{\infty} P_W(\tilde{T},\tau)d\tau.$$

We add that the expediency of use of all the three integral transformations (windowed and adaptive Fourier transforms, as well as wavelet transform) is substantiated in works [142, 143]. The first of them has the best localization by time, the second – by period. The wavelet transform shows the dynamics of the spectra better than other transforms.

Chapter 2
THE MIDDLE IONOSPHERE OF UKRAINIAN REGION UNDER QUIET CONDITIONS

The purpose of the chapter is to study the diurnal-seasonal variations in electron density and wave disturbances in the maximum of the F2-layer of the ionosphere under quiet conditions during the period with low solar activity (2011).

2.1. Space Weather Conditions

The space weather conditions was analyzed using the Wolf numbers W, index $F_{10.7}$, and magnetic indices K_p, D_{st}, AE (Table 2.1). Table 2.1 shows that Sun was quiet during the observational campaigns. Magnetic activity was relatively quiet. Therefore, variations of the electron density described below are considered as caused by diurnal and seasonal changes of the ionosphere and by wave-like processes in the ionosphere.

2.2. Regular Variations in the Electron Density

During the vernal and fall equinoxes, the temporal variations of the electron density N at the maximum of the F2-layer were generally similar (Figs. 2.1*a* and 2.1*b*). In the time interval 00:00–04:00 LT (hereinafter local time), $N \approx 2 \cdot 10^{11}$ m^{-3}. After sunrise at the heights of the F2-layer, the electron density gradually increased to $(6–7) \cdot 10^{11}$ m^{-3} for the vernal equinox and to $(1.0–1.1) \cdot 10^{12}$ m^{-3} for the fall equinox. The maximum of N took place in the time intervals 12:00–13:00 and 10:00–12:00 for the fall and vernal equinoxes, respectively. A slow decrease of N to $(5–7) \cdot 10^{11}$ m^{-3} was observed by the sunset. After sunset in the ionosphere, the electron density increased. At 22:00, the minimum value of N was reached $(2–3) \cdot 10^{11}$ m^{-3}.

During the summer solstice, the sun does not set at altitudes of 300 km and above at all.

Table 2.1. Space Weather Conditions

Data	W	$F_{10.7}$	K_p		D_{st}, nT		AE, nT	
			max	min	max	min	max	min
March 22, 2011	32	100	3.3	0	13	–17	345	23
March 23, 2011	30	105	3.3	2	8	–12	587	51
March 24, 2011	39	108	1.7	0.7	6	–3	89	22
June 20, 2011	26	96	2.7	1	12	–13	472	49
June 21, 2011	33	95	2.7	1	9	–5	445	64
June 22, 2011	33	93	4	1.3	9	–10	552	64
September 19, 2011	92	141	1	0	1	–20	107	17
September 20, 2011	80	144	3	0.7	–2	–16	280	29
September 21, 2011	70	144	2	0	4	–11	417	18
December 20, 2011	72	137	2.7	0.7	4	–11	359	23
December 21, 2011	73	145	2.7	0.3	5	–20	470	20
December 22, 2011	69	146	2.7	0.3	–7	–21	157	25

There was a fall of the density N approximately from $(3–4)\cdot10^{11}$ m^{-3} to (2–2.5) 10^{11} m^{-3} during the time interval 00:00–04:00 (Fig. 2.1*b*). Then, the density increase to $(5–6)\cdot10^{11}$ m^{-3} was observed in the time interval 09:00–10:00. After 10:00–12:00, there was a short-term decrease of the density N to $4\cdot10^{11}$ m^{-3}. Then, the evening increase of the dnsity took place. The maximum values of the electron density in the evening reached $5.5\cdot10^{11}$ m^{-3} at about 20:00.

Also, we analyzed the diurnal variations in the electron density during the winter solstice (Fig. 2.1*d*). In the time interval from 19:00 to 05:00 (the next day), the values of N were close to $2\cdot10^{11}$ m^{-3}. From 06:00 to 10:00–11:00, the density increase to the values $(8–10)\cdot10^{11}$ m^{-3} was observed. After 11:00–12:00 N was decreasing to night values ($2\cdot10^{11}$ m^{-3}) during 6 hours.

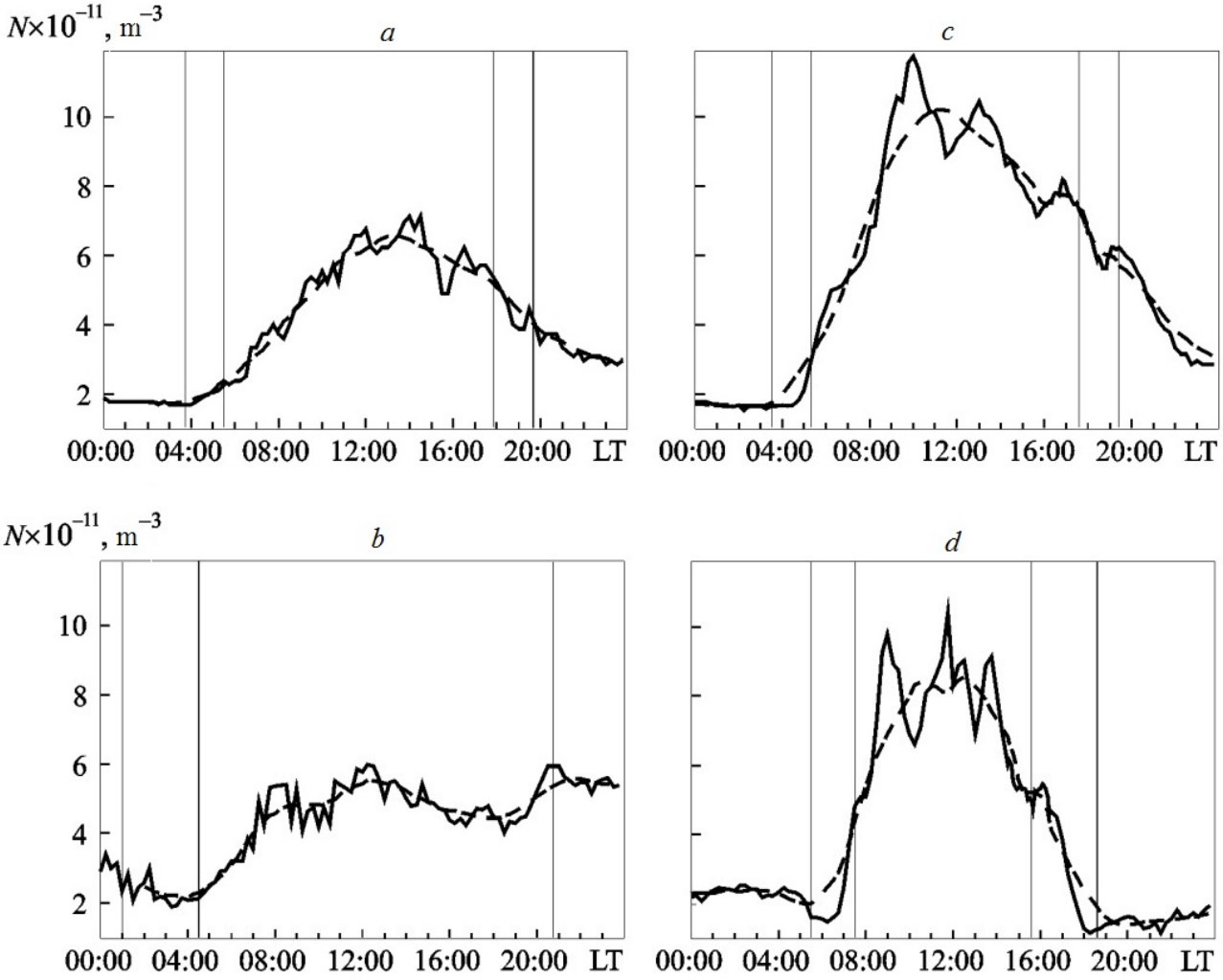

Fig. 2.1. Temporal variations of the electron density in the maximum of F2-layer on March 23, 2011 (*a*); June 21, 2011 (*b*); September 20, 2011 (*c*); December 21, 2011 (*d*). The dashed line is the result of averaging over 3 hours. Here and below, the vertical lines show the moments of sunrise and sunset at altitudes of 300 and 0 km

The temporal variations of the electron density N were generally similar during adjacent days and for the equinoxes and solstices.

Quasi-periodic perturbations were superimposed on regular changes of the density $N(t)$.

2.3. Wave Disturbances of the Electron Density

During the vernal equinox, the disturbances of the electron density ΔN were quasi-periodic (Fig. 2.2*a*, top panel). At night, the amplitude ΔN_a was about $(1–2)\cdot10^{10}$ m^{-3}. During the day, it was $(5–6)\cdot10^{10}$ m^{-3} 3–10 times larger (Fig. 2.2*a*, top panel).

Near the summer solstice, the disturbances of the density $\Delta N(t)$ were quite chaotic, but they also had quasi-periodic oscillations. Their amplitudes were practically independent of the time and were $(2–5)\cdot10^{10}$ m^{-3} (Fig. 2.2*b*, top panel).

During the fall equinox, nighttime ΔN_a was $(1–5)\cdot10^{10}$ m^{-3}, daytime $\Delta N_a \approx (1.0–3.5)\cdot10^{11}$ m^{-3}, i.e. 3–10 times larger (Fig. 2.2*c*, top panel).

Near the winter solstice, density disturbances ΔN also depended significantly on the time. At night, $\Delta N_a \approx 2\cdot10^{10}$ m^{-3}, during the day $\Delta N_a \approx 2\cdot10^{11}$ m^{-3} (Fig. 2.2*d*, top panel). The difference in ΔN_a reached an order of magnitude.

Temporal variations of relative disturbances of the electron density $\delta_N = \Delta N/\overline{N}$, where $\overline{\overline{N}}(t)$ are regular variations of the density N, are shown on the upper panels of Fig. 2.3. It is seen that $\delta_N(t)$ follows the key features of $\Delta N(t)$.

During the vernal equinox, the maximum values of δ_N occur during the daytime. They reached 0.15 but the average amplitude of δ_{Na} was about 0.1 (see Fig. 2.3*a*).

At the end of June fluctuations of δ_N did not exceed ±0.15, on average their amplitude was 0.1 (see Fig. 2.3*b*).

During the fall equinox, the variations in $\delta_N(t)$ were similar to the variations during the vernal equinox. On average, $\delta_{Na} \approx 0.1$ (see Fig. 2.3*c*).

During the winter solstice, δ_N fluctuations reached ±0.4 (see Fig. 2.3*d*). On average, $\delta_{Na} \approx 0.2$.

2.4. The Results of Spectral Analysis

Hereinafter, spectral analysis was performed for both time variations of the primary parameters of ionograms and absolute and relative disturbances of the electron density. Since the frequency spectra of absolute and relative disturbances of electron density differ, there was a need for spectral estimation of absolute and relative disturbances of electron density separately.

2.4.1. Spectral Composition of Diurnal-Seasonal Variations of Absolute Electron Density Disturbances

Spectrograms calculated for the vernal equinox show the oscillation period values T from 140 to 230 min and duration $\Delta T \approx$ 10–12 h prevailed. Oscillations with $T \approx 40$ min and $\Delta T \approx$ 1–2 h were also observed sporadically (see Fig. 2.2*a*). In the evening, there were also fluctuations with $T \approx$ 60–100 min.

Near the summer solstice during the day and night, oscillations with $T \approx 200$ min prevailed (see Fig. 2.2*b*). Their duration ΔT is 5 h. In addition to those oscillations, processes with $T \approx$ 100–150 min were observed, and their amplitude was approximately 2 times smaller than the predominant oscillations. Fluctuations with $T \approx 40$ min and $\Delta T \approx$ 1–2 h also occurred sporadically.

During the fall equinox, fluctuations with a period of $T \approx$ 170–210 min were pronounced in the morning and afternoon (see Fig. 2.2*c*). Their duration were at least 10 h. In the evening and at night, the main oscillations were with $T \approx$ 230–300 min and $\Delta T \approx$ 6–7 h.

During the winter solstice, fluctuations with a period T of 120–160 and 180–220 min prevailed in the morning and in the afternoon (see Fig. 2.2*d*). Their duration was 5–6 h. In the evening and at night, the period of predominant oscillation was close to 180–220 min, $\Delta T \approx$ 5–6 h.

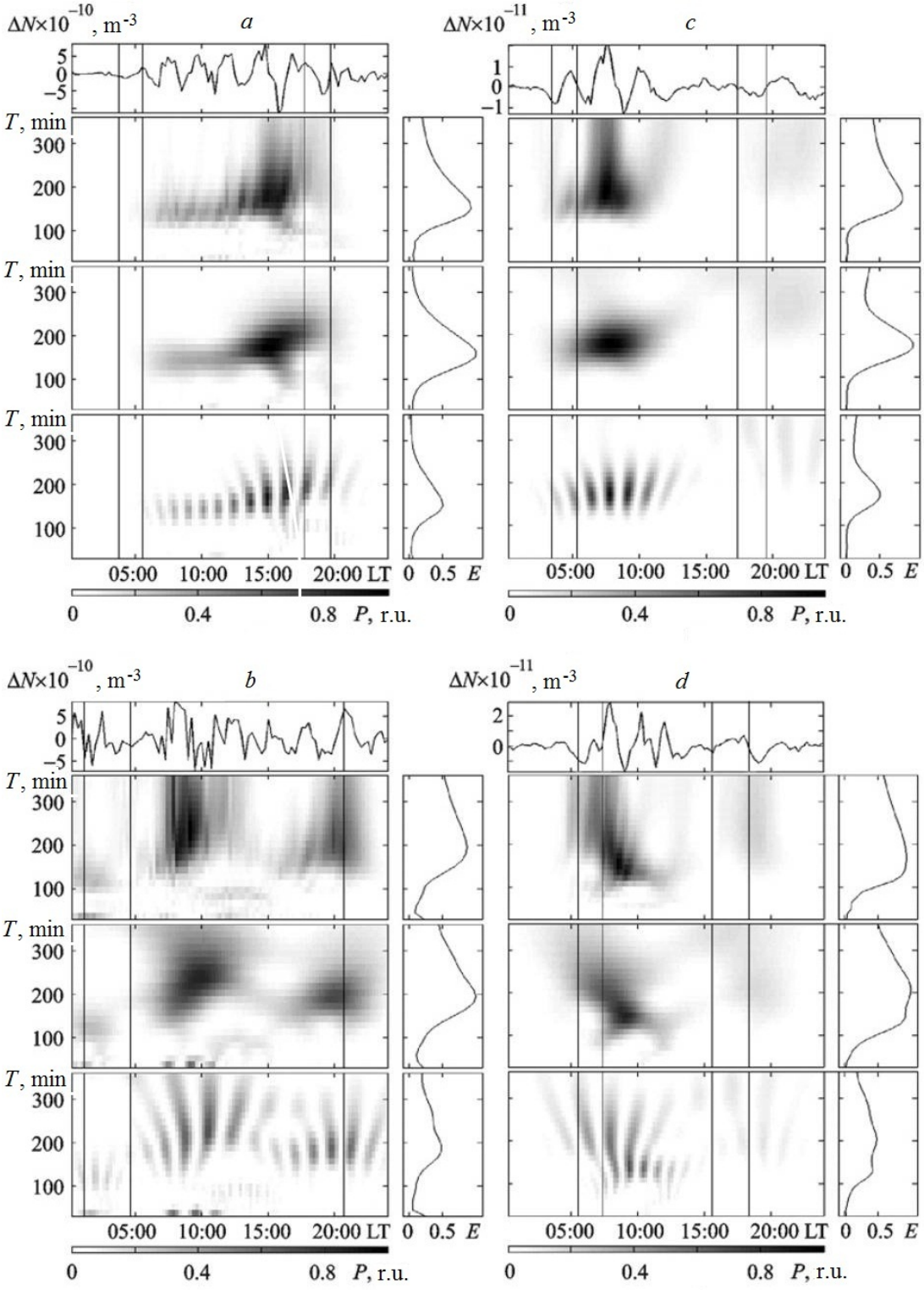

Fig. 2.2. Dependence of $\Delta N(t)$ for March 23, 2011 (*a*), June 21, 2011 (*b*), September 20, 2011 (*c*) and December 21, 2011 (*d*). Additional bottom panels in each figure shows the results of spectral analysis using WFT, AFT and WT (from top to down). The corresponding energy diagrams are shown on the right on small sub-panels

2.4.2. Spectral Composition of Diurnal-Seasonal Variations of Relative Electron Density Disturbances

The results of the spectral analysis of relative disturbances $\delta_N(t)$ are presented in Fig. 2.3. Fig. 2.3*a* shows that during the vernal equinox in daytime, the period of the main oscillation was close to 120–160 min. During the pre-sunset hours and at night, two oscillations with periods close to 60–70 and 180–220 min were clearly distinguished.

Near the summer solstice for almost the whole day on June 21, 2011, fluctuations with $T \approx 150$–240 min prevailed. In addition, fluctuations with periods of 100–120 and about 300 min occurred sporadically (see Fig. 2.3*b*). Their duration ranged from 4 to 6 hours.

During the fall equinox, fluctuations with $T \approx 140$–190 min prevailed in the morning and in the afternoon. Their duration reached 10 hours (see Fig. 2.3*c*). At night, the main oscillations were with $T \approx 230$–300 min and $\Delta T \approx 6$–7 h.

During the winter solstice, the largest variations in relative disturbances $\delta_N(t)$ occurred during the passage of solar terminators and for 4–5 hours after that (see Fig. 2.3*d*). The period of the main oscillation was 180–240 min. In addition to this oscillation, oscillations with periods of 60–110 and 280–330 min were also observed sporadically. For them ΔT is equal to 6–10 h.

2.5. Discussion

Regular diurnal-seasonal variations of $\overline{\overline{N}}$ fully correspond to the theory of physical and chemical processes in the ionosphere (see, for example, [31–56]).

Let us dwell on quasi-periodic variations in the electron density in more detail. Generalized information about these variations are given in the Table 2.2. The table shows that the largest values of ΔN_a occurred in winter, slightly smaller values of ΔN_a occurred in autumn. At night (except for the period close to the summer solstice), the amplitude ΔN_a is 3–10 times smaller than during the day.

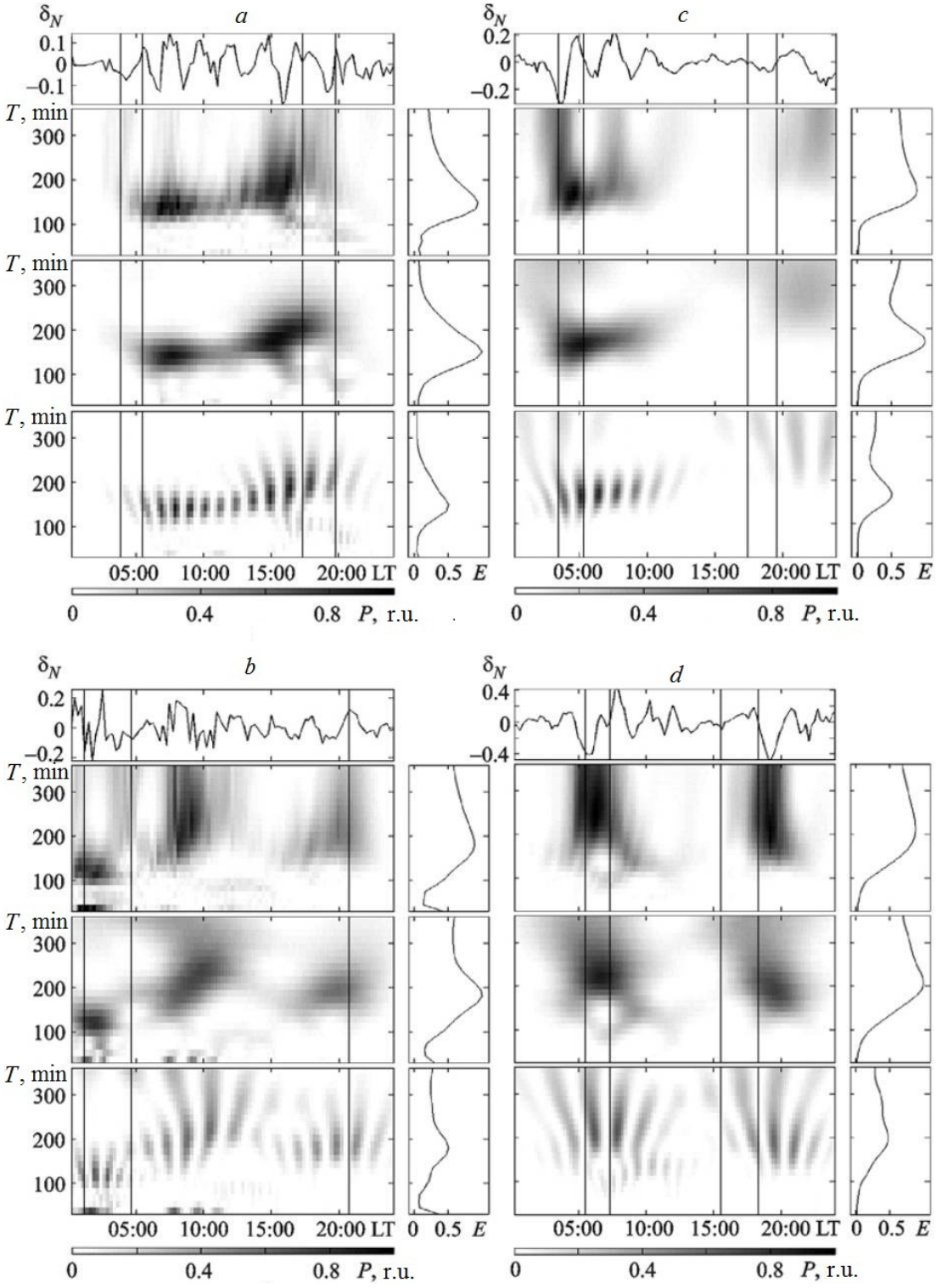

Fig. 2.3. Dependence of $\delta_N(t)$ for March 23, 2011 (*a*), June 21, 2011 (*b*), September 20, 2011 (*c*), December 21, 2011 (*d*). Additional bottom panels in each figure shows the results of spectral analysis using WFT, AFT and WT (from top to down). The corresponding energy diagrams are shown on the right on small sub-panels

The relative amplitudes of quasi-periodic changes in the electron density during the day were close to 0.1. During the winter solstice, it reached 0.2. At night, the values of the relative disturbances δ_N in all seasons were about 2 times smaller than during the day.

The period of predominant oscillations for different seasons was 140, 180, 175 and 200 min (see Table 2.2). Such value is close to the period of the third harmonic of tidal processes in the atmosphere (180 min). Occasionally, there were also oscillations with smaller relative disturbances δ_N and periods of about 60, 100, 220, and 300 min. It is possible that these periods are the periods of harmonics of a single process with a period of about 300 min. Wave processes with the specified periods and amplitudes are inherent in IGWs.

Table 2.2. The main parameters of quasi-periodic processes during the day (night) time

Season	Amplitude of oscillations, m^{-3}	Relative amplitude of oscillations	The period of predominant fluctuations, min	The duration of the quasi-periodic process, h
Vernal equinox	$(5–6)\cdot10^{10}$ ($(1–2)\cdot10^{10}$)	0.1 (0.05)	120–160 (60–70, 180–220)	15
Summer solstice	$(2–5)\cdot10^{10}$	0.1 (0.1)	150–240 (100–120, 300)	24 (4–6)
Fall equinox	$(1.0–1.5)\cdot10^{11}$ ($(1–5)\cdot10^{10}$)	0.1 (0.05)	140–190 (230–300)	10 (6–7)
Winter solstice	$2\cdot10^{11}$ ($2\cdot10^{10}$)	0.2 (0.1)	180–240 (60–110, 280–330)	5–6 (6–10)

The duration of the predominant oscillations was significant: from 5–7 to 24 h (during the summer solstice).

It turned out that the diurnal variations in $\Delta N(t)$ and $\delta_N(t)$ mainly tracked the daytime changes of $\overline{\overline{N}}(t)$. The coefficients of cross correlation for the amplitudes of ΔN_a and $\overline{\overline{N}}$, as well as for δ_{N_a} and $\overline{\overline{N}}$ were 0.6–0.8 for different seasons.

The obtained data on quasi-periodic processes in the maximum of the F2-layer in 2011 and 2016 are generally in good agreement with the results of our observations in the same region by the Kharkiv incoherent scatter radar (see, for example, [26–28]).

Chapter 3
EFFECTS OF SOLAR ECLIPSES IN THE MIDDLE IONOSPHERE

This chapter presents the results of investigation of ionospheric effects of solar eclipses (SE) occurred on January 4, 2011 and on March 20, 2015.

3.1. General Information About the Solar Eclipse on January 4, 2011

3.1.1. Brief Information About the Eclipse

The SE was observed after sunrise in North Africa. Thus, the main phase (0.37) in Morocco took place at about 07:38 (hereinafter universal time UT). The shaded area crossed all of Europe and part of Asia. The SE ended at about 10:25 over Pakistan (phase 0.09). The width of the area of the full SE was about 200 km, and its speed was about 700–800 m/s.

At the measurement site (located 50 km south-east from Kharkiv, near the city of Zmiiv), the coverage of the Sun's disk diameter was about 0.78. The maximum shaded area of the disk $A_{\max} \approx 0.71$. The SE started at 07:30 and ended at 10:29, the main phase took place at 08:59.

3.1.2. Space Weather Conditions

Let's briefly describe the space weather conditions during the period from January 1 to January 5, 2011 which is convenient to represent in terms of temporal variations of density, speed, temperature and dynamic pressure of the solar wind, induction of interplanetary magnetic field (IMF), energy function Akasofu ε_A, and indices of geomagnetic activity (K_p and D_{st}).

During the period of January 1–5, fluctuations in the density, speed, temperature and dynamic pressure of the solar wind did not exceed $1.5 \cdot 10^7$ m^{-3}, 420 km/s, $1.3 \cdot 10^5$ K and 4 nPa, respectively. The bursts of energy function ε_A reached 6 GJ/s.

The eclipse was preceded by a very minor magnetic disturbance (the K_p index varied from 0 to 3). The B_z-component of IMF varied chaotically within ±(5–6) nT. Fluctuations level of the B_y-component were insignificant (about ±(4–6) nT). The values of the D_{st} index also fluctuated chaotically within ±(10–15) nT.

It can be argued that the day of the eclipse, January 4, 2011, and the reference day, January 5, 2011, were quiet. This circumstance facilitated significantly the identification of disturbanes caused by the response of the middle ionosphere to the SE.

3.2. Variations in Ionosphere Parameters During the Solar Eclipse on January 4, 2011

3.2.1. Temporal Variations in Critical Frequencies

In these studies, ionograms were recorded with a data sampling rate of one ionogram per 15 min.

In Fig. 3.1, temporal variations in the critical frequencies of the ionosphere F region f_oF2 are presented. The solid thin line in the figures indicates the variations of the parameters processed by the moving average over 60 min interval. The moments of the beginning, the main phase, and the end of the SE are marked by three vertical lines in all figures. The eclipse near Kharkiv began in the morning when a rapid increase in f_oF2 was in progress.

Fig. 3.1 shows that before the eclipse, the frequency f_oF2 increased from 3.5 to 6.4 MHz. A slight decrease in f_oF2 began approximately 20 min before the onset of the SE. As the Sun's disk was covered, the values of f_oF2 decreased from approximately 6.2 to 4.3 MHz. They corresponded to a decrease in the electron density from $N \approx 4.7 \cdot 10^{11}$ m^{-3} to $N_{min} \approx 2.3 \cdot 10^{11}$ m^{-3}. The maximum value of the decrease of the critical frequency of the F2 layer δf_oF2 ≈ 1.9 MHz.

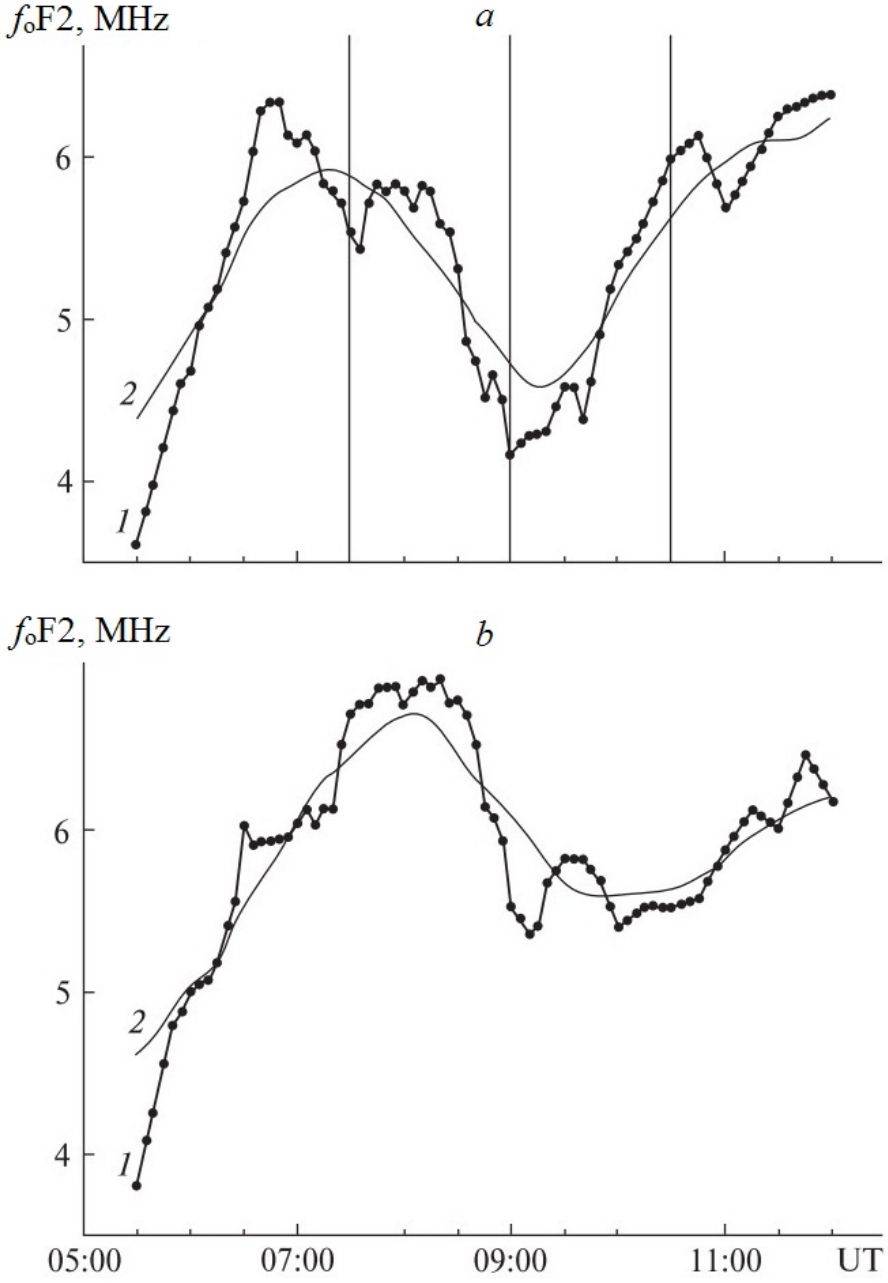

Fig. 3.1 Temporal variations of the critical frequency f_oF2: *a* – on the day of the eclipse on January 4, 2011 (1 – initial dependence, 2 – smoothed by the moving average on time interval of 90 min), *b* – the same but for the reference day January 5, 2011. Vertical lines here and below are the moments of beginning, main phase, and end of the eclipse

The decrease in the electron density $\Delta N = 2.4 \cdot 10^{11}$ m^{-3}, $N_{min}/N \approx 0.48$ and $\delta_N = \Delta N/N \approx 52$ %. Note that the minimum value of f_oF2, and, consequently, the

electron density at the maximum of the layer F2, was observed at 09:15, i.e. with a delay of about 16 min relative to the moment of the main phase of the SE.

Almost immediately after the onset of SE, the values of f_oF2 varied according to the quasi-periodic law. The magnitude of the quasi-periods T was 30 and 60 min, and their amplitude δf_{oa}F2 = 0.2 and 0.4 MHz. The relative amplitude of quasi-periodic disturbances can be estimated from the following formula:

$$\delta_{Na} = \frac{\Delta N}{N} \approx 2\frac{\delta f_{o a}\mathrm{F2}}{f_o\mathrm{F2}}, \tag{3.1}$$

where f_oF2 is average value of the critical frequency for the considered period. Assuming f_oF2 = 5 MHz, from (3.1) we obtain that for T equal to 30 and 60 min, δ_{Na} was 8 and 12%, respectively. The duration of this process was about 2 h.

On the reference day, such a decrease in the values of f_oF2 (and electron density N) was not observed. Note that the data of f_oF2 measurements before the beginning of the SE and after the end of the critical frequency reaction to the SE are close to the values of f_oF2 obtained at the appropriate time points on the reference day.

It is advisable to compare the decrease in f_oF2 on the day of the SE with the reference day. Around 09:15 on the reference day, the average of the frequency f_oF2 was 6.2 MHz. Then the decrease in f_oF2 on the day of the SE was 1.9 MHz. This value agrees with the value of δf_{oa}F2 above.

Let's describe briefly the variations in the critical frequency of the E_s-layer on the day of the SE and on the reference day (Fig. 3.2). It is seen that on January 4 and 5, the frequency f_oE_s fluctuated strongly. Its value varied from approximately 2.5 to 8.5 MHz on the day of the SE and from 2.3 to 8 MHz on the reference day. In general, the values of f_oE_s were larger on the day of the eclipse. The Es-layer was more powerful and significantly shielded the E region.

Temporal variations of the critical frequency of E region are shown in Fig. 3.3. In the time interval 05:00–07:30, the temporal variations of the critical frequency f_oE increased from approximately 1.8 to 2.3–2.6 MHz. On the reference day, the frequency f_oE continued to increase until approximately 08:30.

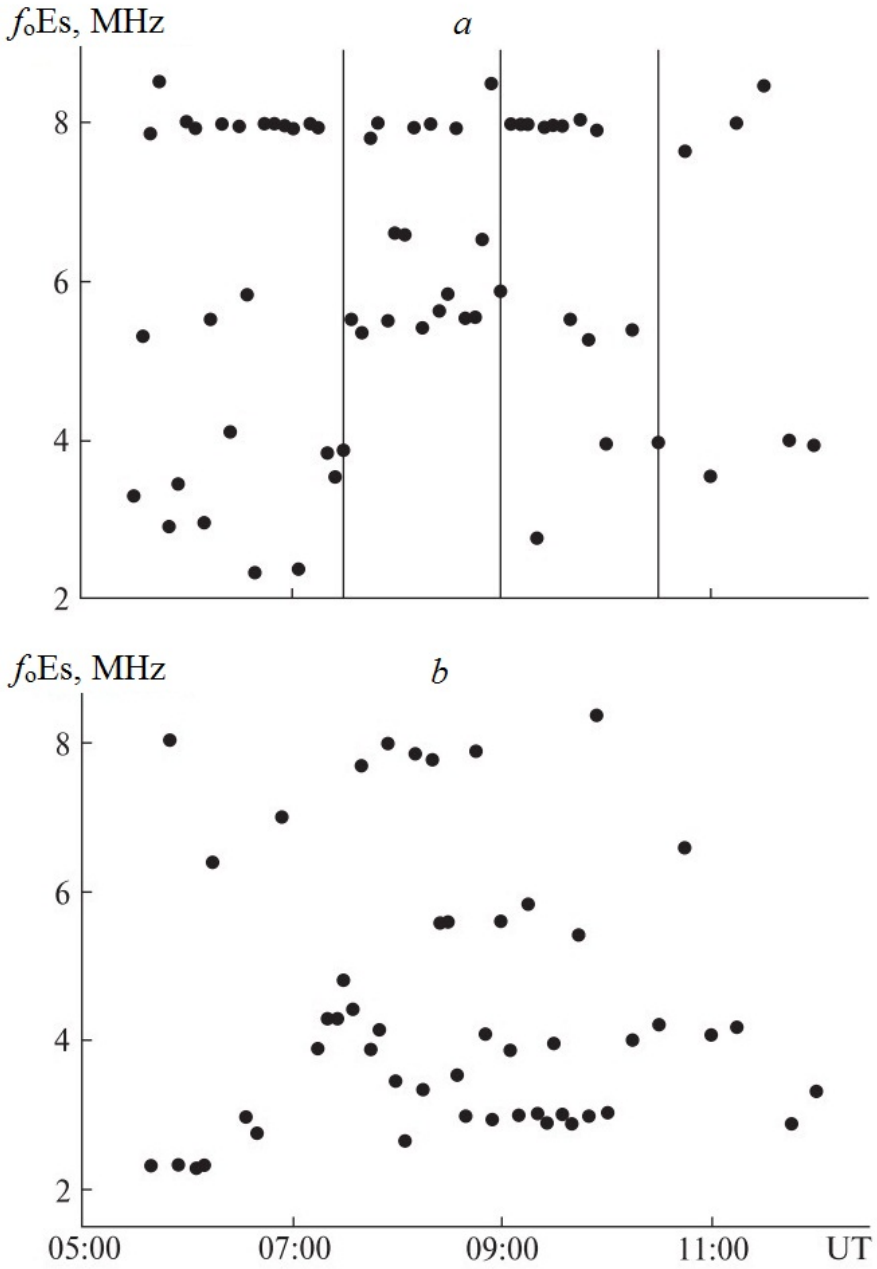

Fig. 3.2. Temporal variations of the critical frequency f_oEs on the day of the solar eclipse on January 4, 2011 (*a*) and on the reference day January 5, 2011 (*b*)

Over the next half hour, the critical frequency f_oE decreased from 2.7 to 2.6 MHz. During the next hour, fluctuations of the f_oE remained in the range of 2.5–2.6 MHz.

On the day of the eclipse, E-layer was observed sporadically. Near the main phase of the SE, the f_oE was approximately equal to 2.2 MHz, i.e. its value decreased

by approximately 0.4 MHz (by 16%) compared to the value that would have been in the absence of the eclipse. After the onset of the main phase, the frequency f_oE gradually increased from 2.2 to 2.8 MHz.

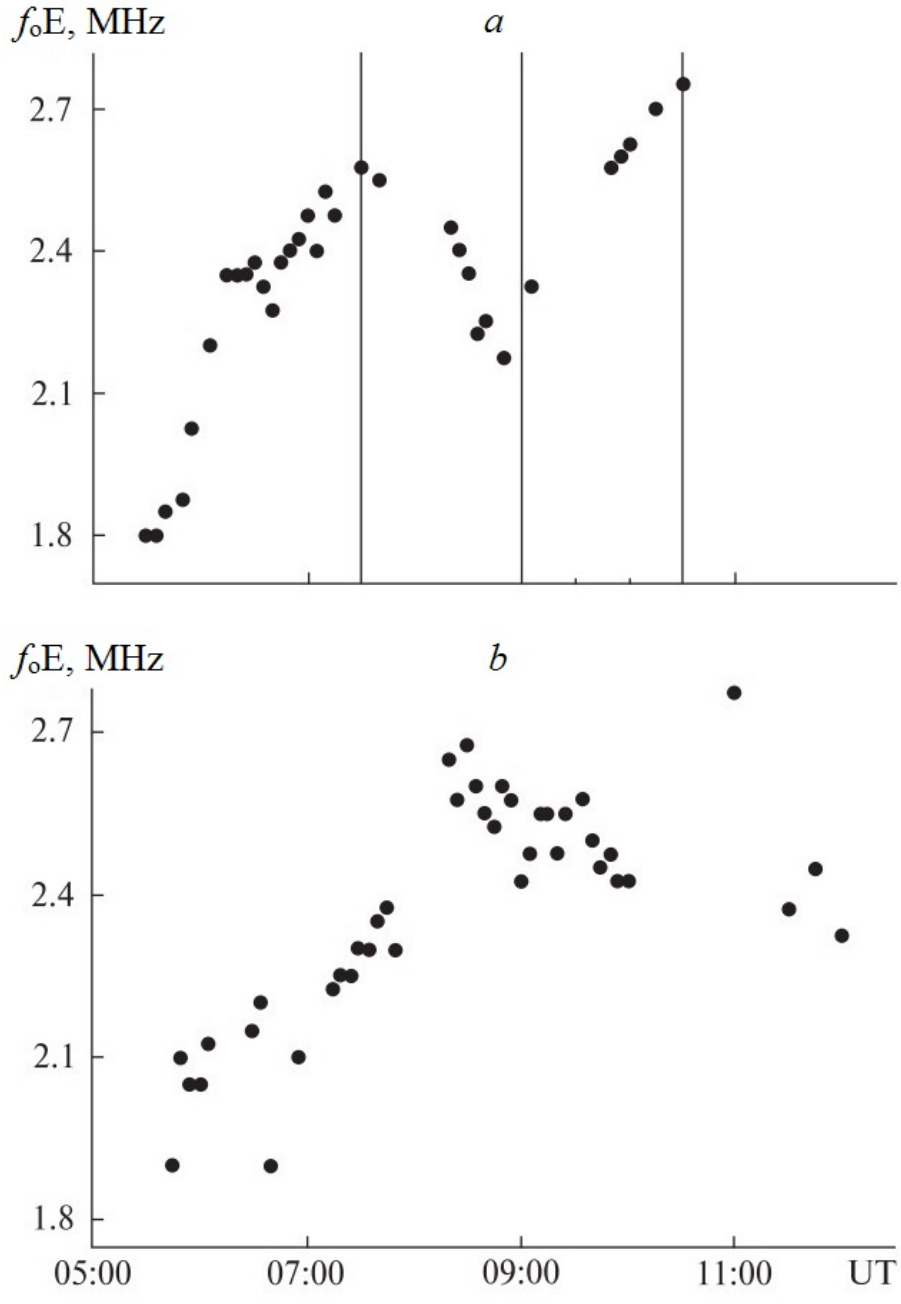

Fig. 3.3. Temporal variations of the critical frequency f_oE on the day of the solar eclipse on January 4, 2011 (*a*) and on the reference day January 5, 2011 (*b*)

3.2.2. Temporal Variations in Effective Heights

Fig. 3.4 shows the temporal variations in the effective heights near the maximum ionization of the F2-layer on the day of the SE on January 4, 2011 and on the reference day January 5, 2011.

The figure shows that as the solar disk is covered, the effective height $h'(f_o\text{F2})$, the value of which was approximately 350 km before the beginning of the SE, increased to almost 420 km at the time of the main phase of the SE (08:59). The rapid increase of $h'(f_o\text{F2})$ occurred from 07:35 to 07:50. During the period from 07:50 to 08:05 the value of the minimum effective height decreased slightly and was 382–387 km during the main phase of the SE.

From 09:45 to 10:30 (i.e. after the end of the eclipse) there was a decrease in the values of $h'(f_o\text{F2})$ to the level corresponding to undisturbed conditions. Note that on the reference day January 5, 2011, the minimum effective height underwent insignificant changes (average $h'(f_o\text{F2}) \approx 365 \pm 15$ km).

3.2.3. Temporal Variations in Reflection Height

Temporal variations in the height h_r(F2) are presented in Fig. 3.5. Since F1-layer was not registered, F2-layer can be approximated by a parabolic layer. The values of the height h_r(F2) are approximately equal to the effective height of the maximum electron density of the layer. Recall that the height h_r(F2) is from the equation $h_r = h'(f_r)$, where $f_r = 0.834 \cdot f_o\text{F2}$.

Consider first the reference day January 5, 2011. The height h_r decreased from 05:30 to 06:30, and it increased in the time interval 06:30–07:45. From 07:45 to 09:25, there was a gradual decrease in h_r(F2). Next, by about 11:45, there was an increase in h_r. In addition to such regular changes in $h_r(t)$, there were fluctuations. Their relative value reached 4%.

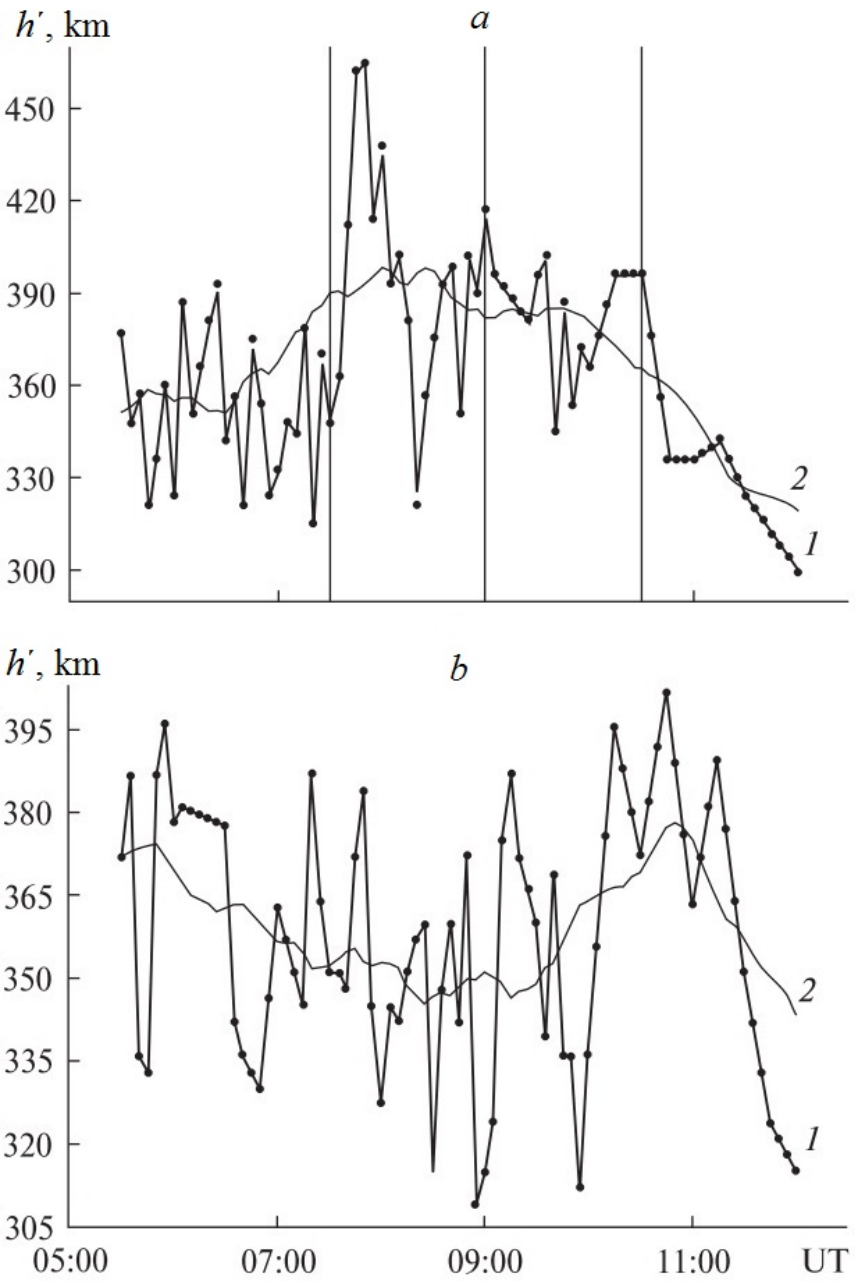

Fig. 3.4. Temporal variations of the effective height h' of reflection near the maximum of the F2- layer ionization: *a* – on the day of the eclipse – January 4, 2011 (1 – initial dependence, 2 – smoothed by the moving average on the time interval of 90 min), *b* – the same but for the reference day January 5, 2011

On January 4, 2011 before the beginning of the SE, there was a decrease in h_r(F2) and its value before the eclipse (07:30) was about 230 km. In the period from 07:30 to 08:30, there is a tendency to increase the h_r, which is typical for nighttime.

From 08:30 until the end of the SE (10:30), the average value of h_r(F2) was about

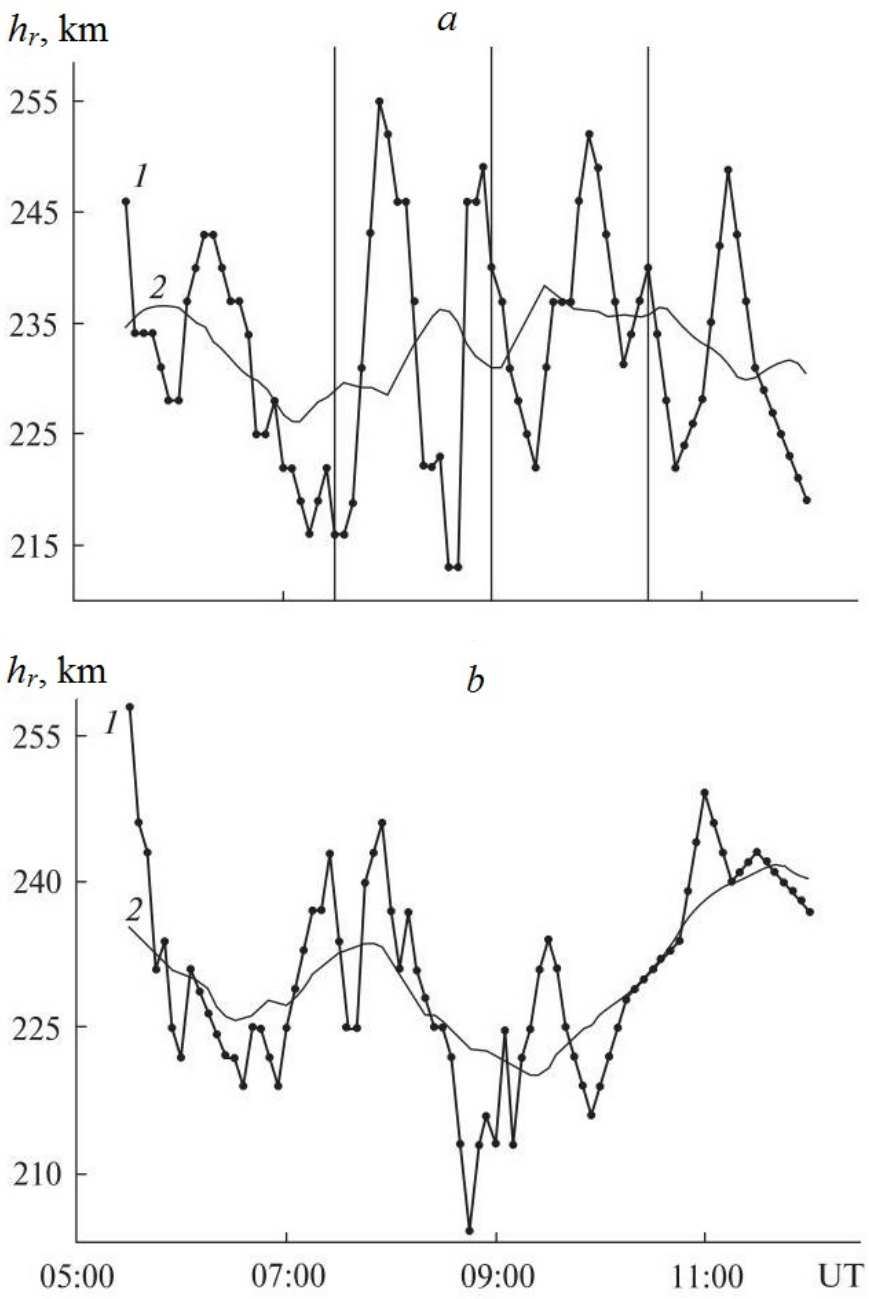

Fig. 3.5. Temporal variations in the reflection height h_r near the maximum ionization of the F2-layer: *a* – on the day of the eclipse January 4, 2011 (1 – initial dependence, 2 – ones smoothed by the moving average on a time interval of 90 min), *b* – the same but on the reference day January 5, 2011

237 km, i.e. the value of height increased by almost 10 km. After 11:20, the h_r values were closer to the values of this parameter preceding the eclipse. The main difference between the temporal variations on January 4 and 5 was that on the day of the SE, there were strong fluctuations in h_r. The amplitude of fluctuations reached 21 km, or 9%. The period of oscillations was close to 60 min.

At 13:15, the height h_r(F2) was approximately 230 km which corresponds to the undisturbed ionosphere.

Thus, an increase in h_r by 10 km indicates the effect of SE on the parameters of the middle ionosphere. The error of the height estimation from the ionogram is 3 km.

3.2.4. Temporal Variations of the Electron Density in the Maximum of Ionization

The dependences of the electron density in the maximum of ionization $N(t)$ on the day of the SE January 4, 2011 and on the reference day January 5, 2011 are shown in Fig. 3.6. The density values are derived from the values of the critical frequencies measured by the ionosonde. Immediately after the onset of SE, there was a decrease in the electron density from $4.0 \cdot 10^{11}$ to $2.1 \cdot 10^{11}$ m^{-3}. The minimum value of the density N_{min} was observed around 09:15, i.e. 16 min after the onset of the main phase of the SE.

The maximum value of the density N_{max} is equal to $1.9 \cdot 10^{11}$ m^{-3}. After the main phase of the eclipse, the electron density increased and by the end of the eclipse it reached values of about $4 \cdot 10^{11}$–$5 \cdot 10^{11}$ m^{-3}.

On the reference day, January 5, 2011, the electron density increased from 05:30 to 08:10. In the time interval 08:10–09:45, the N decreased. From 09:45, there was a gradual increase in the density.

Thus, the temporal variations of the N on the day of the solar eclipse and on the reference day differed significantly.

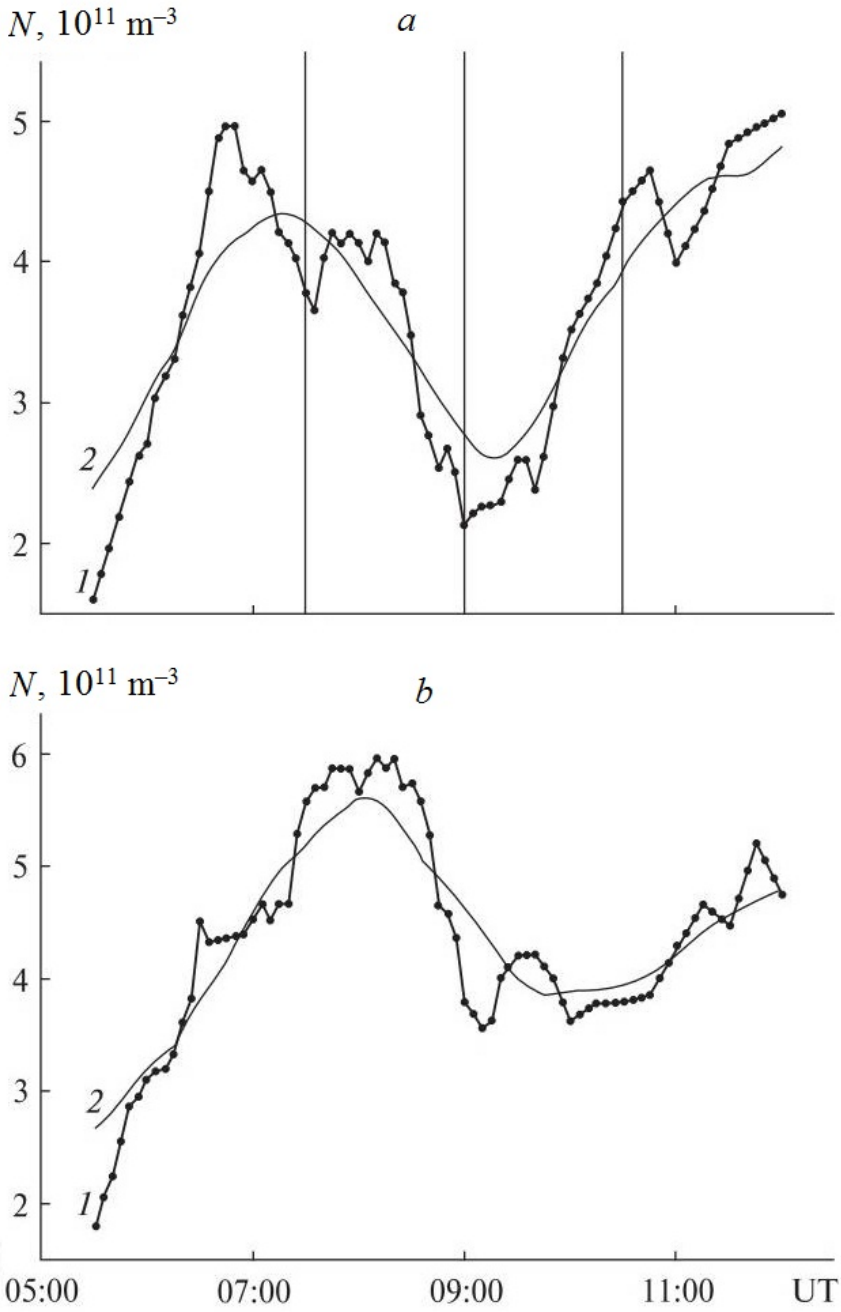

Fig. 3.6. Temporal variations of the electron density in the maximum of ionization of the F2-layer: *a* – on the day of the SE January 4, 2011 (1 – initial dependence, 2 – smoothed by the moving average on the time interval of 90 min), b – the same but on the reference day January 5, 2011

3.3. Wave Disturbances

As shown by spectral analysis, the eclipse was accompanied by an increase in the amplitude of quasi-periodic oscillations of f_oF2 by approximately 0.2 and 0.4 MHz with a period of 30 and 60 min, respectively. The relative amplitude of the oscillations of the electron density δ_{Na} was 8 and 16%. Quasi-periodic variations intensified approximately 1 hour before the onset of SE. The duration of variations with $T \approx 60$ min was about 5–6 h, with $T \approx 30$ min was about 3 h.

On the reference day, f_oF2 fluctuations were weak, at least in the time interval from 07:30 to 08:50. The average amplitude was 0.1–0.2 MHz, i.e. it was about 2 times smaller. At the same time, $\delta_{Na} \approx 3.5$–7%. The period of predominant oscillations varied within 50–90 min.

The difference in the periods and amplitudes of oscillations on the day of the solar eclipse and the reference day suggests that it was the SE that caused the amplification of the oscillations of the ionosphere parameters. The increase in wave activity during the SE period is also evidenced by quasi-periodic variations in height h_r with a period of about 60 min. The relative amplitude of these variations reached 9%.

The nature of the oscillations in the ionosphere is most likely related to the generation of waves in the neutral atmosphere as a result of cooling of atmospheric gas and supersonic motion of the shadow region. Waves in the neutral atmosphere modulated the electron density in the ionosphere, which was observed by the VS method.

The values of the periods and amplitudes of quasi-periodic oscillations indicate that the solar eclipse was accompanied by the generation of internal gravitational waves (IGW).

3.4. Discussion of Observation Results

3.4.1. Variations in Ionogram Parameters

Analysis of ionograms obtained before, during and after the solar eclipse showed that there were significant variations in all their parameters. Of course, the presence of the E_s-layer made it difficult to observe the effects caused by the eclipse. However, a decrease in the critical frequencies of the F2-layer, which reached 1.9 MHz, was confidently observed. After the eclipse, the critical frequencies practically returned to their values that preceded the SE.

The minimum values of f_oF2 were recorded with a delay relative to the time of the main phase of the eclipse, with an accuracy of σ close to 16 minutes. Here σ is an error in counting time at the value of the discrete Δt. We know that $\sigma = \Delta t / \sqrt{12}$. If Δt = 5 min, we have σ ≈ 1.4 min. Thus the delay was 16.0±1.4 min. Simultaneously with the variations of f_oF2, an increase of approximately 70 km of the effective height $h'(f_o\text{F2})$ was observed, and then its decrease by the same value.

As expected, our event which is close to full solar eclipse caused the ionosphere to rearrange first from day to night, and then in the opposite direction.

In addition to those variations, there were quasi-periodic changes in the parameters of ionograms, indicating that the SE was accompanied by an increase in wave activity in the ionosphere.

This behavior of ionograms is quite typical for the periods of SE and generally corresponds to the results of previous observations (see, for example, [144]).

3.4.2. Diffuse Reflections

During the eclipse from 7:30 to 11:30, altitude-frequency characteristics were diffuse in nature. In the whole range of frequencies and heights, there were strong violations of the layered structure of the ionosphere. Most likely, the entire space

between the maximum of E and F2-layers was filled with intense ionospheric irregularities. The reason for their strengthening was apparently hydrodynamic instability in the thermosphere [145].

3.4.3. Variations in Electron Density

Consider in more detail the altitude-temporal variations of the electron density N that accompany the solar eclipse.

Taking into account the processes of producing of electrons and ions, their recombination and the plasma drift in the vertical direction with a velocity V_z for the middle-latitude ionosphere, the continuity equation for N is the following [179]:

$$\frac{\partial N}{\partial t} + \frac{\partial}{\partial z}\left(NV_z\right) = q(t) - L, \tag{3.2}$$

where q – ionization rate, L – electron loss rate.

At the rather low solar activity, the maximum of F2-layer height does not exceed 230–250 km under quiet conditions. If the altitudinal variations in NV_z can be neglected, the relation (3.2) is reduced to the following equation:

$$\frac{dN}{dt} = q(t) - L, \tag{3.3}$$

Where $q(t) = q_0[1 - A(t)]$, $A(t) = S(t)/S_0$ – Sun disk coverage function, S is the area of the shaded part of the Sun's disk, S_0 is the area of the Sun's disk.

Since the characteristic time of this solar eclipse $t_e \approx 90$ min is much longer than the time of recombination processes at altitudes $z \le 250$ km, the relation (3.3) can be roughly replaced by the following:

$$q \approx L. \tag{3.4}$$

At the maximum of the F2-layer, the rate of loss [146]

$$L = \beta N, \tag{3.5}$$

where β – coefficient of loss. Assuming that during a solar eclipse, the coefficient β changes insignificantly, from (3.4) and (3.5) we obtain that at a given height

$$\frac{N}{N_0} = \frac{q}{q_0} = 1 - A \equiv B\,. \tag{3.6}$$

Here $B(t) = 1 - A(t)$, N_0 – value of the density N in the absence of SE. Near the main phase $A_{max} \approx 0.71$, $B_{min} \approx 0.29$. Then, based on (3.6), the calculated value $N_{min}/N_0 = 0.29$ with $\Delta N/N_0 = 1 - N_{min}/N_0 = 0.71$. The value of $N_{min}/N_0 = 0.29$ differs markedly from the experimentally obtained value of 0.48. There are three reasons for the discrepancy. First, at altitudes of 230–250 km, it can no longer be assumed that $V_z = 0$. Second, when a solar eclipse lasted for about 3 hours, the parameters of the neutral atmosphere changed markedly, which caused a change in the coefficient β. Third, the shift of the F2-layer height up during the SE led to a decrease in β.

Consider these reasons in more detail. As shown by synchronous observations by the Kharkiv incoherent scattering radar, during the main phase of the eclipse, in the altitude range of 200–250 km, the drift velocity $V_z(z) \approx$ –50 m/s. Near the maximum of the F2-layer the density $N(z)$ = const; in addition, in a wide range of heights, the drift velocity $V_z(z) \approx$ const. For this reason, in equation (3.2) $\partial(N V_z)/\partial z \approx 0$, i.e. the transfer process could not significantly affect the variations of the density $N(t)$ associated with the eclipse.

It can be shown that variations in the neutral particle density and the coefficient β during the transition period of the day at altitudes of 200–300 km are approximately described by a linear dependence. With

$$\beta(\Delta t) \approx \beta_0 (1 - \frac{\Delta t}{2\tau}),$$

where $\tau \approx 4.5$ hour – characteristic time of transients, Δt – time interval after sunset (beginning of the eclipse). During the main phase of solar eclipse $\Delta t \approx 1.5$ h. Then $\beta(1.5) = 0.83\ \beta_0$.

By reducing the density N, the region of reflection of the radio wave shifts upwards by $\Delta z \approx 10$ km. As a result, β decreases by law

$$\beta(z) = \beta_0 e^{-\Delta z / H},$$

where H is the reduced (geopotential) height of the neutral atmosphere. According to the known international models of the neutral atmosphere, near altitudes 230–240 km (i.e. near the maximum of the F2-layer height on January 4, 2011) $H \approx 45$ km. Then the total decrease in β due to the last two reasons at time $\Delta t \approx 1.5$ hours, given that $\Delta z << H$ is described by the relation:

$$\beta \approx \beta_0 (1 - \frac{\Delta t}{2\tau} - \frac{\Delta z}{H}) \approx 0.61 \beta_0 .$$

In this case, according to (3.5) and (3.6), the calculated value

$$\frac{N_{\min}}{N_0} = \frac{q}{q_0} \frac{\beta_0}{\beta} = B_{\min} \frac{\beta_0}{\beta} \approx 0.49 ,$$

which is very close to the experimentally obtained value (0.48).

Thus, the solar eclipse led not only to a decrease in the electron density N, but also to the ratio decrease of approximately $\Delta t/2\tau \approx 17\%$ of the neutral particle density at heights near the F2-layer.

Based on the altitude dependence of the coefficient β, given, for example, in [147, 148], we can show that in the F2-layer at an altitude of $z = 230$ km $\beta \approx 10^{-3}$ s^{-1}. Thus, the time of the electron density producing $t_N = \beta^{-1} \approx 1000$ s ≈ 16.7 min. The value of the time t_N is close to what was observed experimentally (16.0±1.4 min).

The quadratic law of recombination is valid for the E region. Instead of (3.4), (3.5), we have the following relations:

$$q = \alpha N^2 ,$$

where α – recombination coefficient. In the absence of eclipse, $q_0 = \alpha_0 N_0^2$. Then

$$\frac{N}{N_0} = \sqrt{\frac{\alpha_0}{\alpha} \frac{q}{q_0}} = \sqrt{\frac{\alpha_0}{\alpha} B(t)} .$$

With $B_{\min} = 0.29$ and $\alpha \approx \alpha_0$ we have $N_{\min}/N_0 \approx 0.54$, and $fE_{\min}/fE \approx 0.73$. The relative change in f_oE should be 27%. From ionograms, it was found that the relative change was close to 16%, and $N_{\min}/N_0 \approx 0.70$. Thus, experimental $N_{\min}/N_0$ exceeded the estimated value by 16%. This difference may be due to the mid-latitude precipitation of electrons from the magnetosphere [149].

Thus, the spatial-temporal variations of the density N during the solar eclipse generally correspond to the existing theories on physical chemical processes in the middle ionosphere (altitudes of 100–250 km).

3.5. General Information About the Solar Eclipse on March 20, 2015

There was an increase of more than an order of magnitude in the density of solar wind particles n_{sw} (Fig. 3.7) during March 16 and 17, 2015. The solar wind speed V_{sw} increased by 1.5 times in the period from March 17 to March 22. On March 17, the solar wind temperature T_{sw} increased by an order of magnitude. The increase in the density and the temperature led to an increase in dynamic pressure p_{sw} of the solar wind. The B_z-component of the interplanetary magnetic field returned to the south, i.e. there was a situation when $B_z < 0$. The minimum value of B_z was –15 nT.

A magnetic storm began, which was accompanied by an increase of 1–2 orders of magnitude in the energy ε_A coming into the magnetosphere from the solar wind as well as by significant changes in the indices AE, K_p and D_{st}. The geomagnetic indexes reached 1600 nT, 8, and –230 nT, respectively.

This storm, which was called St. Patrick's Storm, was the strongest in the 24th cycle of solar activity. The storm, gradually subsiding, lasted for a week. On March 20 and 21, the total index $\sum K_p$ was 27 and 22, respectively. In the afternoon of March 20, there was a relaxing ionospheric storm, or rather its negative phase. The values of the critical frequency f_oF2 were approximately 1–2 MHz lower than on the reference day March 21.

To study the effects of SE on March 20, 2015, data from 10 European ionosondes were used, which are available for free access on the Internet [http://umlcar.uml.edu/stationlist.html], as well as the ionosonde near Kharkiv (Gaidary village). The list of the ionosondes is presented in Table. 3.1 (hereinafter the names of ionosondes will correspond to the names of settlements near which they are located).

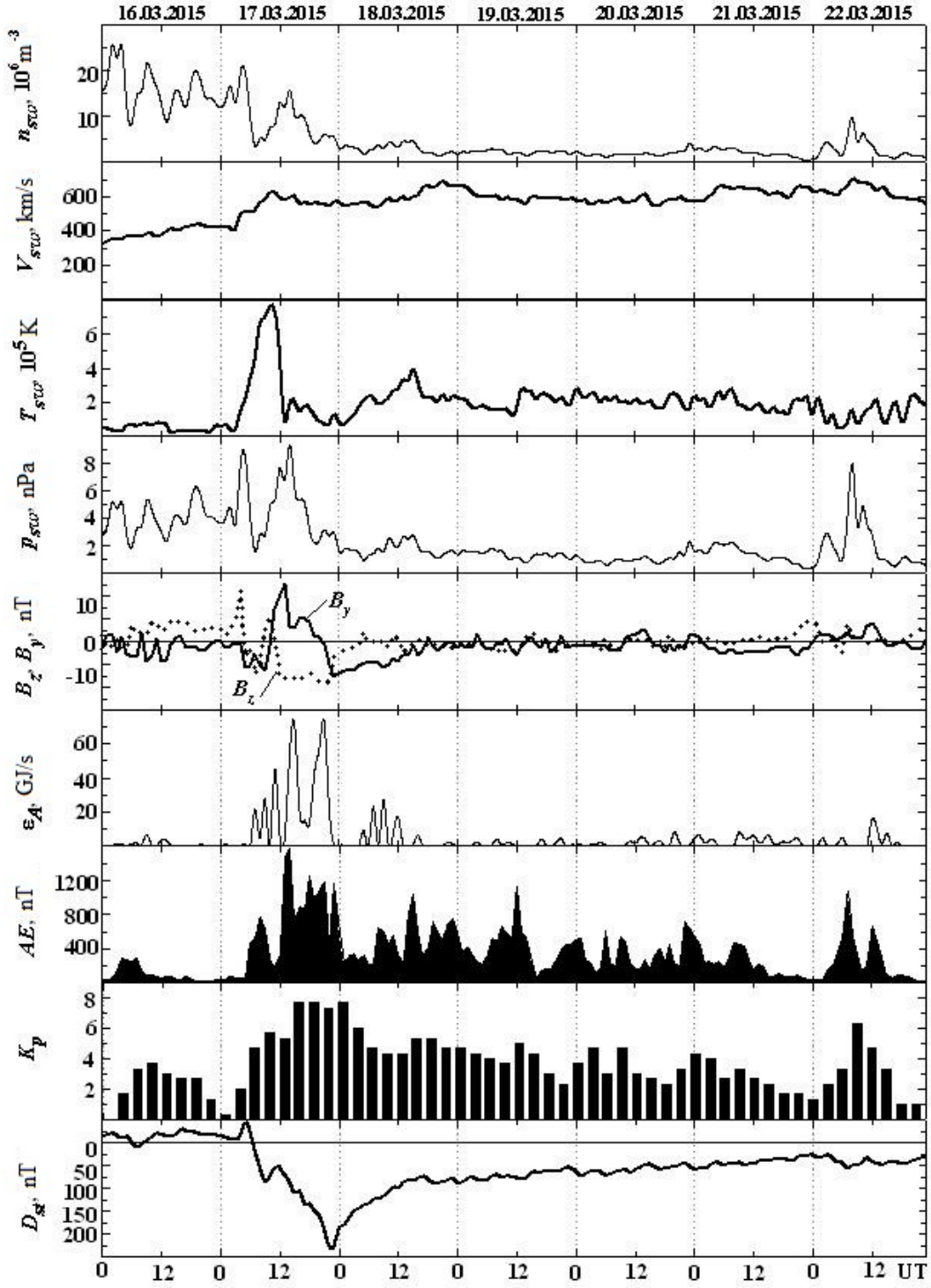

Fig. 3.7. Temporal variations of solar wind parameters during March 16–22, 2015: particle density n_{sw}, radial speed V_{sw}, temperature T_{sw}, and dynamic pressure p_{sw}; B_z and B_y-components of the interplanetary magnetic field (provided by ACE Satellite); ε_A – Akasofu function; indeces of geomagnetic activity AE (provided by WDC Kyoto), K_p (provided by Air Force Weather Agency) and D_{st} (WDC-C2 for Geomagnetism Kyoto University)

Table 3.1. Geographic coordinates of ionosondes and general information about the position of the Sun and the solar eclipse

Ionosonde	Latitude φ	Longitude λ	Time of occurrence of the event	The SE phase	Disk cover	Angular altitude of the Sun above the horizon	Azimuth of the Sun	Discreteness of ionogram registration March 20/21, min
“Tromsö”	69.6°N	19.2°E	09:04:52 10:08:49 11:13:19	0.95	0.95	17.9° 19.8° 20.1°	152.1° 168.8° 186.0°	15/15
“Fairford”	51.7°N	1.5°W	08:24:10 09:29:54 10:39:40	0.88	0.86	19.3° 27.7° 34.5°	116.8° 132.3° 151.1°	15/15
“Dourbes”	50.1°N	4.6°E	08:26:25 09:33:42 10:44:48	0.82	0.78	23.8° 32.0° 37.9°	122.3° 138.9° 159.4°	0.5/0.5
“Juliusruh”	54.6°N	13.4°E	08:41:34 09:49:53 11:00:29	0.82	0.78	26.9° 32.5° 35.1°	136.2° 154.8° 175.8°	15/15
“Pruhonice”	50.0°N	14.6°E	08:36:41 09:45:36 10:57:10	0.74	0.68	30.1° 36.7° 39.7°	134.4° 153.5° 176.1°	3/15
“Rocuetes”	40.8°N	0.5°E	08:08:53 09:13:58 10:24:21	0.70	0.64	22.6° 33.5° 43.0°	111.5° 125.3° 144.2°	5/5
“El Arinosillo”	37.1°N	6.7°W	07:58:27 09:00:12 10:07:43	0.69	0.62	16.5° 28.1° 39.6°	103.2° 114.2° 129.2	15/15
“Troitsk” (Moscow)	55.5°N	37.3°E	09:12:25 10:19:38 11:25:57	0.65	0.57	34.1° 33.7° 30.2°	172.2° 192.4° 211.6°	3/15
“San Vito”	40.6°N	17.8°E	08:30:25 09:37:23 10:47:23	0.54	0.45	37.4° 45.4° 49.1°	131.5° 151.2° 176.6°	15/15
“Gaidary” (Kharkiv)	49.6°N	36.3°E	09:09:25 10:15:52 11:21:33	0.54	0.44	39.6° 39.6° 35.8°	169.3° 190.9° 211.2°	5/5
“Athens”	38.0°N	23.5°E	08:39:15 09:43:13 10:49:11	0.43	0.32	43.6° 50.1° 51.6°	138.6° 160.1° 186.3°	2/5

Note: the first, second, and third points in time correspond to the beginning, maximum phase, and end of the SE

The Table 3.1 shows that the eclipse took place in the morning and afternoon, the angular height of the Sun above the horizon varied from 17° to 51°. The

maximum phase and coverage area varied between 0.43–0.95 and 0.32–0.95, respectively.

The measurement error of the frequency and effective height for standard ionosondes is 25 or 50 kHz and 5 km, respectively.

3.6. Ionospheric Parameters Variations during the Solar Eclipse on March 20, 2015 over Europe

3.6.1. Temporal Variations in Critical Frequency f_oF2

The temporal dependencies of the critical frequency f_oF2 as well as its smoothed moving average in the interval of 120 min values for 11 European ionosondes are shown in Fig. 3.8 and Fig. 3.9.

These figures show that on March 20, 2015, the smoothed critical frequency dependencies $\overline{f_o\mathrm{F2}}(t)$ decreased near the maximum phase of the solar eclipse. The dashed line indicates the expected variations of f_oF2(t) in the absence of solar eclipse. The vertical lines here and below show the moments of time of beginning, maximum phase, and end of the SE.

For the “Gaidary” ionosonde, the frequency decrease is masked by the positive disturbance observed in the time interval 10:00–10:50. In the absence of this disturbance, the value of $f_o\mathrm{F2}_{\min}$ would be 7.8 MHz, and without solar eclipse $f_o\mathrm{F2}_0 \approx 8.3$ MHz. These values were further used in estimating the ratio $N_{\min}/N_0$ (Table 3.2). The minimum values of $\overline{f_o\mathrm{F2}}(t)$ were observed with a delay time $\Delta t \approx$ 5–30 min after the onset of the maximum eclipse phase (see Table 3.2).

Note that similar reducing of $\overline{f_o\mathrm{F2}}(t)$ on the reference day March 21, 2015 were absent.

In addition to the regular behavior of f_oF2(t), quasi-periodic variations of the critical frequency took place.

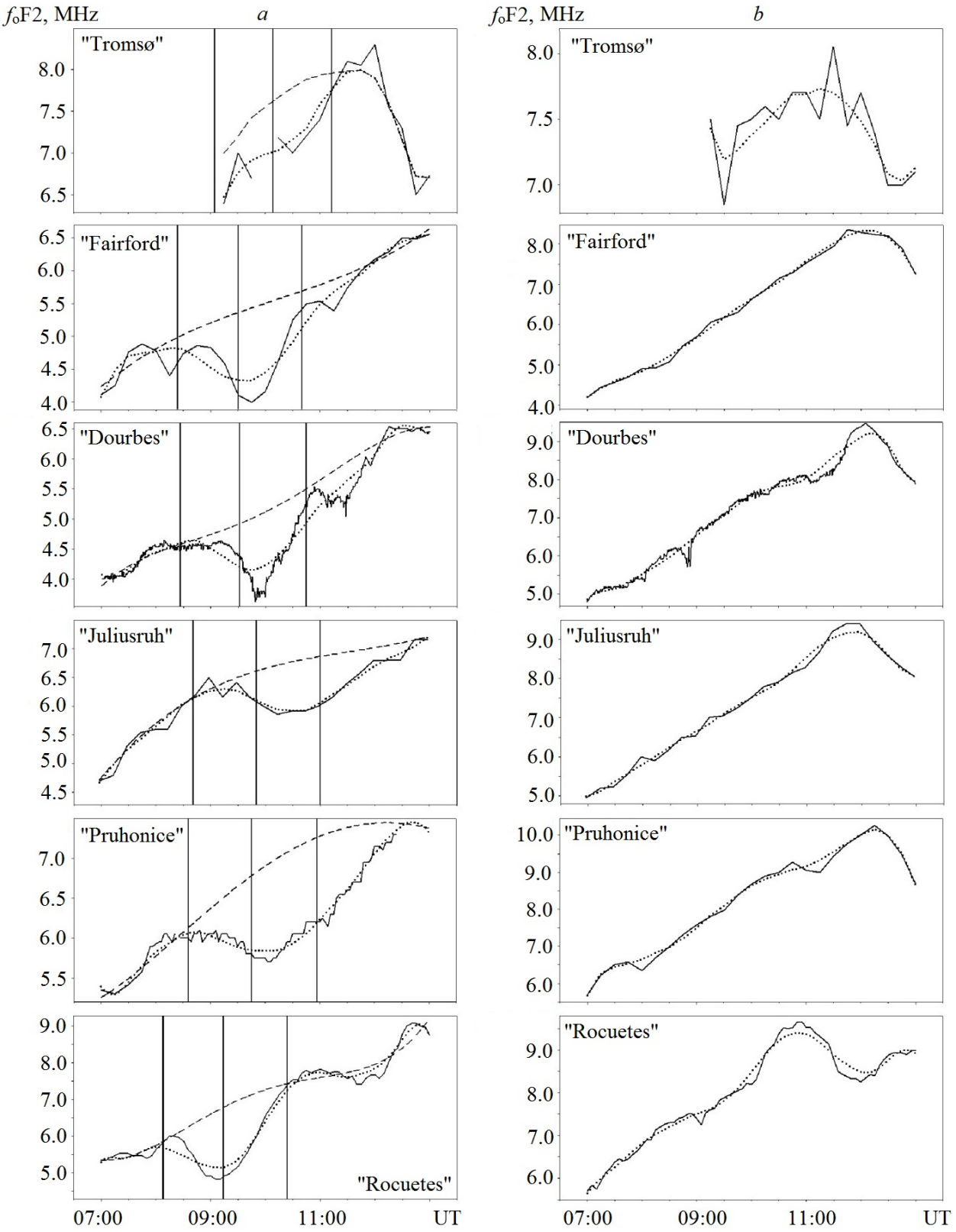

Fig. 3.8. Temporal variations of the f_oF2 (solid line) and the $\overline{f_o F2}(t)$ (dotted line) for ionosondes: *a* – March 20, *b* – March 21, 2015.

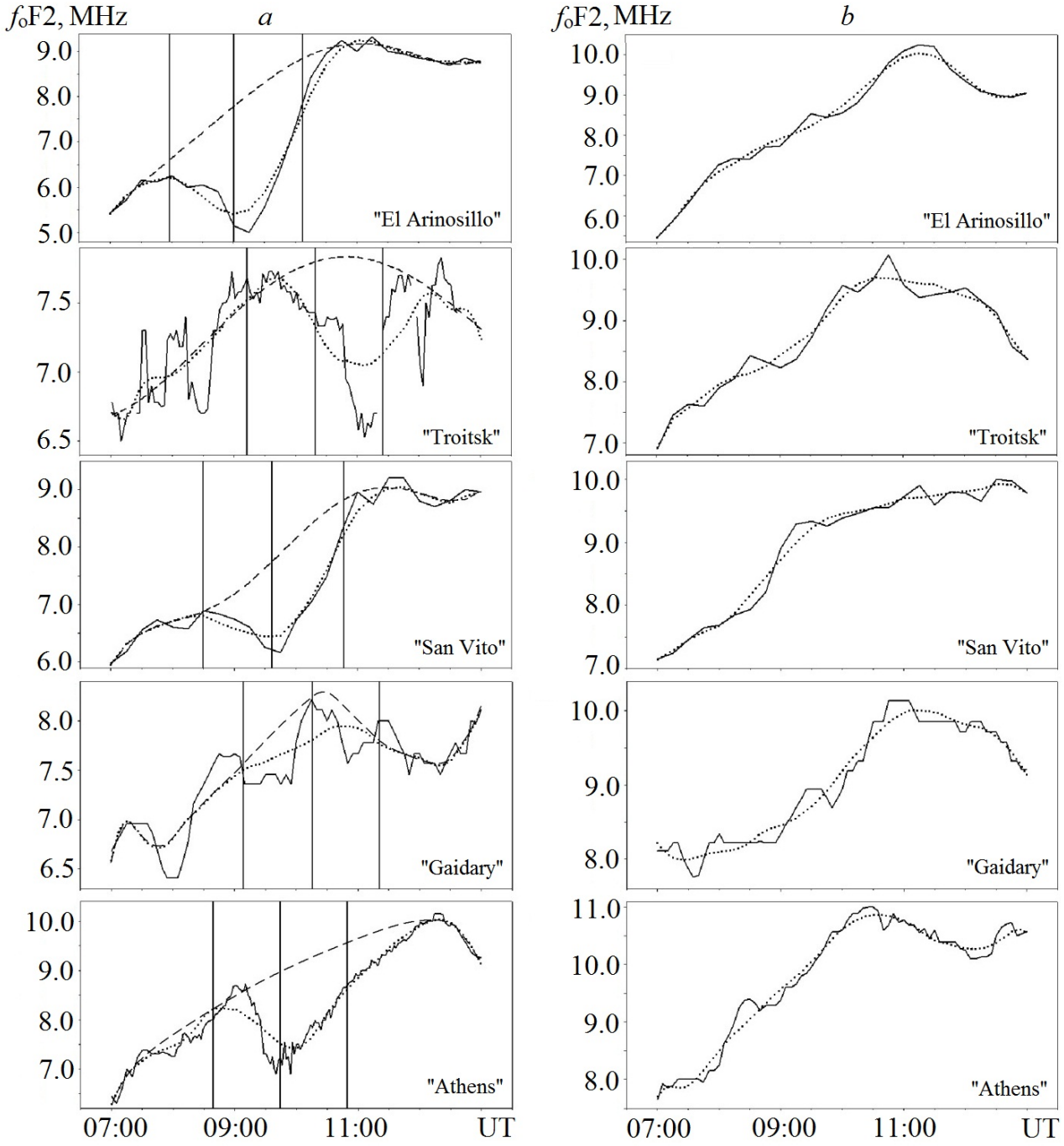

Fig. 3.9. Temporal variations of the f_oF2 (solid line) and the $\overline{f_o F2}(t)$ (dotted line) for ionosondes: *a* – March 20, 2015; *b* – March 21, 2015.

3.6.2. Temporal Variations in Reflection Height

Temporal variations in reflection height h_r for March 20 and 21, 2015 are shown in Figs 3.10 and 3.11. The dashed line indicates the expected variations of $h_r(t)$ in the absence of solar eclipse.

Table 3.2. Variations of the main parameters of the observed ionograms, parameter N_{min}/N_0 and calculated parameter $(N_{min}/N_0)_{cal}$. f_oF2_0 and f_oF2_{min} are actual and expected values of f_oF2 on the reference day and the day of eclipse near the maximum phase of the solar eclipse

Ionosonde	f_oF2_0, MHz	f_oF2_{min}, MHz	$\frac{N_{min}}{N_0}$	$\left(\frac{N_{min}}{N_0}\right)_{cal}$	Δh_{rmax}, km	Δt, min	β_0/β
“Tromsø”	8	7.0	0.77	0.05	40	30	15.4
“Fairford”	5.3	4.1	0.60	0.14	50	15	4.3
“Dourbes”	5.3	4.25	0.49	0.22	22	15	2.2
“Juliusruh”	6.8	5.9	0.75	0.22	25	30	3.4
“Pruhonice”	6.7	5.8	0.75	0.32	25	30	2.3
“Rocuetes”	6.5	4.8	0.55	0.36	75	5–10	1.5
“El Arinosillo”	7.9	5.0	0.40	0.38	70	15	1.05
“Troitsk” (Moscow)	7.8	6.9	0.78	0.43	10	30	1.8
San Vito	8.2	6.2	0.57	0.55	50	5–10	1.04
“Gaidary” (Kharkiv)	8.3	7.8	0.88	0.56	25	15	1.6
“Athens”	8.7	7.2	0.62	0.68	15	20	1

From these figures, it can be seen that for all ionosondes the value of height h_r during the solar eclipse exceeded by 40–70 km the value of h_r on the reference day, and it also exceeded by 25–50 km the value of h_r, which would have been obreved in the absence of the eclipse. In addition to the regular increase in h_r observed during the eclipse, the height of the h_r experienced quasi-periodic variations with an amplitude of 15–30 km and a quasi-period of 45–90 min. The values of amplitudes δh_{ra} and quasi-periods T_h on the day of the eclipse and on the reference day differed markedly (Table 3.3).

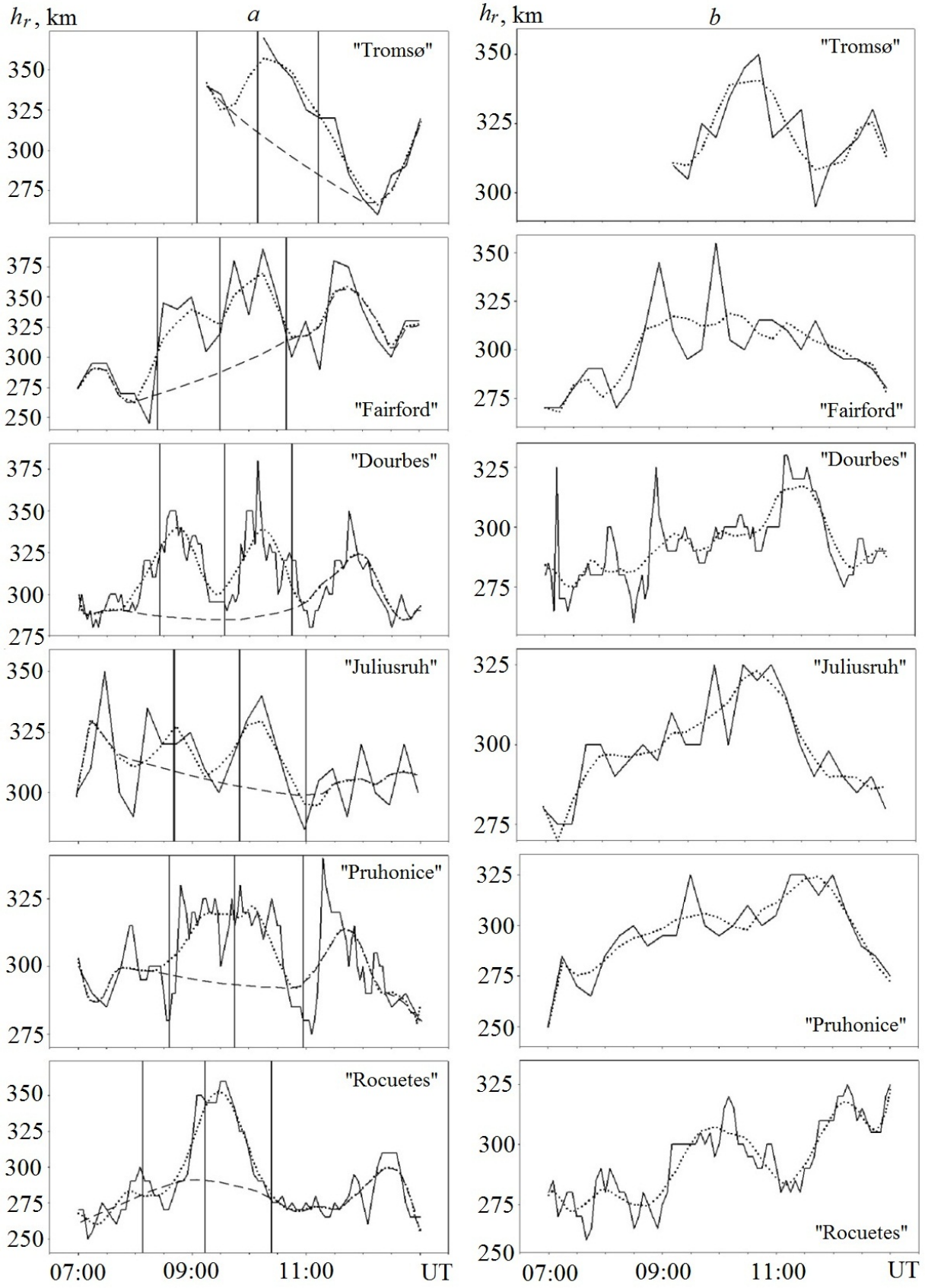

Fig. 3.10. Temporal variations of the height h_r (solid line) and smoothed moving average $\overline{h}_r$ (dotted line) for ionosondes: *a* – March 20, *b* – March 21, 2015

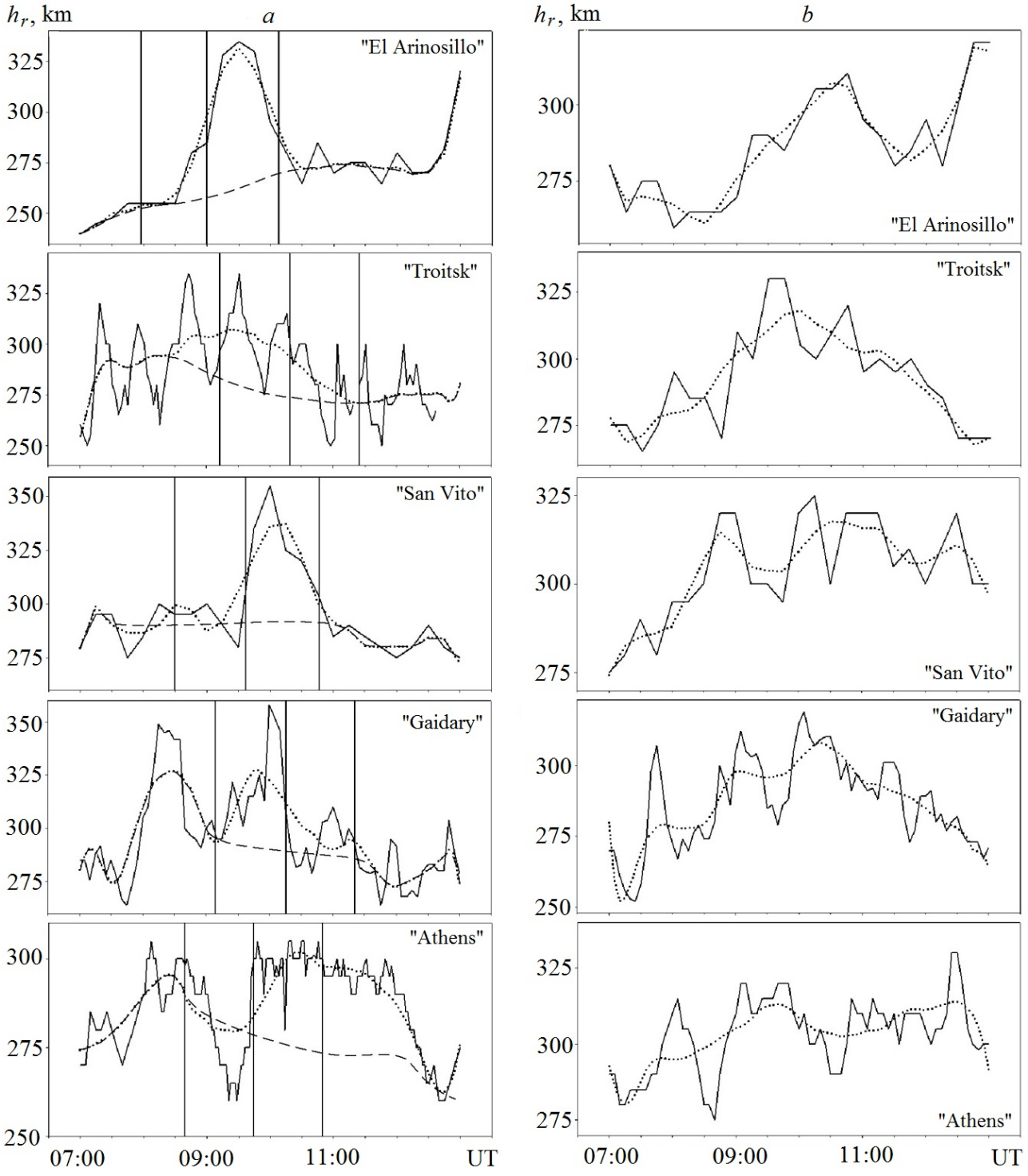

Fig. 3.11. Temporal variations of the height h_r (solid line) and smoothed moving average $\overline{h}_r$ (dotted line) for European ionosondes: *a* – March 20, *b* – March 21, 2015

Table 3.3. The main parameters of quasi-periodic disturbances in the ionosphere

Ionosonde	March 20, 2015				March 21, 2015			
	T_f, min	T_z, min	δf_a, MHz	δh_{ra}, km	T_f, min	T_z, min	δf_a, MHz	δh_{ra}, km
"Tromsø"	30–40	45–60	0.2	10–15	60	60	0.15–0.2	10
"Fairford"	80–100	30–45	0.3	25–30	75	60	0.1	15–20
"Dourbes"	80–100	50–60	0.2–0.4	10–25	60	30–40	0.15–0.20	10–15
"Juliusruh"	50–70	45–60	0.15–0.20	10–15	60–80	30–60	0.10–0.20	10
"Pruhonice"	80–90	40–60	0.15	10–20	60–120	45–60	0.10–0.20	10
"Rocuetes"	60–90	30–60	0.25–0.35	10–15	60	45–60	0.2	10
"El Arinosillo"	60–90	30–45	0.3–0.4	5–10	90	30–45	0.15–0.20	5–7
"Troitsk" (Moscow)	50–60	45–60	0.4	20–25	50–60	45–60	0.2–0.3	15
"San Vito"	40–60	45–75	0.2	10–20	45–75	45–60	0.15–0.20	5–10
"Gaidary" (Kharkiv)	80–100	60	0.4	20–25	60–70	30–60	0.2	10–15
"Athens"	60	45–60	0.4–0.6	10–15	60	40–60	0.15–0.20	5–10

3.7. Wave Perturbations during the Solar Eclipse on March 20, 2015 over Europe

3.7.1. Temporal Variations of Critical Frequency Changes

Temporal variations in the critical frequency changes δf_oF2 on March 20 and 21, 2015 are shown in Figs 3.12–3.14.

It can be seen that the nature of the quasi-periodic variations on the day of the eclipse and on the reference day differed markedly. On the day of the eclipse, the temporal variations were more regular, quasi-periodic variations were more clearly observed, and the amplitude δf_a of these variations was 2–3 times larger than on the

reference day (Table 3.3). In addition, the periods of quasi-periodic oscillations T_f on the day of the eclipse and on the reference day differed markedly (see also Table 3.3).

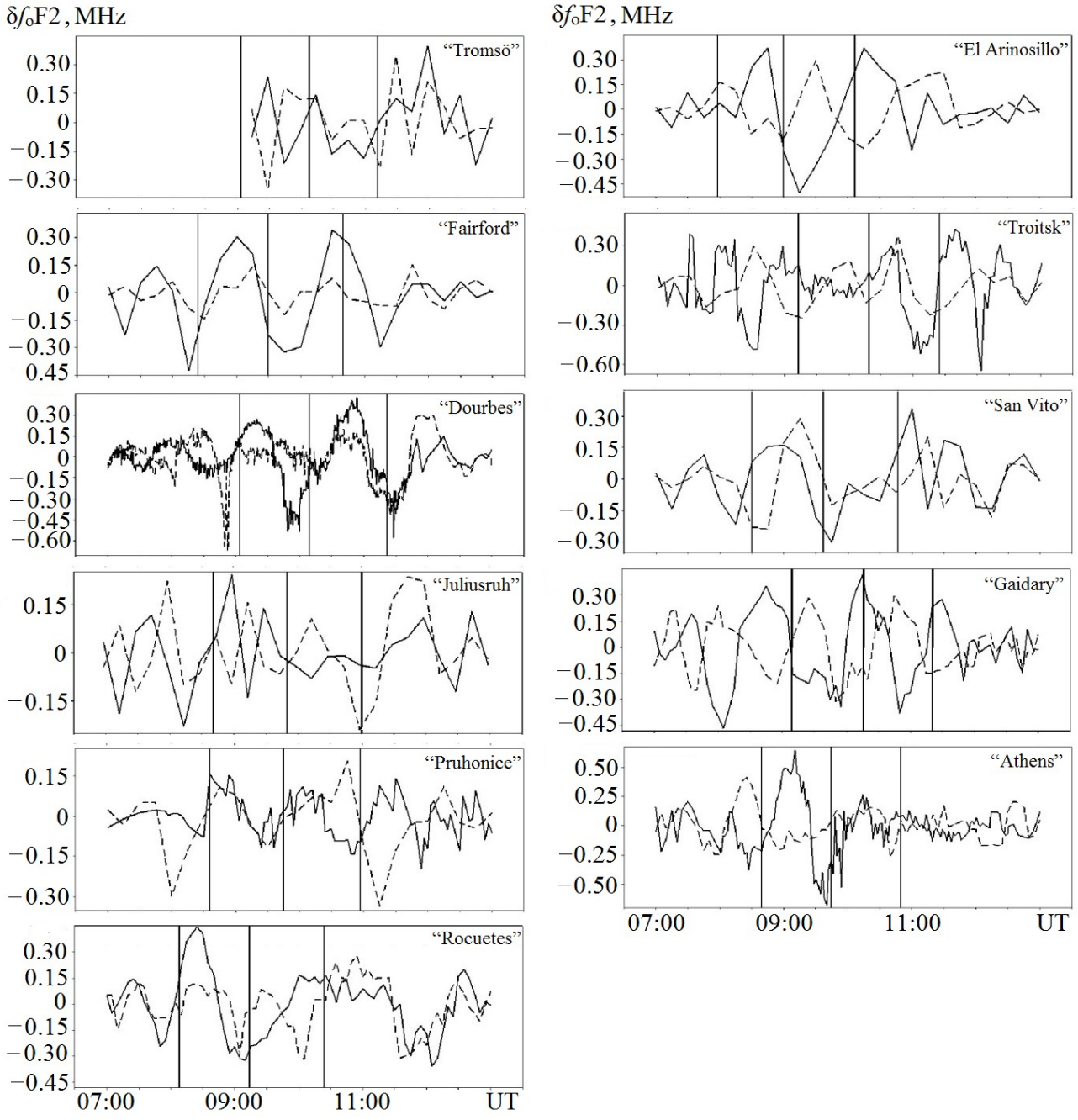

Fig. 3.12. Temporal variations of δf_oF2 on March 20, 2015 (solid line) and March 21, 2015 (dashed line) for European ionosondes

Temporal variations in reflection height changes δh_r for March 20 and 21, 2015 are shown in Fig. 3.12. It can be seen that the amplitude δh_r on the day of the eclipse

and on the reference day differed markedly. The amplitude of δh_r was on average 1.5–2 times larger on the day of the eclipse than on the refrerence day (see also Table 3.2). The values of the quasi-period T_z on the day of the solar eclipse and March 21, 2015 differed slightly (see also Table 3.3). The values of quasi-periods calculated from the variations of δf_oF2 and δh_r were close (see Table 3.3).

3.7.2. Temporal Variations in Reflection Height Changes

3.7.3. Results of System Spectral Analysis

Spectral analysis of $\delta f_oF2(t)$ dependencies. Examples of the results of system spectral analysis for $\delta f_o\text{F2}(t)$ variations for San Vito and Pruhonice ionosondes are shown in Figs. 3.13 and 3.14, respectively. It can be seen that during the solar eclipse, the spectral composition and amplitude of oscillations changed significantly. For the San Vito ionosonde, the oscillation with $T_f \approx 50$–60 min was changed by the oscillation with $T_f \approx 75$–120 min (see Fig. 3.13).

The low frequency of ionogram registration (1 ionogram per 15 min), unfortunately, did not allow estimating the T_f period more accurately. For the Pruhonice ionosonde, the interval between ionogram registrations was 3 min, which provided better results of spectral analysis (see Fig. 3.14). From Fig. 3.14, it is clear that during the SE the oscillations with $T_f \approx 80$–90 min increased. The main results of spectral analysis are presented in Tables 3.2 and 3.3.

Comparison of amplitudes and periods of oscillations for March 20 and 21, 2015 showed that on the day of the SE, they were significantly different from those that were on the reference day.

Spectral analysis of $\delta h_p(t)$ variations. Examples of the results of system spectral analysis of $\delta h_r(t)$ variations for ionosondes “San Vito” and “Trinity” are shown in Figs 3.15 and 3.16, respectively. From Fig. 3.15, it is seen that the solar eclipse was accompanied by noticeable changes in the spectral composition and amplitudes of

oscillations, during the SE the oscillations with $T_z \approx 45–75$ min intensified, and their amplitudes doubled.

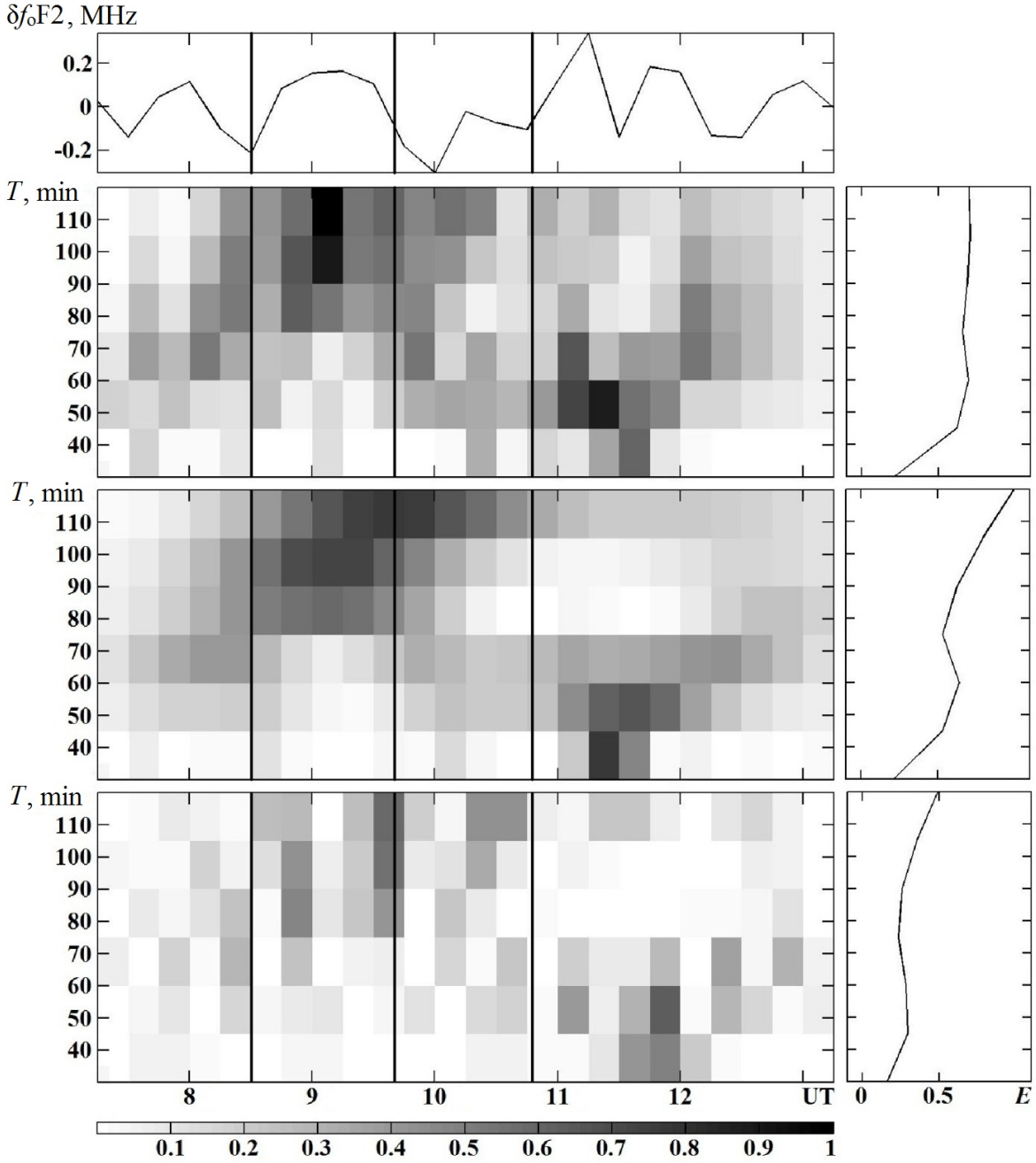

Fig. 3.13. Results of the system spectral analysis of the δf_oF2 changes for the "San Vito" ionosonde on March 20, 2015. From top to down panels, the following parameners shown: δf_oF2(t); WFT spectrogram; AFT spectrogram, and WT spectrogram. The energy diagrams of the corresponding spectrograms are shown on the right panels

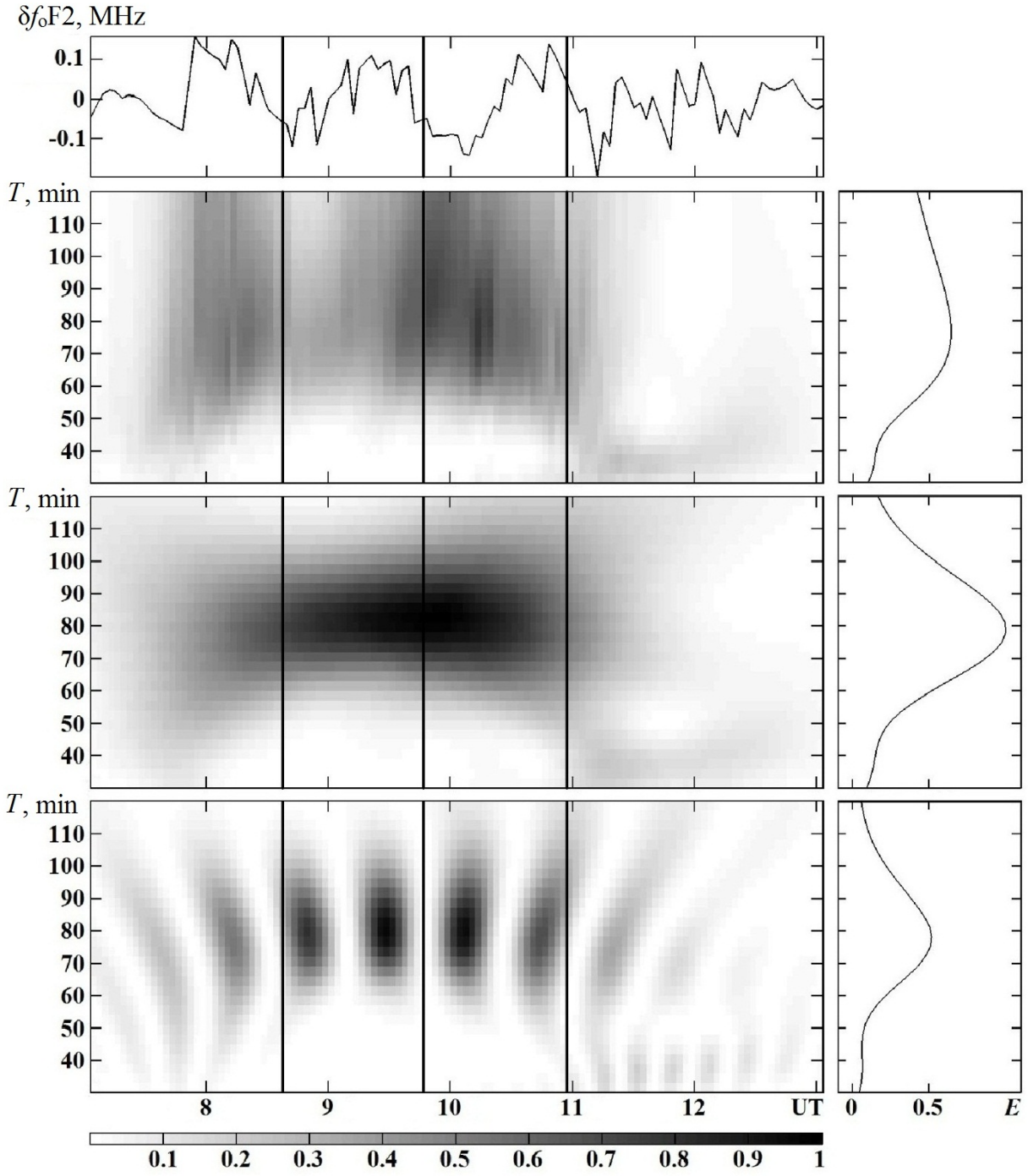

Fig. 3.14. Results of the system spectral analysis of the δf_oF2 changes for the "Pruhonice" ionosonde on March 20, 2015. From top to down panels, the following parameners shown: δf_oF2(t); WFT spectrogram; AFT spectrogram, and WT spectrogram. The energy diagrams of the corresponding spectrograms are shown on the right panels

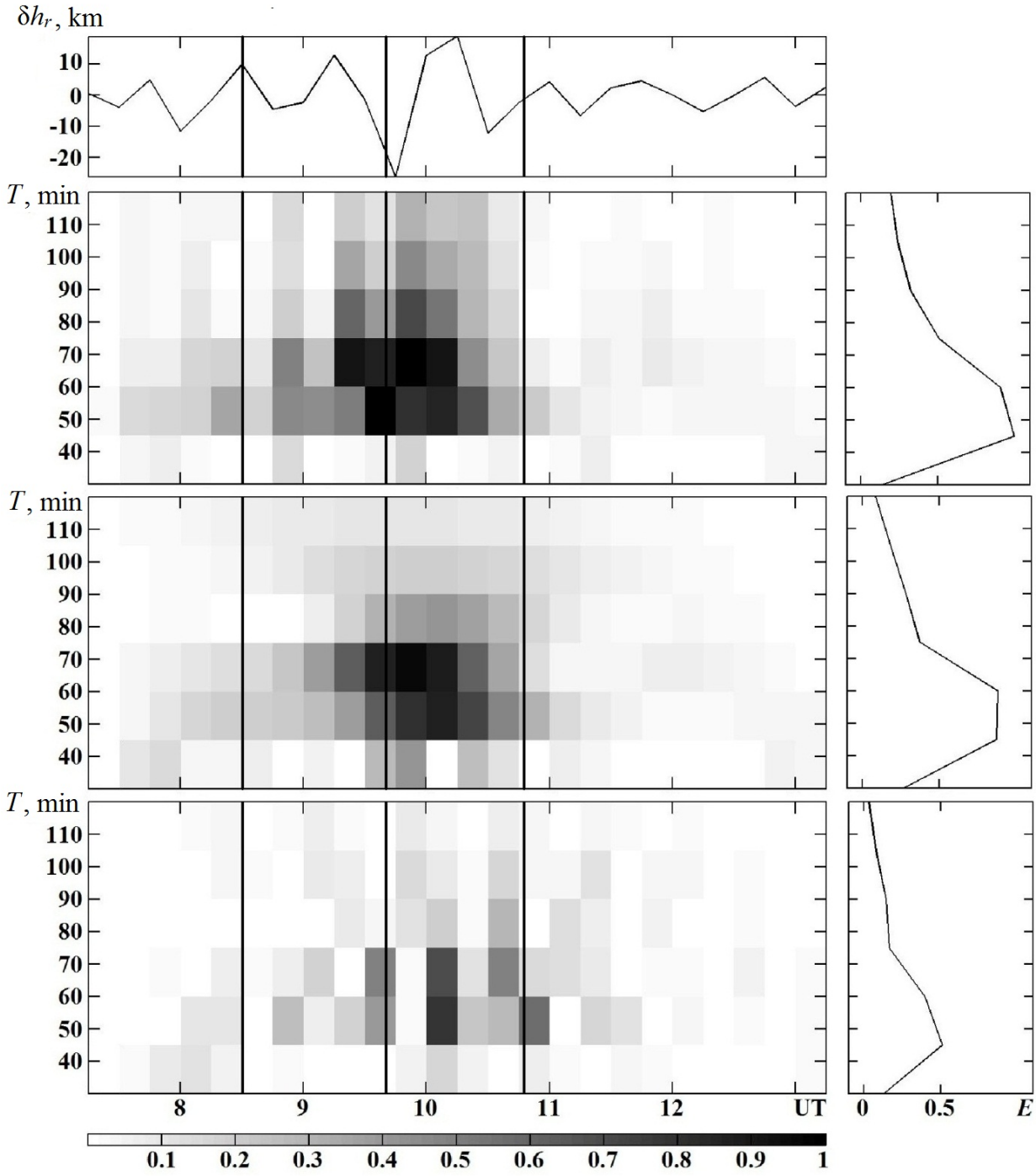

Fig. 3.15. Results of the system spectral analysis of the δh_r changes for the "San Vito" ionosonde on March 20, 2015. From top to down panels, the following parameners shown: $\delta h_r(t)$; WFT spectrogram; AFT spectrogram, and WT spectrogram. The energy diagrams of the corresponding spectrograms are shown on the right panels

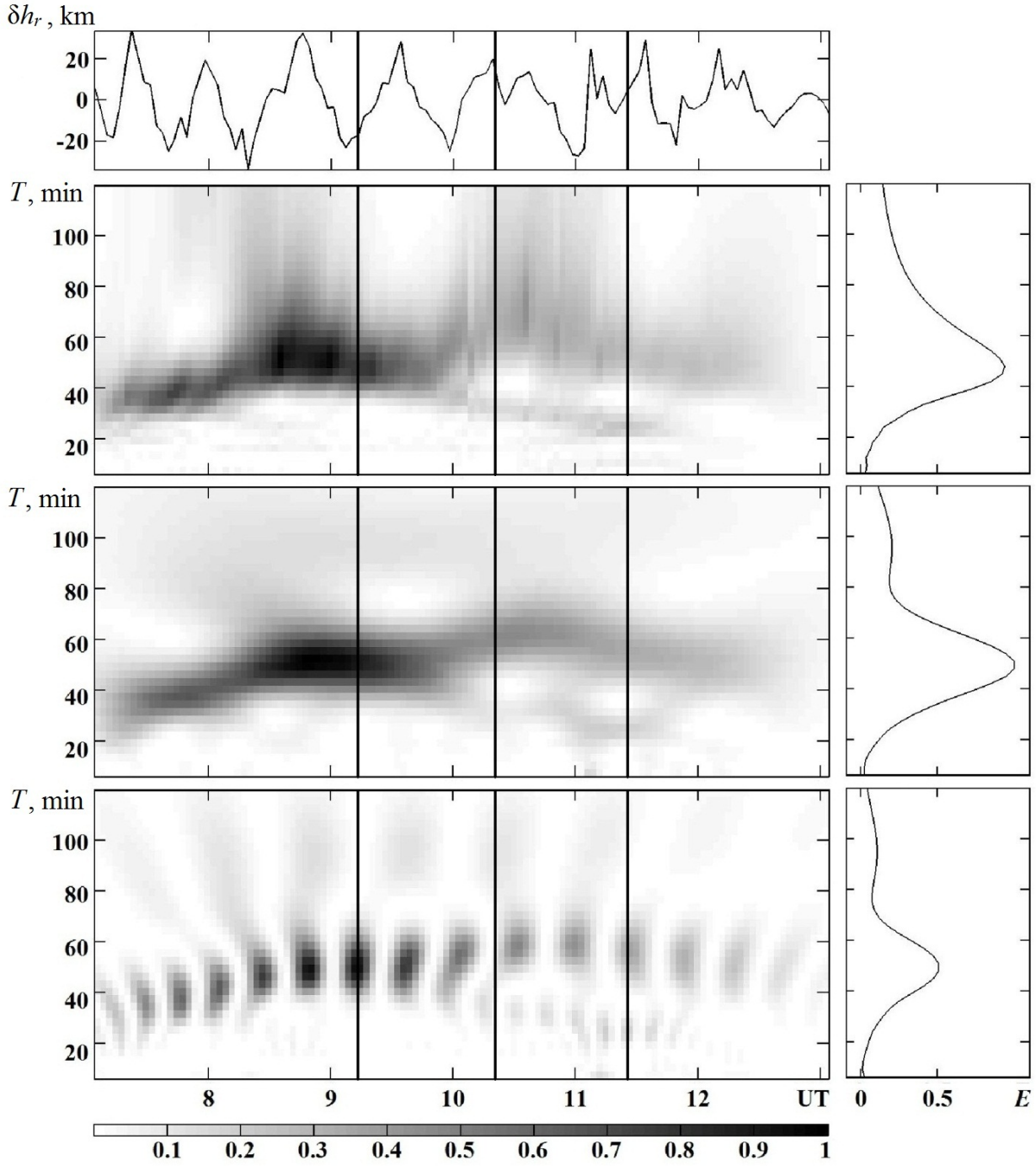

Fig. 3.16. Results of the system spectral analysis of the δh_r changes for the "Troitsk" ionosonde on March 20, 2015. From top to down panels, the following parameners shown: $\delta h_r(t)$; WFT spectrogram; AFT spectrogram, and WT spectrogram. The energy diagrams of the corresponding spectrograms are shown on the right panels

Fig. 3.16 shows that during the solar eclipse, the powerful oscillations with an amplitude of about 20–25 km and $T_z \approx 45$–60 min split into two oscillations with T_z of about 30 and 60 min and amplitudes of about 10 and 15 km, respectively. This is evidenced by the comparison of spectrograms for March 20 and 21, 2015. Data on amplitudes and periods obtained from the results of the system spectral analysis are summarized in Tables 3.2 and 3.3.

3.8. Discussion

The analysis of temporal variations of $\delta f_o F2(t)$ and $h_r(t)$ confirmed that the solar eclipse led to electron density decrease by tens of percent, an increase in h_r by 40–70 km compared to the reference day, and to the generation of quasi-periodic disturbances in $f_o F2$, i.e., in the electron density, and in the height h_r with periods of 30–60 min. Larger phases of the eclipse did not necessarily correspond to larger disturbances of the electron density. At the same values of the phase, the disturbances of the density N could not be the same.

This applies to the ionsondes “Dourbes” and “Juliusruh”. The decrease of the density N for the “Tromsø” ionosonde was much smaller than expected at almost total eclipse. This is due to the geographical location of the ionosonde, which is at a latitude of 69°N. It is known that the high-latitude ionosphere differs significantly from the middle-latitude ionosphere, the former is less stable, it is more prone to disturbances of natural origin, especially during geomagnetic storms, which was observed during this measurement campaign. The decrease in the electron density caused by the solar eclipse was largely offset by its increase, most likely as a result of the downward movement of the plasma flows from the plasmasphere, and by the precipitation of energetic electrons from the magnetosphere. The latter process at high latitudes usually accompanies geomagnetic storms (see, for example, [98]).

The main feature of the SE on March 20, 2015 was that the eclipse occurred on the background of a relaxing geomagnetic storm accompanied by a negative ionospheric storm. The storm significantly affected the slow variations in the

ionosphere parameters. At the same time, the geomagnetic storm did not appear to have a significant effect on the quasi-periodic disturbances of the electron density.

The next feature of the observations of the eclipse effects on March 20, 2015 is associated with relatively large values of the relative decrease in the electron density

$$\delta_{N\max} = 1 - \frac{N_{\min}}{N_0}$$

for ionosonde “San Vito”.

With almost the same values of the coverage function of $A_{\max}$ in Kharkiv and San Vito (0.44 and 0.45), the values of the relative decrease $\delta_{N\max}$ were 0.12 and 0.43, respectively. This difference is due to a noticeable difference in the density of the downward plasma flow for mid-latitude and low-latitude ionosondes, as well as due to different angular height of the Sun above the horizon at the maximum phase, which was about 45° and 50° for ionosondes “San Vito” and “Gaidari”, respectively.

For all ionosondes, the values of $N_{\min} / N_0$ and $\delta_{N\max}$ were well described by the linear law of recombination and the following quasi-stationary continuity equations, which are valid during the solar eclipse and on the reference day, i.e. in the absence of eclipse (index “0”):

$$q - \beta N + \Delta q = 0, \tag{3.7}$$

$$q_0 - \beta_0 N_0 + \Delta q_0 = 0, \tag{3.8}$$

where q and q_0 are ionization rate, β and β_0 are linear recombination coefficients, Δq and Δq_0 are additional sources of plasma caused by its downward drift. Their size depend on the geographical location of the ionosonde. Following [146, 150],

$$\Delta q = -\mathrm{div} N\vec{v} \approx -\frac{d}{dz} N v_z .$$

According to our estimates, $\Delta q \approx 2\cdot 10^8$ m^{-3}s^{-1} for most of ionsondes, $\Delta q \approx 10\cdot 10^8$ m^{-3}s^{-1} for the high-latitude “Tromsø” ionsonde, and $\Delta q \approx \Delta q_0 \approx 0.5\cdot 10^8$ m^{-3}s^{-1} for low-latitude ionsondes “El Arinosillo”, “San Vito” and “Athens”.

From the eqations (3.7) and (3.8), it follows that

$$\frac{N_{\min}}{N_0} = \frac{\beta_0}{\beta}\frac{q_{\min} + \Delta q}{q_0 + \Delta q_0} = \frac{\beta_0}{\beta}\frac{q_0(1 - A_{\max}) + \Delta q}{q_0 + \Delta q_0}. \quad (3.9)$$

Here $q_0 = \beta_0 N_0 - \Delta q_0$. Near the maximum of ionization, where $N_0 \approx (5–8)\cdot 10^{11}$ m^{-3}, $\beta_0 \approx 10^{-3}$ m^{-1}, we have $\beta_0 N_0 \approx (5–8)\cdot 10^8$ m^{-3}s^{-1}.

For weak flows, from equation (3.9), we obtain

$$\frac{N_{\min}}{N_0} = \frac{\beta_0}{\beta}(1 - A_{\max}). \quad (3.10)$$

In the general case $\beta \neq \beta_0$, when the density N decreases as a result of the solar eclipse, the reflection region of the probing radio wave shifts upwards, where the role of recombination is smaller. It is this circumstance that prevents a significant decrease in N for total or almost total eclipse. The dependence of β on height is given by the following equation (see, for example, [146, 150]):

$$\beta(z) = \beta_0 \exp\left(-\int_{z_0}^{z} \frac{dz}{H(z)}\right),$$

where z_0 is the height of the radio wave reflection in the absence of SE. H – the scale height of the neutral atmosphere. In F2-layer, the height $H \approx 50$ km. At altitude 300 km, $\beta_0 \approx 10^{-3}$ s^{-1} [146, 150]. When the region of reflection is shifted by 50 km, β decreases by approximately 2.7 times. In this case, according to expression (3.10), the ratio $N_{\min}/N_0$ increases by the same number of times.

The results of calculations β_0/β in accordance to (3.10) are given in Table 3.2. It is seen that for the low-latitude ionosondes “El Arinosillo”, “San Vito” and “Athens”, the ratio $\beta_0/\beta \approx 1$. For high-latitude ionosondes, $\beta_0/\beta > 1$. For the “Tromsö” ionosonde, this ratio is 15.4. In fact, instead of (3.10), it is necessary to use equation (3.9) which takes into account the downward flow of plasma. For $q_0 + \Delta q_0 \approx 6\cdot 10^8$ m^{-3}s^{-1}, $\Delta q \approx 10\cdot 10^8$ m^{-3}s^{-1}, we have $\beta_0/\beta \approx 9.2$. These estimates are close to the truth.

The value of the time delay between $N_{\min}$ $A_{\max}$ occurances is equal to $\Delta t = \beta^{-1}$. For a typical atmosphere model at altitudes of 250, 290, and 330 km, the β is about

$2.7 \cdot 10^{-3}$, $1.2 \cdot 10^{-3}$, and $5.5 \cdot 10^{-4}$ s^{-1}, respectively. In this case, Δt is approximately 6, 14, and 30 min. Very close values were obtained in the observations (see Table 3.2).

The results of (N_{min}/N_0) calculations in accordance with equation (3.9) are also shown in Table 3.2.

Thus, our study confirmes the conclusion of the work [1]: the processes during each solar eclipse, in addition to general patterns, have their own individual characteristics depending on the space weather conditions, season, time of day, geographical coordinates, etc.

Chapter 4
EFFECTS OF THE CHELYABINSK METEOR IN THE MIDDLE IONOSPHERE

4.1. General Information

As it was noted above, the meteor entered the Earth's atmosphere on February 15, 2012 at 03:20:26 UT. The cosmic body moved approximately from east to west (azimuth was about 270°) at an angle to the horizon of about 20°. The initial body mass $m_0 \approx 11$ kt, the initial velocity $v_0 \approx 18.5$ km/s, and the initial body diameter $d_0 \approx 18$ m (see, for example, [68]).

The search for disturbances in the atmosphere and ionosphere at considerable distances from the place of the Chelyabinsk meteor fall has an undoubted interest. Because its invasion of the Earth's atmosphere took place by surprise, purposeful measurements of the whole complex of the physical effects of the space body fall in all environments (in all geospheres) proved impossible. Some effects are registered by "regular" instruments. These include a network of ionosondes, which allows for almost continuous monitoring of the ionosphere on an almost global scale.

The state of solar activity was evaluated by Wolf numbers W and index $F_{10.7}$, and indices of geomagnetic activity: K_p, D_{st}, AE (Table 4.1). Table 4.1 shows that the space weather conditions was characterized as calm. This fact facilitated the search for the effects caused by the fall of the cosmic body.

Ionosonde network. To assess the ionosphere state, ionograms of ionosondes located to the west of the meteor explosion site ("Troitsk" station (near Moscow), geographical coordinates: 55.5° N, 37.3 E) and to the east ("Almaty" station, (near Almaty), geographical coordinates: 43.15° N, 76.54° E) were used. The results of observations at the stations "Pruhonice" (geographical coordinates: 50.0° N, 14.6° E) and "Juliusruh" (geographical coordinates: 54.6° N, 13.4° E) were used to assess the possibility of spreading ionospheric disturbances over long distances ($R > 3000$ km). Ionograms are posted on the site [151].

Table 4.1. Space weather conditions (according to [152])

Date	W	$F_{10.7}$	K_p		D_{st}, nT		AE, nT	
			max	min	max	min	max	min
February 14, 2013	38	100	4	1	–11	–36	944	23
February 15, 2013	48	100	1	1	1	–19	328	20
February 16, 2013	54	103	4	1	15	–20	1219	23

4.2. Instruments and Methods of Research

The distance along the Earth's surface from the place of the explosion of the space body to the stations "Troitsk", "Almaty", "Pruhonice" and "Juliusruh" was about 1510, 1730, 3145 and 3020 km, respectively. Ionograms at all stations operating in the standby mode were taken every 15 min. Only at the "Almaty" station, the time interval δt between ionogram registration was 5 minutes. In this case, the statistical error in estimating the delay time of perturbations is

$$\Delta = \frac{\delta t}{\sqrt{12}},$$

i.e. 3.5 min (for the "Almaty" station 1.4 min).

Methods of analysis. The main parameter that describes the state of the ionosphere near the maximum of ionization is the critical frequency of the ionospheric F2-layer

$$f_{\text{o}}\text{F2} = \frac{1}{2\pi}\sqrt{\frac{e^2 N}{\varepsilon_0 m}},$$

where e and m – charge and mass of the electron, ε_0 – electric constant, N – electron density. Variations of the density N lead to changes in $\delta f_{\text{o}}\text{F2}$ as follows:

$$\delta_N = \frac{\Delta N}{N} \approx 2\frac{\delta f_{\text{o}}\text{F2}}{f_{\text{o}}\text{F2}}. \qquad (4.1)$$

This takes into account that $f_{\text{o}}\text{F2} \sim \sqrt{N}$.

Equation (4.1) is valid at $\delta N << 1$. In the general case

$$\delta_N = (f_o\mathrm{F2} - \overline{f_o\mathrm{F2}})^2 - 1 \qquad (4.2)$$

where $\overline{f_o\mathrm{F2}}$ is smoothed or undisturbed values of f_oF2.

Time variations of $\delta f_o\mathrm{F2}(t)$ on February 15, 2013 and on the reference days February 14 and 16, 2013 were subject to analysis. In addition to $\delta f_o\mathrm{F2}(t)$, temporal variations of fluctuations were also analyzed

$$\delta f_o\mathrm{F2}(t) = f_o\mathrm{F2}(t) - \overline{f_o\mathrm{F2}(t)},$$

where $\overline{f_o\mathrm{F2}(t)}$ is trend calculated on a time interval of 180 min with a slip of 15 min (for the station "Almaty", for 5 min).

Further, the dependencies of $\delta f_o\mathrm{F2}(t)$ were subjected to system spectral analysis using complementary window, adaptive Fourier transforms and wavelet transforms [146, 150]. In the latter case, the Morlet function was used as the basic function. As is known (see, for example, [146, 150]), the Morlet wavelet has the form

$$\psi(t) = \exp\left(-\frac{t^2}{2}\right)\cos\omega t,$$

where t and ω – dimensionless time and frequency. This type of wavelet should be used to detect oscillation trains [150].

Spectral analysis was performed in the range of periods $T \approx 30$–180 min. The choice of the minimum value of $T = 30$ min is determined by the frequency of ionograms (one ionogram per 15 min). The choice of the maximum value of $T = 180$ min is explained by the fact that such periods belong to the atmospheric gravitational waves. At $T > 180$ min, the daily variations of $\delta f_o\mathrm{F2}$ and tidal fluctuations of this parameter, more precisely their higher harmonics, are significantly affected (see, for example, [153]).

4.3. Temporal Variations in Critical Frequency

"Troitsk" station. Sunrise at an altitude of $z \approx 300$ km was at 03:00, and at ground level it was at 04:45 (hereinafter UT). On February 14–16, 2013, the

minimum value of the critical frequency f_oF2 was observed in the time interval 03:30–04:30 (Fig. 4.1). After that, there was an increase in f_oF2 from about 3 to 7–8 MHz. After 10:00–11:00 on reference days 14 and 16 February 2013, there was a gradual decrease in f_oF2.

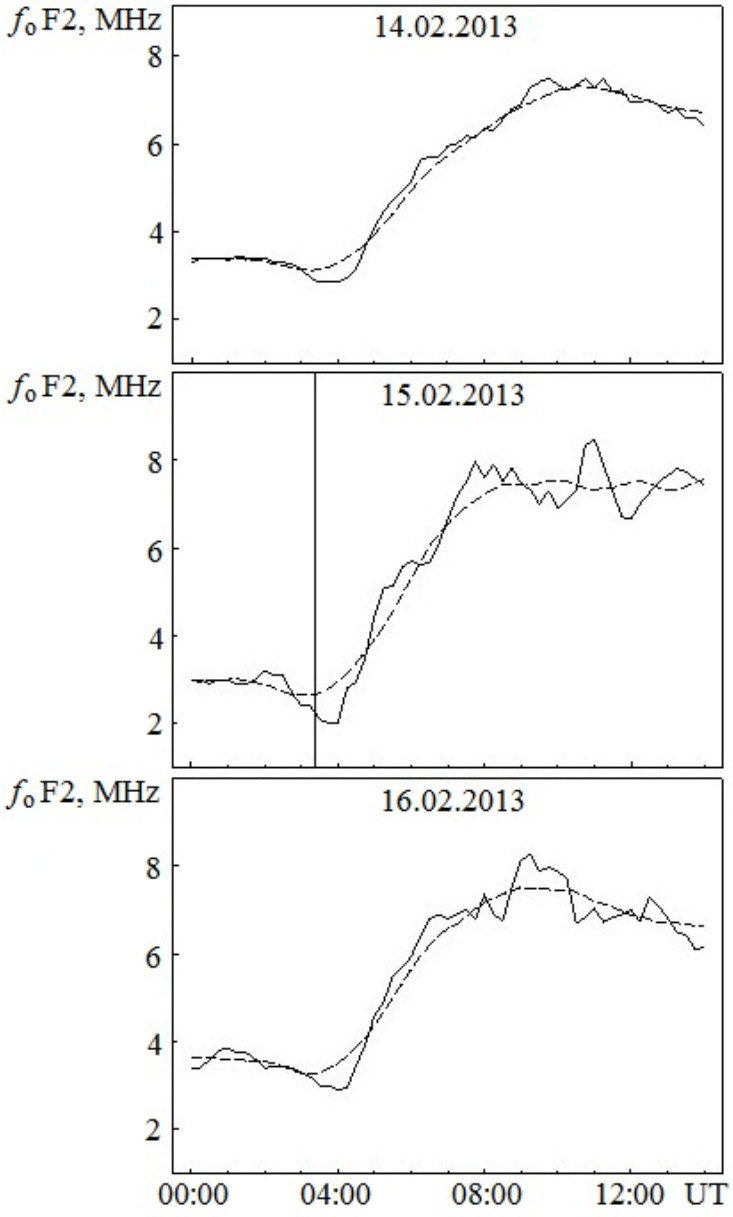

Fig. 4.1. Temporal variations in the f_oF2 for “Troitsk” station. The vertical line shows the moment of the Chelyabinsk meteorite fall, and the dashed line shows $\overline{f_o\mathrm{F2}}(t)$ calculated by the moving average

Fluctuations with a deviation, as a rule, in several tenths of a megahertz, were superimposed on the regular course $\overline{f_o F2}(t)$. On the day of the meteorite fall, the level of fluctuations (amplitude of oscillations $f_o F2$) increased. Noticeable deviations (increased depth of reduction) from the regular course began at about 04:00. Their level increased significantly in the time interval from 07:00 to 14:00 (see Fig. 4.1, Fig. 4.5*b*). The amplitude of $f_o F2$ reached 1 MHz. A quasi-periodic change in the $f_o F2$ with a period of $T \approx 135$ min was observed. No similar quasi-periodic process was observed on the reference days (see Fig. 4.1). In addition, the decrease in the $f_o F2$ after 10:00–11:00, which occurred on the reference days, was absent until 14:00.

In the time interval 07:00–09:00, there was a clear quasi-periodic disturbance of the critical frequency. Most likely, it is caused by the Chelyabinsk meteoroid.

"Almaty" station. Sunrise at an altitude of 300 km was observed at 00:20, and at an altitude of $z \approx 0$ – at 02:00. The nighttime values of the $f_o F2$ did not exceed 4 MHz (Fig. 4.2). After approximately 01:00, $f_o F2$ values began to increase to 8–10 MHz. Fluctuation changes with a deviation of up to 1 MHz were superimposed on the regular course $\overline{f_o F2}(t)$.

On the day of the meteorite fall, a noticeable change in $f_o F2$ began at about 04:00–04:15. Perhaps it was to suppress the existing quasi-periodic process. Most likely, a negative half-wave of a new quasi-periodic process with a period of 80–100 min and an amplitude of the $\delta f_o F2 \approx 0.5$ MHz ($\overline{f_o F2} \approx 8$–9 MHz) came. This process was observed for 4–5 hours (see Fig. 4.2, middle panel).

Significant fluctuations in $f_o F2$ also occurred on the reference days, but quasi-periodic processes were less pronounced.

"Pruhonice" station. Sunrise at altitudes of about 300 and 0 was at about 03:50 and 05:35, respectively. The nighttime values of the $f_o F2$ were close to 3.5–4 MHz (Fig. 4.3). After approximately 5:00, the frequency $f_o F2$ began to grow rapidly from night values to 7–8 MHz. In addition to the regular course, the $f_o F2$ fluctuations of 0.5–1 MHz were observed.

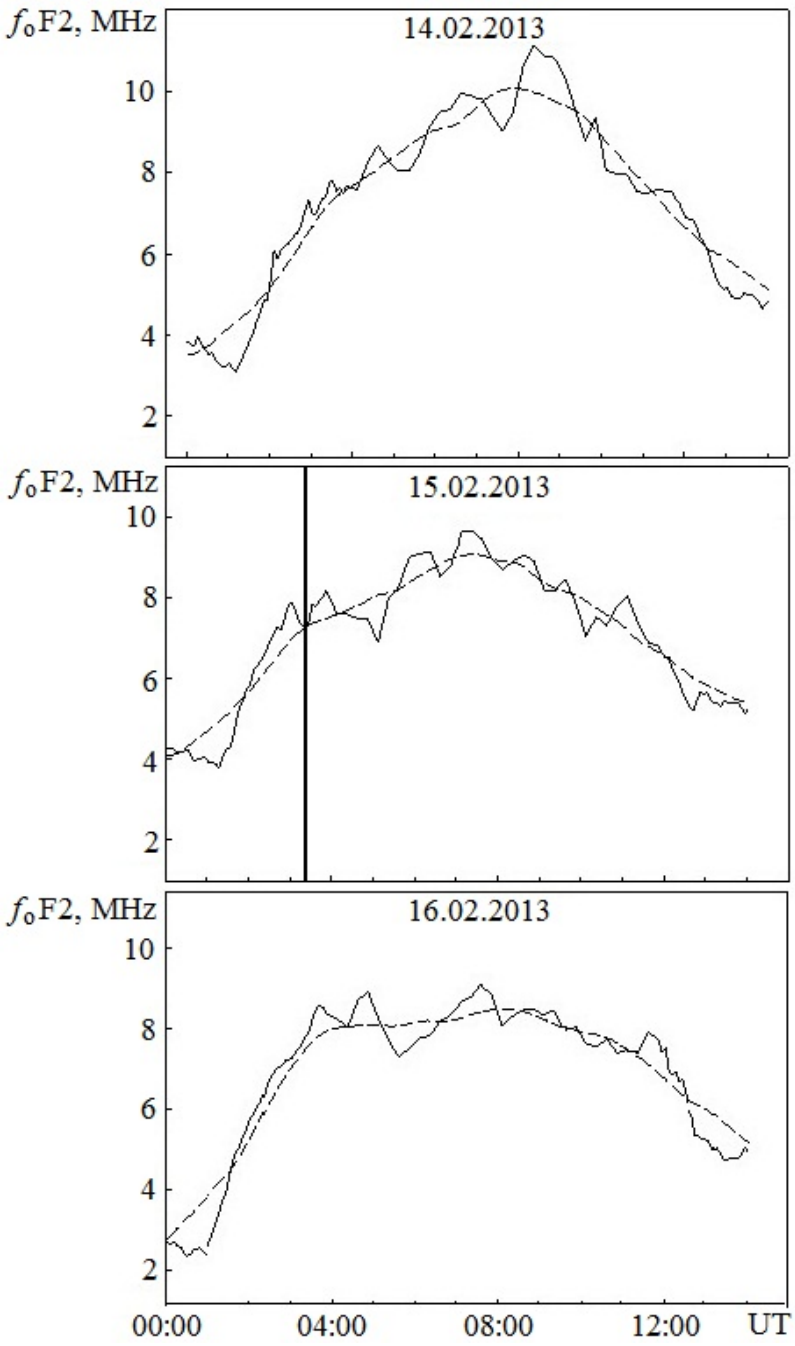

Fig. 4.2. Temporal variations in the f_oF2 for “Almaty” station. The vertical line shows the moment of the Chelyabinsk meteorite fall, and the dashed line shows $\overline{f_o\mathrm{F2}}(t)$ calculated by the moving average

On the day of the cosmic body fall, the fluctuations of the critical frequency f_oF2, which began at approximately 04:30–04:45, became quasi-periodic with a period of T = 135 min and an amplitude of 0.4–0.6 MHz. In this case, $\overline{f_o\mathrm{F2}} \approx$ 4–

6 MHz. A particularly strong burst of f_oF2 up to 1.7 MHz was observed at about 11:00, i.e. almost when a similar burst was recorded at the "Troitsk" station (see Fig. 4.1). Note that in the reference days, similar train of fluctuations was not observed.

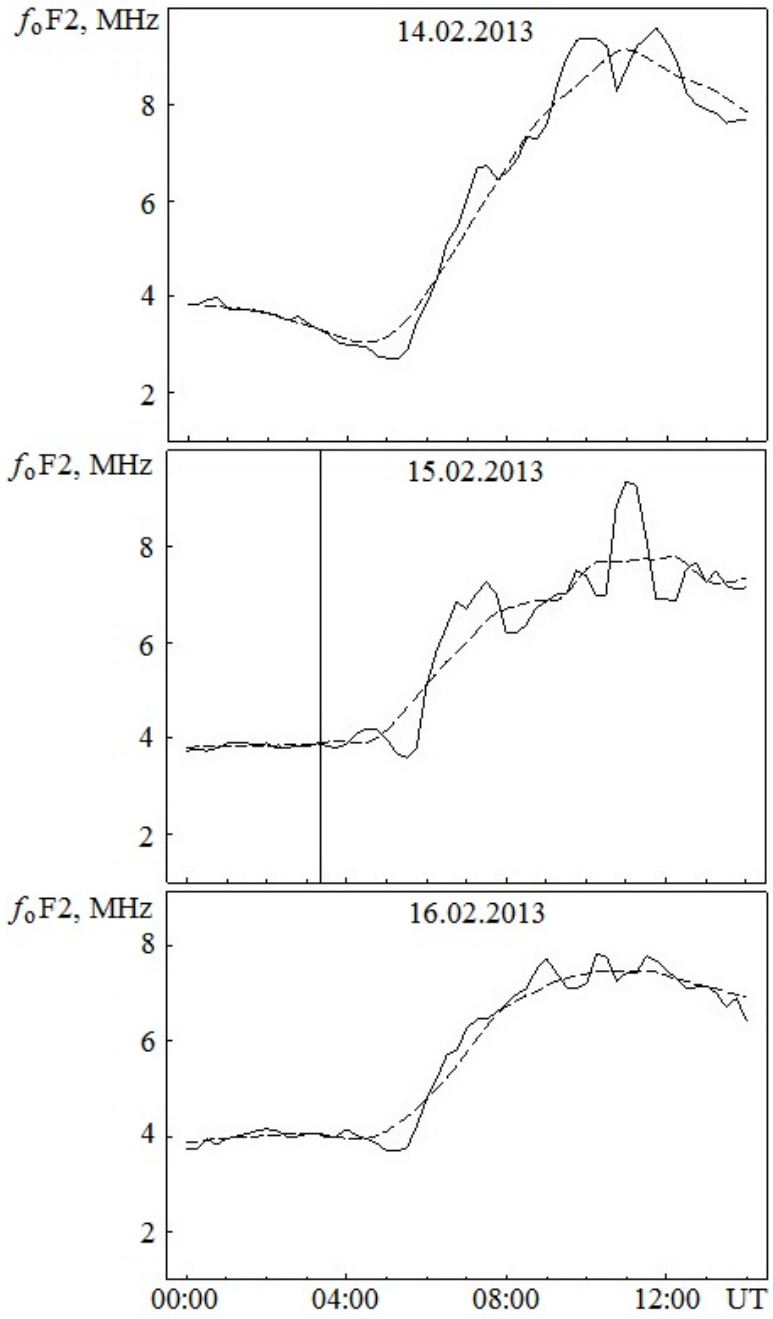

Fig. 4.3. Temporal variations in the f_oF2 for "Pruhonice" station. The vertical line shows the moment of the Chelyabinsk meteorite fall, and the dashed line shows $\overline{f_o\mathrm{F2}}(t)$ calculated by the moving average

"Juliusruh" station. Sunrise at the stations "Pruhonice" and "Juliusruh" was at about the same time. The nighttime values of the f_oF2 were close to 3.5 MHz, the minimum value of this parameter was observed at about 05:00, after which it began to grow rapidly to 7–8 MHz (Fig. 4.4). As at other stations, f_oF2 fluctuations with a deviation of 0.3–0.5 MHz were superimposed on the regular course.

On the day of the Chelyabinsk meteorite fall around 04:30–04:35, a slight (0.2 MHz) increase in f_oF2 began, which lasted until approximately 09:00. From 09:00 to 16:00 there was a strong oscillation of the f_oF2 with a period of about 70 min, duration $\Delta T \approx 5$ h and amplitude 0.5–1.0 MHz, with $\overline{f_o F2} \approx 7$ MHz. Strong bursts of the f_oF2 (up to 0.5–1 MHz) were also observed on the reference days, but they were not quasi-periodic.

4.4. The Results of Spectral Analysis

The results of the system spectral analysis of the $\delta f_o F2(t)$ for the station "Troitsk" are shown in Fig. 4.5. The figure shows that the spectral composition of the variations of the $\delta f_o F2(t)$ on the day of the meteorite fall and on the reference days differed significantly. The differences began at about 04:00 and lasted until 14:00 February 15, 2013, the spectrum of fluctuations was narrower, it was dominated by a component with a period of about 160 min. The amplitude of this component was 2–3 times larger than in the reference days.

Fig. 4.6 shows the results of the system spectral analysis of temporal variations in the $\delta f_o F2(t)$ for the station "Almaty". From Fig. 4.6*b*, it is seen that the spectral composition of the critical frequency fluctuations differed significantly, starting from the time interval 04:00–05:00. In the fluctuation spectrum of the $\delta f_o F2(t)$, the component with a period of about 70–80 min increased. In addition to this component, the component with $T \approx 100$–120 min was also enhanced. On the reference days, the components with a period of 140–160 min predominated.

The results of the system spectral analysis of the the critical frequency fluctuations for the "Pruhonice" station are shown in Fig. 4.7.

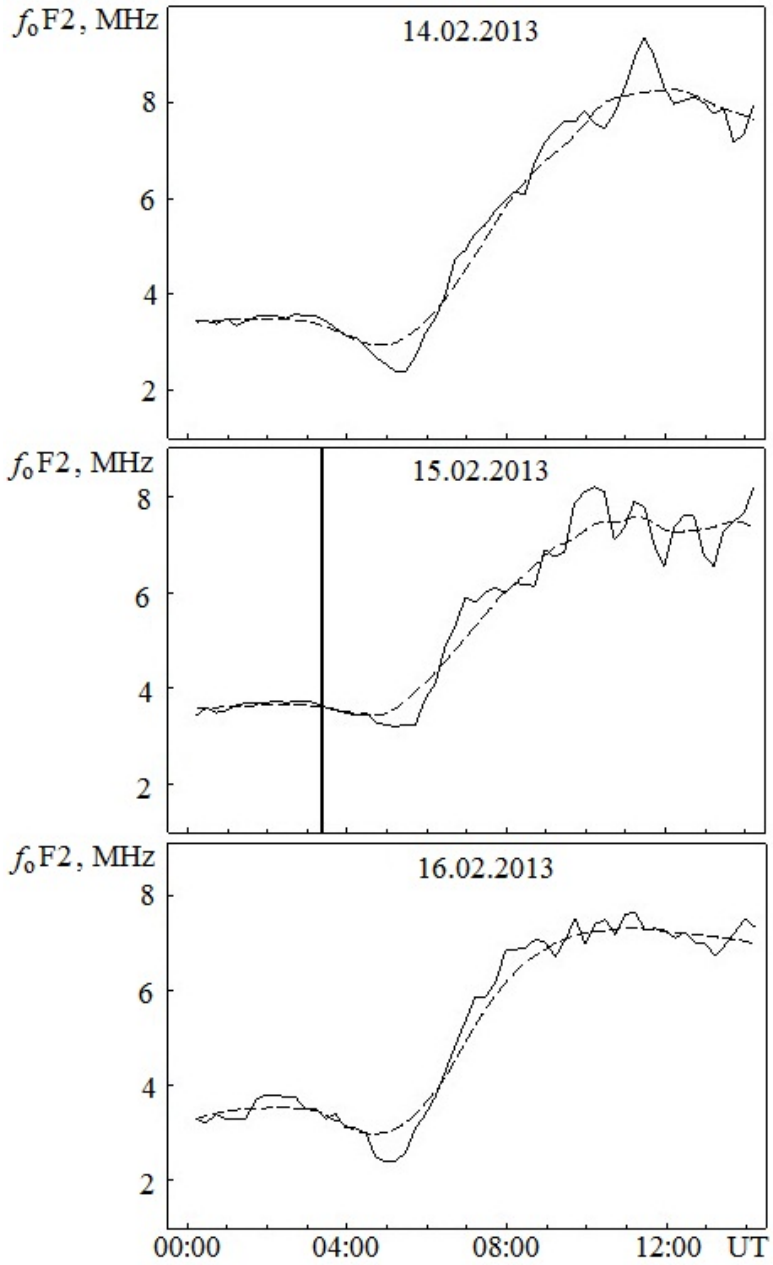

Fig. 4.4. Temporal variations in the f_oF2 for "Juliusruh" station. The vertical line shows the moment of the Chelyabinsk meteorite fall, and the dashed line shows $\overline{f_o\mathrm{F2}}(t)$ calculated by the moving average

Significant differences in the spectral characteristics on the day of the cosmic body explosion and on the reference days on February 14 and 16, 2013 are visible. The spectra were dominated by components with $T \approx 140$–180 min, and on February 15, 2013 – with $T \approx 100$–140 min. On the day of the meteorite fall, the amplitude of the main oscillation was 1.5–2 times larger than on the reference days.

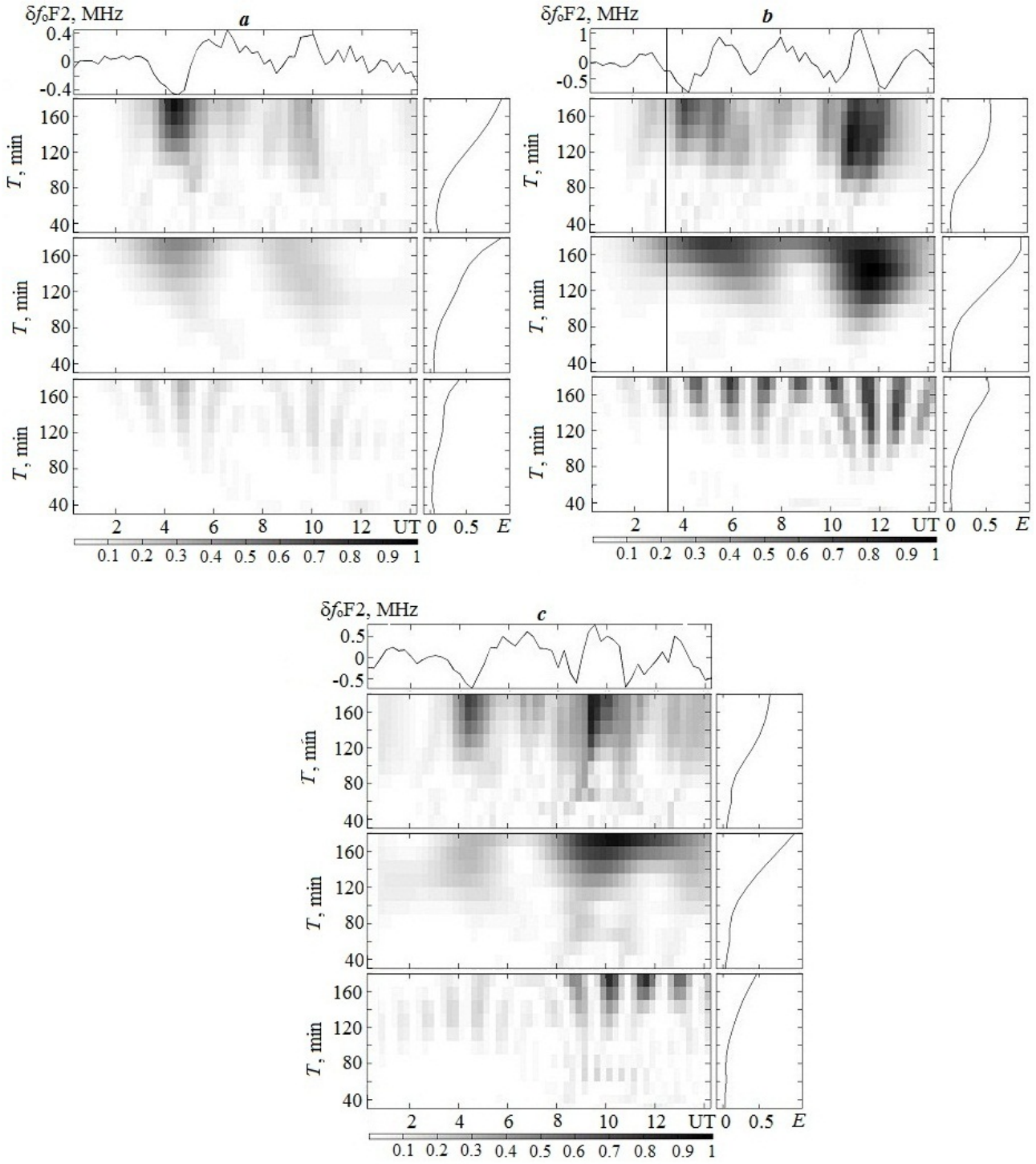

Fig. 4.5. Results of the system analysis of the time dependence of the critical frequency fluctuations for “Troitsk” station: *a* – February 14, 2013, *b* – February 15, 2013 and *c* – February 16, 2013: the fluctuation (top panel), spectrograms by the windowed and adaptive Fourier transform, and wavelet transform (from top to down panels). Energograms are shown on the right panels

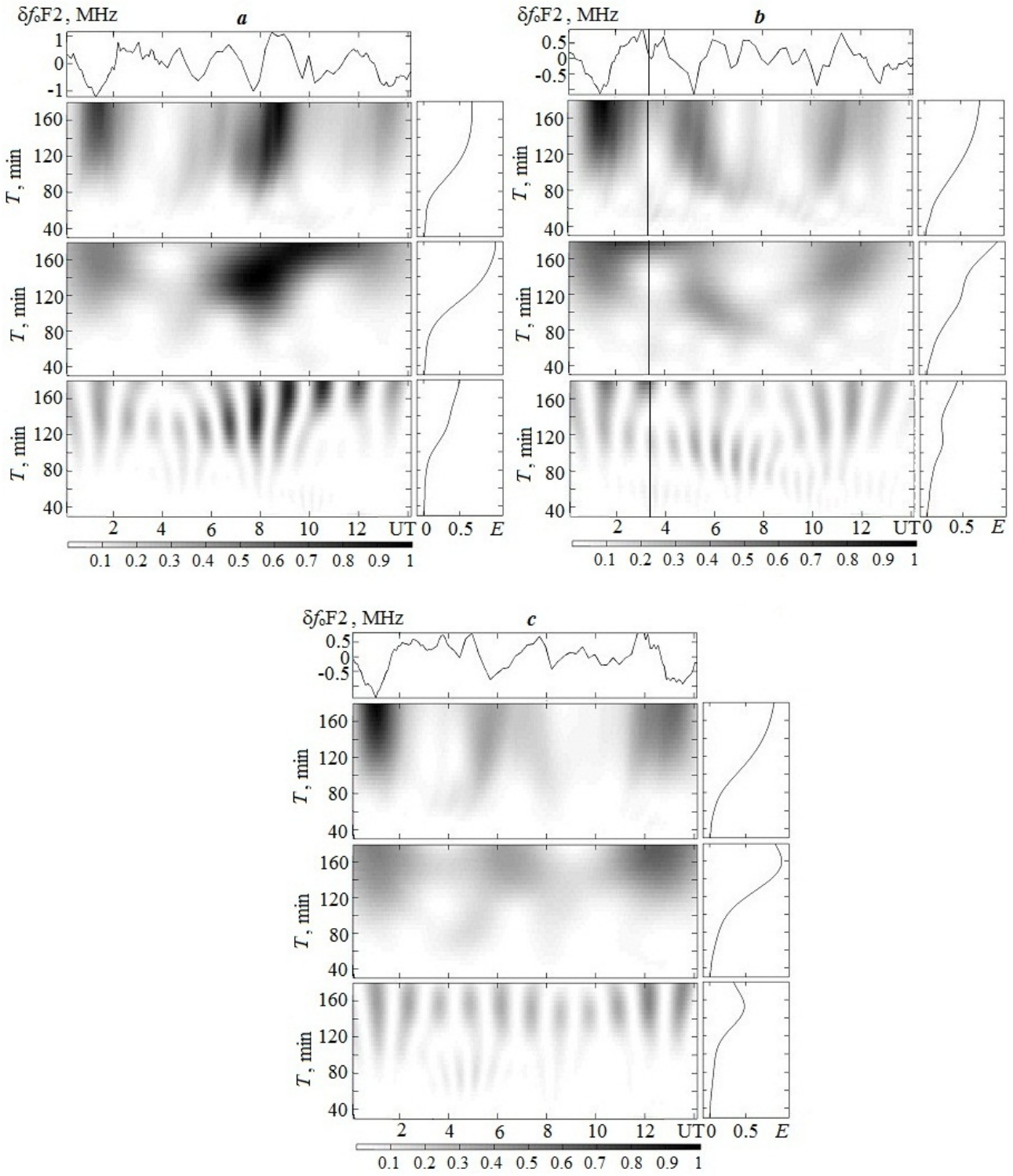

Fig. 4.6. Results of the system analysis of the time dependence of the critical frequency fluctuations for “Almaty” station: *a* – February 14, 2013, *b* – February 15, 2013 and *c* – February 16, 2013: the fluctuation (top panel), spectrograms by the windowed and adaptive Fourier transform, and wavelet transform (from top to down panels). Energograms are shown on the right panels

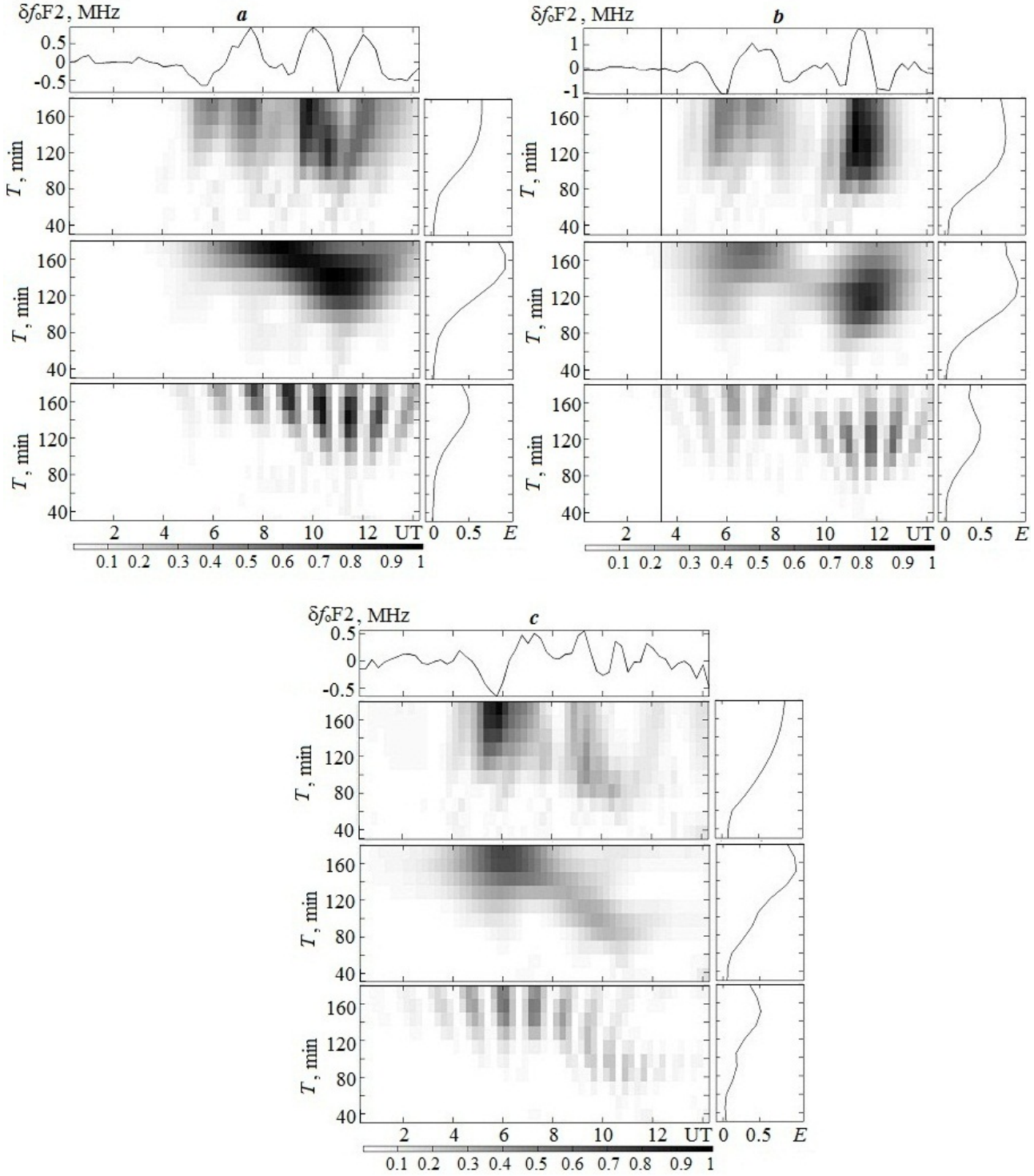

Fig. 4.7. Results of the system analysis of the time dependence of the critical frequency fluctuations for “Pruhonice” station: *a* – February 14, 2013, *b* – February 15, 2013 and *c* – February 16, 2013: the fluctuation (top panel), spectrograms by the windowed and adaptive Fourier transform, and wavelet transform (from top to down panels). Energograms are shown on the right panels

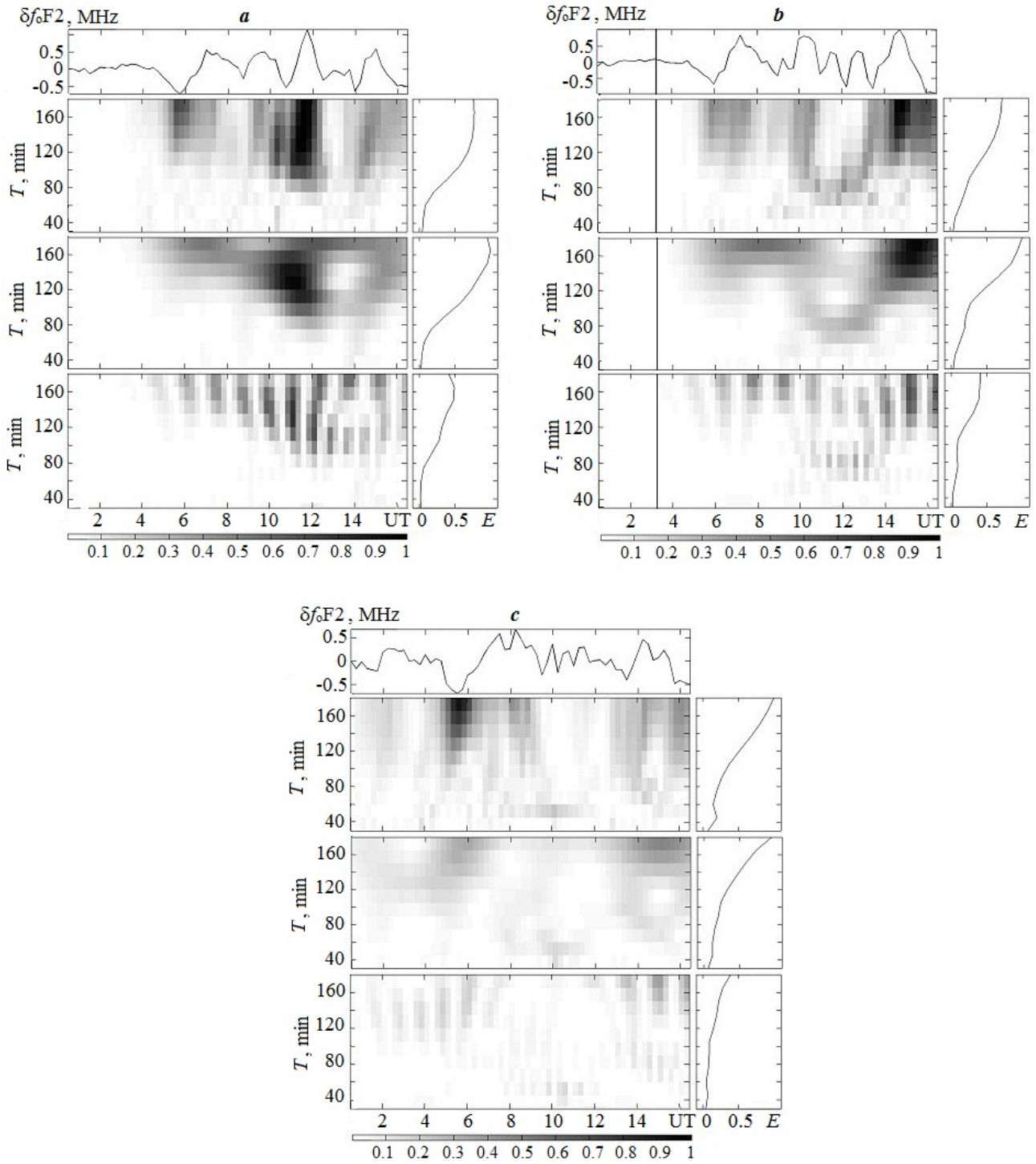

Fig. 4.8. Results of the system analysis of the time dependence of the critical frequency fluctuations for “Juliusruh” station: *a* – February 14, 2013, *b* – February 15, 2013 and *c* – February 16, 2013: the fluctuation (top panel), spectrograms by the windowed and adaptive Fourier transform, and wavelet transform (from top to down panels). Energograms are shown on the right panels

Fig. 4.8 shows the results of the system spectral analysis of the time dependence $\delta f_o F2(t)$ for the "Juliusruh" station. Spectrograms and energograms for February 14, 15, and 16, 2013 differed markedly. On the day of the Chelyabinsk body fall, the components intensified with periods of first 130–160 and then 60–80 min. Their amplitude was noticeably larger (1.5–2 times) than in the reference days. On February 14 and 16, 2013, oscillations with $T \approx$ 160–180 min prevailed, their amplitude did not exceed 0.5 MHz.

4.5. Discussion on the Observation Results

Temporal variations in the critical frequency. At the stations "Troitsk", "Pruhonice" and "Juliusruh", the moments of the reaction to the space body explosion and the sunrise almost coincided. This seriously complicated the separation of disturbances associated with the movement of the meteoroid.

At the "Almaty" station, the processes caused directly by the sunrise ended before the space body fall. However, the wave processes generated by the movement of the morning terminator could continue.

At "Troitsk" station the first noticeable deviation of the frequency $f_o F2$ from the regular course was observed at about 04:00. If it is caused by the meteoroid explosion, the delay time of the perturbation $\Delta t \approx$ 40 min. Knowing Δt and the wavelength of the wave, it is possible in principle to calculate the average velocity of propagation of wave disturbances (WD). Unfortunately, the exact trajectory of the wave is unknown. At greater (more than 1000 km) distances of the ionosonde from the place of explosion, we can assume that the wave propagates to the ionosphere almost vertically, then it is captured in atmospheric waveguides and then propagates almost horizontally. The average speed can be estimated by the obvious formula

$$v = \frac{R}{\Delta t - \Delta t_0}, \tag{4.3}$$

where R is the distance along the Earth's surface between the place of the body explosion and the ionosonde, Δt_0 is the time of propagation of WD to the atmospheric

waveguide (F region of the ionosphere). The time Δt_0 is easy to estimate knowing the altitude profile of the speed of sound v_s in the upper atmosphere:

$$\Delta t_0 = \int_{z_e}^{z_m} \frac{dz}{v_s}, \tag{4.4}$$

where z_e is the altitude of the space body explosion, z_m is the height of the F2-layer maximum, which corresponds to the frequency f_oF2. For a typical model $v_s(z)$, the equation (4.4) gives $\Delta t_0 \approx 9$ min. Velocity $v_s \approx 300$–700 m/s at altitudes of 25–300 km. Using the average value $\overline{v}_s \approx 500$ m/s and $\Delta z = 275$ km we receive $\Delta t_0 \approx 550$ s $\approx$ 9.2 min. At $\Delta t_0 \approx 9$ min and $R \approx 1510$ km, from (4.3) we have $v \approx 810$ m/s.

For station "Troitsk", δf_oF2 $\approx$ 0.3–0.5 MHz and $\overline{f_o\text{F2}} \approx 3$–$6$ MHz. Thus, $\delta_N \approx 17$–20%. Near 11:00, $\overline{f_o\text{F2}} \approx 7$ MHz, and $\delta f_o\text{F2}_{\max} \approx 8.5$ MHz. Thus, $\delta_N = (f_o\text{F2}/\overline{f_o\text{F2}})^2 - 1 \approx 47\%$ (see (4.2)).

At the "Pruhonice" and "Juliusruh" stations, a noticeable deviation of the frequency f_oF2 from the regular course began in the time interval 04:30–04:45, with $\Delta t \approx 70$–85 min. At $R \approx 3100$ km, we have $v \approx 690$–860 m/s (average speed velocity value is about 780 m/s). Around 11:00 at the station "Pruhonice", the f_oF2 ≈ 9.4 MHz and $\overline{f_o\text{F2}} \approx 7$ MHz. According to (4.2), $\delta_N \approx 80\%$. At the same time, at the "Juliusruh" station, the f_oF2 ≈ 8 MHz, and the $\overline{f_o\text{F2}}(t) \approx 7$ MHz, whicn gives $\delta_N \approx 31\%$.

At the "Almaty" station, a noticeable deviation of the f_oF2 began at about 04:00–04:45. If it is caused by a meteoroid fall, $\Delta t \approx 40$–55 min. For $\Delta t_0 \approx 9$ min and $R \approx 1760$ km, we obtain $v \approx 650$–980 m/s (average speed velocity value is about $v \approx 810$–820 m/s). For $\delta f_o\text{F2} \approx 0.5$ MHz and $\overline{f_o\text{F2}}(t) \approx 7.5$–$8.5$ MHz, we have $\delta_N \approx 12$–13%.

If the propagation of the wave cannot be separated to the horizontal and vertical motion, (4.3) is enough to estimate the average speed where $\Delta t_0 = 0$. For stations "Troitsk", "Almaty", "Pruhonice" and "Juliusruh", the following values of the

average speed v was obtained: 630, 520–720, 610–740, and 610–740 m/s, respectively.

Thus, for all four ionosondes, the disturbances propagated in the horizontal direction with an average velocity of about 600–700 m/s. The value of the WD period was 70–135 min. Such parameters are typical for gravitational waves in the atmosphere at altitudes $z \approx 300$ km (see, for example, [5, 153]).

Let's discuss the nature of strong f_oF2 bursts during the day and, in particular, around 11:00. They were observed almost simultaneously on strongly spaced ionosondes. This means that they were large-scale (about 4–5 thousand km) and could be caused by an external source, such as a non-stationary process on the Sun. The analysis of the space weather conditions did not allow attributing the change of the f_oF2 (and hence, the density N) to the processes on the Sun. The authors have no information about any large-scale source in the tectonosphere, lithosphere or atmosphere which could cause such a large-scale disturbance at altitudes of about 300 km.

It can be assumed that the mentioned values of the frequency f_oF2 during the day are associated with long-lived disturbances in the upper atmosphere. Similar perturbations were observed by the authors [154, 155] with rather weak ground explosions with an energy release of only ~ 1 t of TNT (trinitrotoluene).

The possibility of the existence of long-lived vortices, first described by the author [156] and mentioned in [157], requires, however, more investigations. It cannot be ruled out that long-lived perturbations may be associated with disruption of the interaction of subsystems in the system Earth – atmosphere – ionosphere – magnetosphere occurred before the flight of the meteoroid [75, 158, 159].

The results of spectral analysis. The system analysis performed in this work confirmed that the spectral composition of δf_oF2 in the reference days and the day of the Chelyabinsk meteoroid explosion differed significantly. These differences were observed both shortly (40–70 min) after the explosive release of energy, and for 9–10 h after that.

According to the energy digrams (this is best seen for the adaptive Fourier transform), the average values of the disturbance periods on February 15 were 170, 110, 130 and 170 min for the stations “Troitsk”, “Almaty”, “Pruhonice” and “Juliusruh”, respectively. On the reference days, they generally differed markedly. Moreover, during the reference days, in some cases, there was no maximum in the distribution of energy by periods.

The estimated values of the periods and amplitudes of WD confirmed that the fall of the space body was accompanied by the generation and propagation of gravitational waves in the upper atmosphere, as well as, possibly, by the occurrence of long-lived disturbances.

We emphasize that the parameters of WD described above are in good agreement with the results of theoretical studies described in [71, 76–79]. The fact of generation of gravitational waves in the atmosphere is theoretically predicted by the authors [160].

Chapter 5
APERIODIC LARGE-SCALE DISTURBANCES IN THE IONOSPHERE ACCOMPANYING THE MODIFICATION OF THE IONOSPHERIC PLASMA BY INTENSE RADIO WAVES

5.1. General Information

A qualitatively new level of understanding of physicochemical processes in the near-Earth space medium is associated with a change in the system paradigm [75, 158, 159, 161–164]. It was argued that the description of the Earth's crust is not self-sufficient. There is an interaction between the regions. Direct and inverse, positive and negative connections are revealed. Therefore, it is necessary to consider the system Sun – interplanetary medium – magnetosphere – ionosphere – atmosphere – Earth (its inner shells) (SIMMIAE). When studying the role of flows "from below", it is often sufficient to consider the system Earth – atmosphere – ionosphere – magnetosphere (EAIM) (see, for example, [158, 164]). It is important that the formation of EAIM (as well as SIMMIAE) refers to an open dynamic nonlinear physical system. Such systems have a number of non-trivial properties. For example, in these systems triggering mechanisms of the energy release are possible [75, 158, 164].

To study the interaction of subsystems in the EAIM system, active experiments are convenient and effective. In this case, the energy of the source, place and time of energy release are known a priori.

Among the active experiments, a special place is occupied by the modification of near-Earth plasma by powerful radio transmission. Such experiments are environmentally friendly, they can be repeated many times. For this reason, considerable attention has been paid to the interaction of high-power radio transmission with ionospheric-magnetospheric plasma for the last forty years (see, for example, [165–167]). In this case, as a rule, the processes arising within the pattern of

the antenna of the heating stand are investigated. Such processes have been called localized [109]. Their horizontal size usually did not exceed 10–100 km.

According to the study results of localized disturbances in the ionosphere caused by powerful radio transmission, several hundred works by scientists from Ukraine, Russia, the United States, Norway, etc. have been published. A review of such works is made in the most complete monograph of V.L. Frolov [168].

At the same time, there is another scientific field, the purpose of which is to study the possibility of disturbances in the ionosphere far beyond the transmission pattern of the heating stand antenna. Such disturbances were first detected about 45 years ago (see, for example, [108–114, 127, 128]). They were called large-scale. Their horizontal size is about several thousand kilometers.

There are two causes of large-scale disturbances. The first of them is the generation and propagation of acoustic-gravitational waves at the heights of the F region of the ionosphere. The results of nowadays studies of these waves are presented in [107, 115–119].

At the altitudes of the D and E regions, the cause of large-scale disturbances is different [113, 114]. Most likely, it is caused by the interaction of subsystems ionosphere – magnetosphere – energetic electrons – atmosphere, more precisely – it is associated with the precipitation of high-energy electrons from the magnetosphere into the atmosphere. In this case, large-scale disturbances are aperiodic. The results of recent studies of such disturbances are described in [120, 121].

The purpose of this chapter is to consider the observation results of the spatial distribution of aperiodic large-scale disturbances in the lower ionosphere, which accompanied the impact on the plasma by powerful radio transmission of the stand “Sura” on August 28–30, 2012.

5.2. Space Weather Conditions

Space weather conditions were monitored using the solar wind parameters (particle density n_{sw}, speed V_{sw}, temperature T_{sw} and pressure p_{sw}), the B_y and B_z

components of the interplanetary magnetic field (INF), Akasofu energy function ε_A, and indices of geomagnetic activity (a_p, A_p, K_p and D_{st}) (some values of these parameters are listed in Table 5.1).

Table 5.1. Indices of geomagnetiv activity

Date	AE_{max}, nT	K_{pmax}	ΣK_p	a_{pmax}, nT	A_p, nT	D_{st}, nT
August 26, 2012	527	3.7	18.7	22	11	–6 – +4
August 27, 2012	297	3	10.7	15	6	–8 – +1
August 28, 2012	100	1.3	5.3	5	3	–8 – 0
August 29, 2012	110	1.3	6	5	3	–4 – +3
August 30, 2012	88	1	5	4	3	–1 – +10

On August 26, 2012, the geospace medium was slightly disturbed, there was a slight perturbation of the IMF (up to –(5–6) nT) and the geomagnetic field ($K_{pmax} < 4$).

From August 27 to August 30, 2012, the space weather conditions were characterized as quiet: the parameters of the solar wind, the IMF and geomagnetic field fluctuated weakly around their undisturbed values (see Table 5.1). The quiet state of space weather provided favorable conditions for the separation of the effects caused by the influence of powerful radio radiation on the ionosphere.

5.3. Instruments and Methods of Research

5.3.1. “Sura” Heating Stand

Ionospheric plasma disturbance by radio transmission of the “Sura” stand was carried out from August 27 to August 30, 2012. The stand is located near the city of Novgorod (Russia); its geographical coordinates: 56.15° N, 46.1° E. The modes of operation of the stand and its parameters are described below. The carrier frequency

of the stand in various experiments varied from 4785 to 6720 kHz, the polarization of radio waves was always normal, the effective transmission power of the stand was approximately equal to 150 MW. The duration of the exposure pulses varied from 5 to 30 minutes, and in some cases a longer mode of powerful radio wave transmission was used. To fulfill the conditions of the "magnetic zenith effect", the antenna pattern of all experiments was tilted to the south by 12°.

5.3.2. Observation Means

Four digital ionosondes were used to observe ionosphere disturbances caused by strong radio transmission (see Table 5.2).

Table 5.2. Information about ionosondes

Station (location)	Type	Latitude	Longitude	Distance to the heating stand, km
"Vasilsursk" (near N. Novgorod)	Automated digital ionosonde "BASIS"	56°09′ N	46°06′ E	~0
"Troitsk" (near Moscow)	Digital ionosonde "Parus"	55°28′ N	37°18′ E	560
"Gaidary" (near Kharkiv)	Digital ionosonde	49°38′ N	36°20′ E	960
"Pruhonice" (near Pruhonice)	Digital ionosonde DPS-4	50°00′ N	14°36′ E	2200

Frequency of ionogram sampling is 1 ionogram per 15 min ("Gaidary" is 1 ionogram per 5 min).

All the main parameters of ionograms were analyzed. It turned out that the effect of powerful radio transmission on the ionospheric plasma was accompanied by noticeable disturbances of the minimum observed frequency. Other parameters of the ionograms changed insignificantly, within natural fluctuations. Therefore, the results of the analysis of temporal variations of the minimum observed frequency are given below. Its bursts indicated an increase in the absorption of radio signals at the

altitudes of the lower ionosphere, which was most likely due to the appearance of an additional layer of ionization.

The distance *R* from the “Sura” stand to the ionosondes varied from 0 to about 2200 km.

The ionosonde of the Scientific Research Radio-Physical Institute (SRRPI) (Vasilsursk subdivision) of the “CADI” type is located directly next to the heating stand.

Ionosonde of the N.V. Pushkov Institute of Earth Magnetism, Ionosphere and Radio Wave Propagation of the Russian Academy of Sciences (IZMIRAN) (Moscow station, Russia), located in Troitsk, is approximately at the same latitude as the SRRFI ionosonde at a distance of about 560 km from the heating stand.

The ionosonde of the V.N. Karazin Kharkiv National University (Gaidary station, Ukraine) is located in the Radio-Physical Observatory of the V.N. Karazin Kharkiv National University (the village of Gaidary near Kharkiv). Its distance from the stand “Sura” is about 960 km. This ionosonde is approximately the same longitude as the IZMIRAN ionosonde.

The ionospheric station “Pruhonice” (Pruhonice, Czech Republic) is located at the latitude of the V.N. Karazin Kharkiv National University. The ionosonde dislocation made it possible to study the dependence of large-scale disturbances on the latitude, longitude, and distance from the heating stand to the instruments of observation.

The ionograms of the stations “Toitsk” (Moscow) and “Pruhonice” (Pruhonice) are presented at the website http://ulcar.uml.edu/Didbase/. The error in digitizing the frequency and effective altitude on the ionograms was about 50 kHz and 5 km, respectively.

5.4. Observational Results

We describe the results of experiments made during August 27–30, 2012. The day of August 27 was chosen as the reference day. On this day, the “Sura” stand was

turned on in the evening (from 17:00 to 18:30 (hereinafter UT)) in the mode of 5 min – transmission, 5 min – pause ([+5 min; –5 min]). As it turned out, this mode of the stand operation in the evening was not accompanied by noticeable disturbances of the ionosphere at distances of 560–2200 km from the stand. For other days, a search was made for the effects associated with the operation of the heating stand.

5.4.1. Examples of Ionograms

An example of an ionogram registered in Vasilsursk village on August 29, 2012 at 09:45 shown in Fig. 5.1. It is seen that an ionized layer (Es-layer of type C) with critical frequencies f_oEs = 2.6 and f_xEs = 3.5 MHz appeared in the lower ionosphere. The virtual altitudes of the layer varied within 120–160 km, and the actual altitudes varied from about 110 to 130 km. This ionogram was obtained shortly after the end of the heating of the ionosphere in the mode [+30 min; –30 min]. No similar layer was observed on the previous and subsequent time intervals.

On the same day, on ionograms from Troitsk obtained in the time interval 14:31–15:31, in addition to E-layer, layer Es of type C with 3.1–3.2 MHz in the range of effective altitudes of 120–160 km was also observed (Fig. 5.2). In this time interval, the heating stand transmitted in the mode [+30 min; –30 min].

In addition to E-layer, Es-layer type C was observed in Troitsk on August 30, 2012 at 14:16 (Fig. 5.3), as well as at 15:16–15:31. Critical frequencies of about 3.4 and 3.5 MHz were detected. The layers were observed in approximately the same altitude range (about 110–130 km). It is known that the Es-layer of type C is formed, as a rule, due to additional ionization, which was caused by the electron precipitation [1].

The search for layers of additional ionization at altitudes $z' \leq 110$ km should be carried out by looking at the values of the minimum observed frequency on ionograms (f_{min}). The following sections of work are devoted to that.

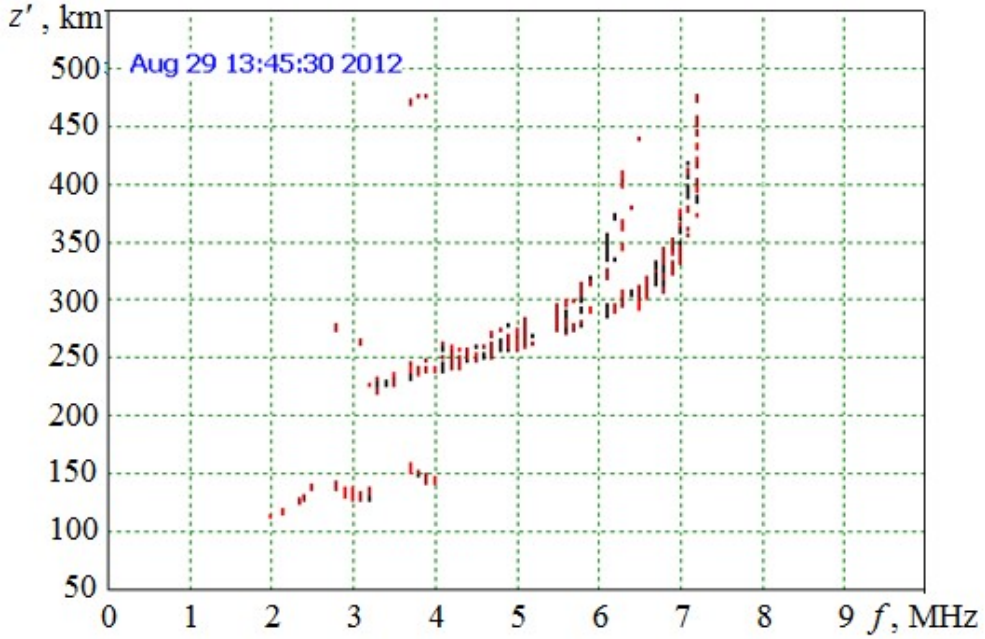

Fig. 5.1. The ionogram with a sporadic layer of type C obtained on August 29, 2012 at 09:45:30 in Vasilsursk village

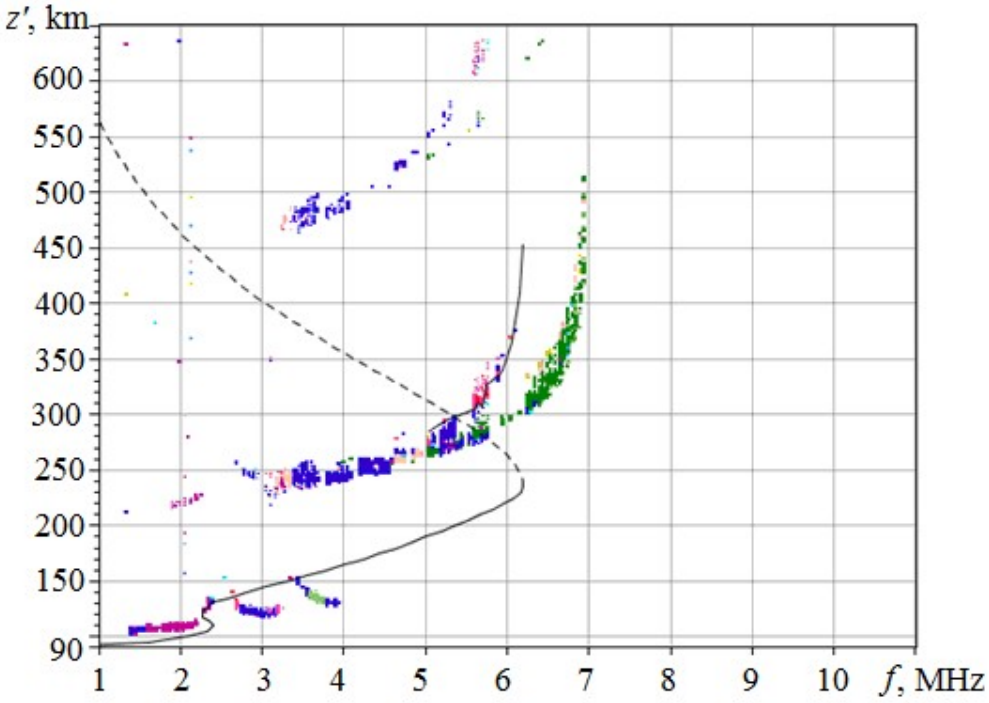

Fig. 5.2. The ionogram with a sporadic layer of type C obtained on August 29, 2012 at 14:31 in Troitsk city

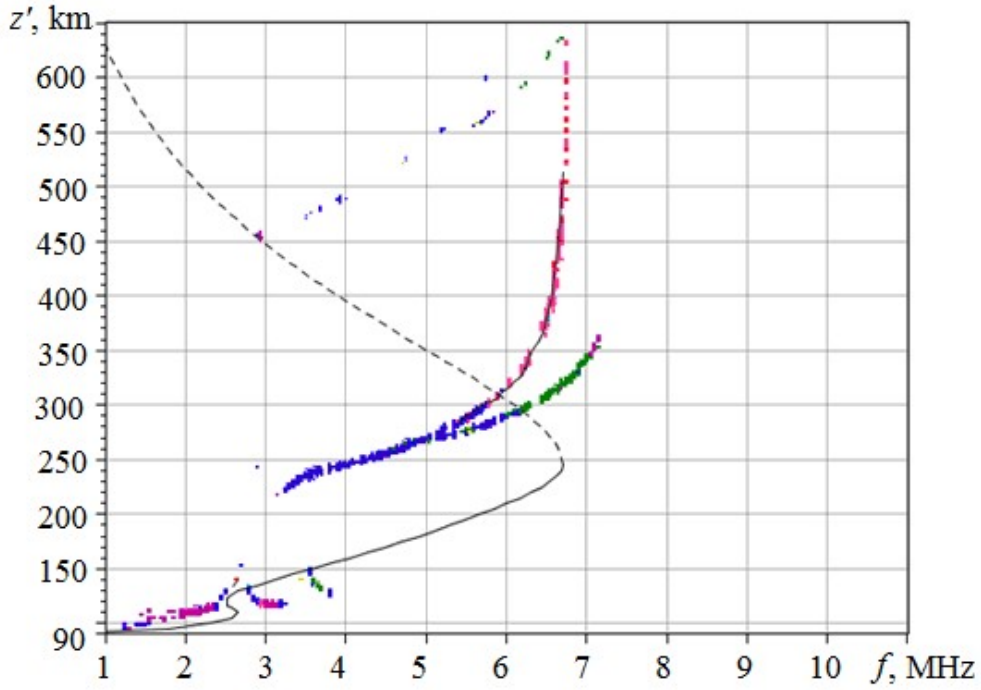

Fig. 5.3. The ionogram with a sporadic layer of type C obtained on August 30, 2012 at 14:16 in Troitsk city

5.4.2. Variations in f_{min} on August 27, 2012

The temporal variations of the minimum observed frequency f_{min} for the four above-mentioned ionosondes are shown in Fig. 5.4. For the "Vasilsursk" ionosonde, during the day (06:00–10:00) $f_{min} \approx 1.8$–2 MHz. From 10:00 to 14:00, there was an increase in f_{min} to 2.3 MHz. In the time interval 14:00–22:00, f_{min} values were close to 1.6 MHz. After 22:00, there was a gradual increase in f_{min} to about 2 MHz.

For the "Troitsk" ionosonde, the frequency f_{min} varied between 1.4 and 1.8 MHz during the day. Before sunset, f_{min} decreased to 1.3 MHz for approximately 1.5 hours. After that, for a long time (from 15:00 to 24:00), $f_{min} \approx 1.6$ MHz.

Analysis of ionograms from the ionosonde in the village Gaidary showed that from 06:00 to 08:00, f_{min} fluctuation gradually increased from 1.9 to 2.1 MHz. Approximately during 08:00–10:00, the frequency f_{min} was 2.2 MHz. After 10:00, f_{min} decreased to nighttime values of approximately 1.4–1.6 MHz.

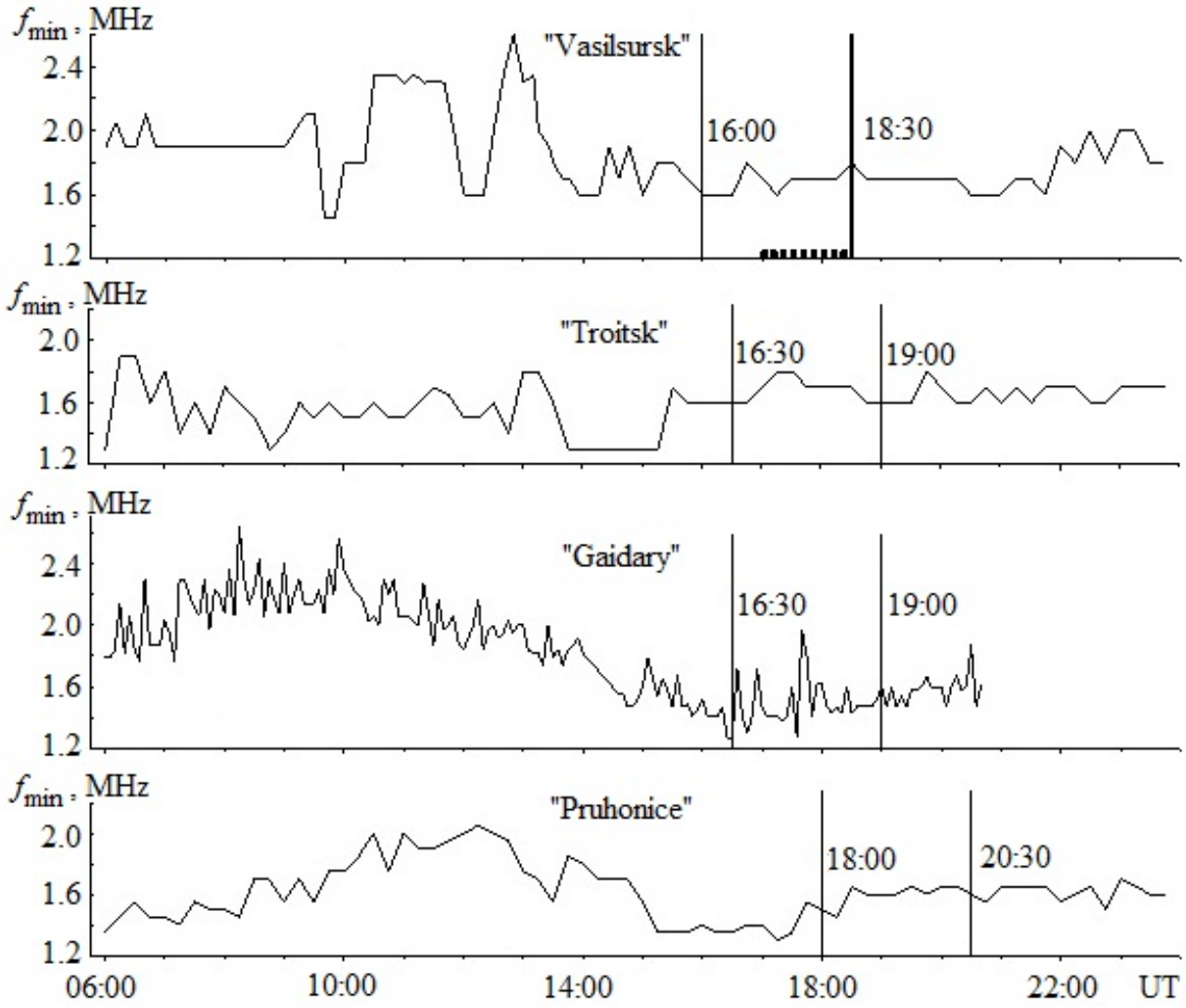

Fig. 5.4. Temporal variations in f_{min} on August 27, 2012 for four ionosondes. Vertical lines show the moments of sunset at ground level and at altitude of 400 km

For the “Pruhonice” ionosonde, f_{min} increased from 1.4 to 2 MHz in the time interval 06:00–10:00. Then, for the next 3–4 hours, it remained approximately constant. From 14:00 to 15:00, it decreased from 1.8 to 1.3 MHz. Then, there was an increase in f_{min} from 1.3 to 1.6 MHz and the subsequent stabilization in the time interval 18:30–24:00.

5.4.3. Variations in f_{min} on August 28, 2012

Temporal variations in f_{min} on August 28, 2012 are shown in Fig. 5.5. On the ionograms obtained in Vasilsursk, $f_{min} \approx 2$ MHz in the time interval 06:00–09:45. Approximately from 10:00 to 12:00, $f_{min} \approx 2.4$ MHz. From 12:00 to 15:00, f_{min} varied in the range of 1.6–2.0 MHz. In the time interval 15:15–18:00, f_{min} was minimal (about 1.6 MHz). Then, f_{min} fluctuated in the range of 1.7–1.9 MHz.

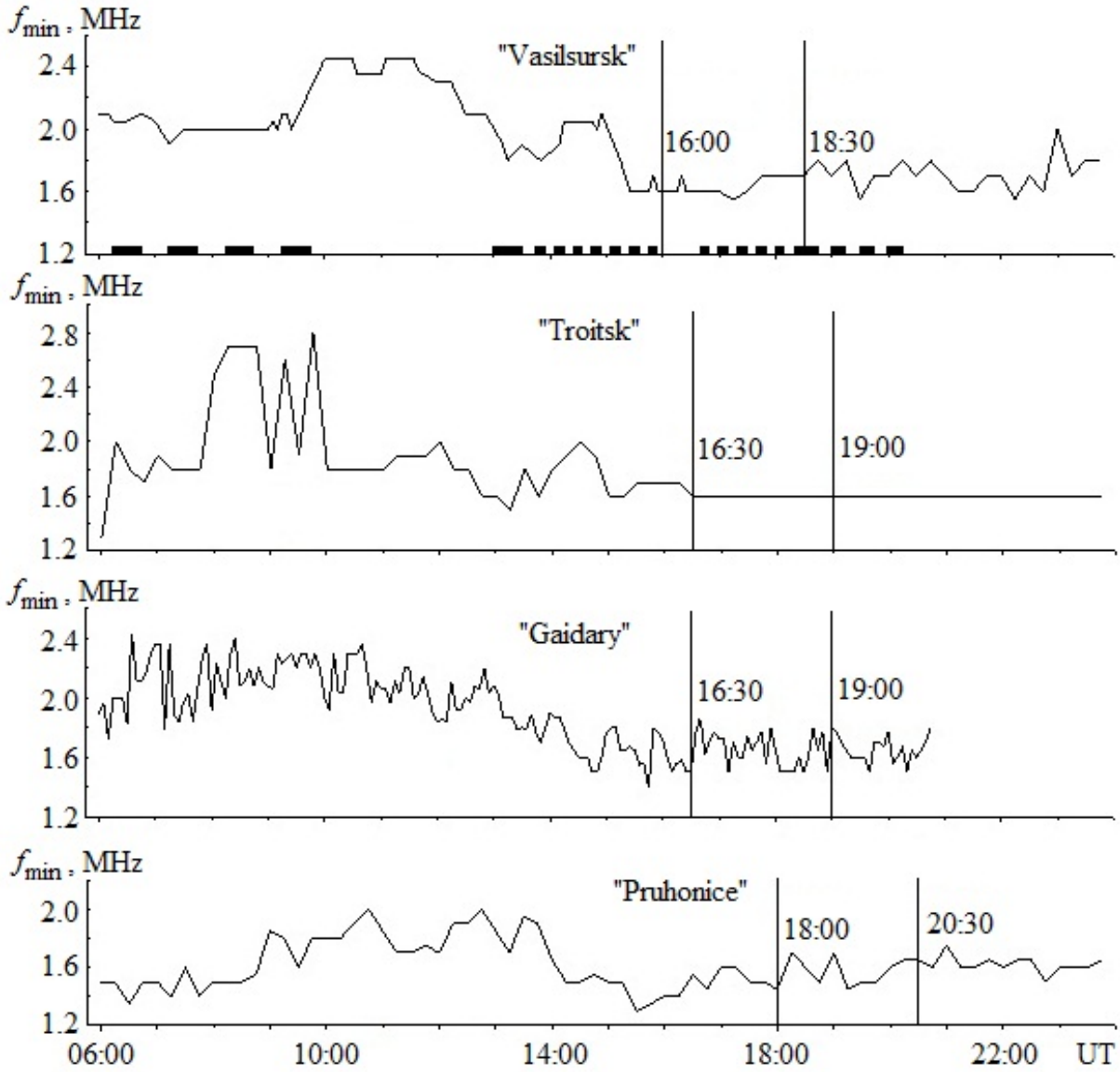

Fig. 5.5. Temporal variations in f_{min} on August 28, 2012 for four ionosondes. Vertical lines show the moments of sunset at ground level and at altitude of 400 km

The behavior of the f_{min} for the ionosonde in Troitsk was as follows. In the time interval 06:00–07:45, $f_{min} \approx 1.8$ MHz. From approximately 08:00 to 10:00, f_{min} bursts of up to 2.7 MHz were observed. Then, for 2 hours, $f_{min} \approx 1.8$ MHz. During 12:00–13:00, there was a drop in f_{min} from 1.8 to 1.6 MHz, and then, over the next hour, there was an increase to 2.0 MHz. From 14:00 to 14:30, f_{min} decreased from 2.0 to 1.6 MHz. Then, for 9 hours, it remained 1.6 MHz.

For "Gaidary" ionosonde, f_{min} increased from the nighttime values 1.6 MHz to daytime values of about 2.2 MHz. From approximately 06:30 to 10:30, f_{min} fluctuations varied from 2.0 to 2.4 MHz. In the time interval 10:30–14:30, a decrease in f_{min} from 2.2 to 1.6 MHz was observed. After that, the frequency f_{min} fluctuated in the range of 1.5–1.7 MHz.

Variations of $f_{min}(t)$ in Pruhonice were as follows. From 06:00 to 09:00, f_{min} increased from 1.4 to 1.8 MHz. In the time interval 09:00–14:00, it fluctuated in the range of 1.7–2.0 MHz. From approximately 14:00 to 15:30, the f_{min} dropped from 1.8 to 1.3–1.4 MHz. Next, the f_{min} values fluctuated in the range of 1.5–1.6 MHz.

5.4.4. Variations in f_{min} on August 29, 2012

Quasi-periodic variations of f_{min} with a quasi-period $T \approx 1$ h were observed on "Vasilsursk" ionosonde from 06:00 to 13:00 (Fig. 5.6). The f_{min} values varied from 2 to 2.4 MHz. After 13:00, there was a decrease in f_{min} to 1.6–2.0 MHz. From 15:00 to 22:00, $f_{min} \approx 1.6$ MHz.

For the ionosonde in Gaidary, the fluctuations of f_{min} values increased initially from 1.9 to 2.5 MHz. After 09:00, f_{min} decreased on average from 2.5 to 1.4 MHz. Individual f_{min} bursts had an amplitude of 0.2–0.3 MHz.

Observations on the ionosonde in Troitsk showed that during time interval 07:00–11:00, the values of f_{min} varied according to the quasi-periodic law with $T \approx 1$ h from 1.8 to 2.8–3.2 MHz. From 11:00 to 15:00, f_{min} fluctuations decreased from 1.8 to 1.4 MHz. Approximately from 16:00 to 24:00, $f_{min} \approx 1.6$ MHz.

As see from the ionograms obtained in Gaidary from 06:00 to 08:00, the average value of f_{min} increased from 1.9 to 2.2 MHz. In the time interval from 06:30 to 10:30, f_{min} bursts from 2.0 to 2.2–2.4 MHz were observed. On average, f_{min} was 2.0–2.1 MHz.

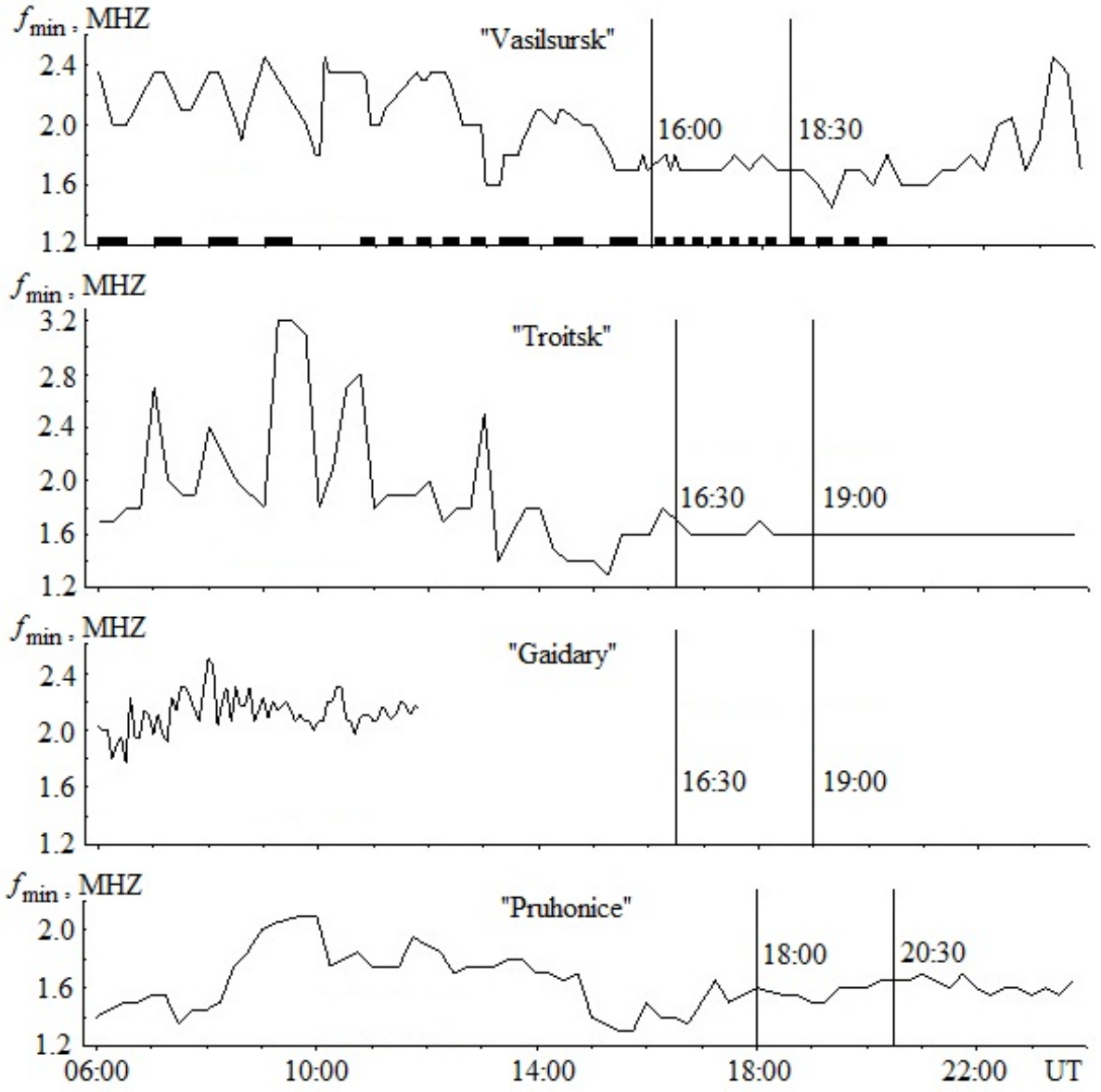

Fig. 5.6. Temporal variations in f_{min} on August 29, 2012 for four ionosondes. Vertical lines show the moments of sunset at ground level and at altitude of 400 km

For “Pruhonice” ionosonde, from 06:00 to 09:00, f_{min} increased from 1.4 to 1.8–2.0 MHz. During 09:00–15:00, the f_{min} values gradually decreased from 2.0 to

1.6 MHz. In the interval 13:00–14:00, f_{min} took the minimum value equal to 1.3–1.4 MHz. From 15:00 to 22:00, f_{min} was 1.6 MHz.

5.4.5. Variations in f_{min} on August 30, 2012

Observations by the ionosonde in Vasilsursk showed that from 06:00 to 10:00, f_{min} was 2.4 MHz (Fig. 5.7). In the time interval 10:00–16:00, there was a sporadic Es-layer. Its occurrence was accompanied by bursts of f_{min} from 2.4 to 2.8 MHz and from 1.6 to 2.4 MHz.

From 16:00 to 22:00, f_{min} was 1.6 MHz. In the time interval 22:00–24:00, there were f_{min} bursts up to 2.4 MHz.

In Troitsk, the values of f_{min} increased on average from 1.6 to 2.0 MHz in the time interval 06:00–07:00. From 07:30 to 10:00, f_{min} bursts from 1.8 to 2.8–3.0 MHz were observed. From 10:00 to 13:00, f_{min} was 1.6–2.2 MHz. At around 14:00, the minimum values of $f_{min} \approx 1.3$ MHz were observed. From 15:00 to 24:00, f_{min} was 1.6 MHz.

On ionograms registered in Pruhonice, f_{min} increased from 1.4 to 2.4 MHz in the time interval 06:00–09:00. During 09:00–10:00, the f_{min} burst of 1.8 to 2.4 MHz was observed. From 10:00 to 15:00, f_{min} was 1.8 MHz. From 17:00 to 18:00, the minimum value of $f_{min} \approx 1.4$ MHz was observed. In the time interval 18:30–24:00, f_{min} was 1.6 MHz.

5.5. Discussion of Observations Result

5.5.1. Variations in f_{min} in Vasilsursk

The largest variations in f_{min} were observed in the time interval 10:00–12:00 on August 28, 2012 (see Fig. 5.5). The increase of f_{min} reached 0.4 MHz. On the reference day at about the same time, the increase of f_{min} was also about 0.4 MHz. The f_{min} increase on August 28, 2012 was preceded by the ionospheric plasma heating

by powerful radio transmission of the stand “Sura” in the mode [+30 min; –30 min]. A comparison of the f_{min} variations on August 27 and 28 shows that the ionosphere heating did not affect their magnitude significantly.

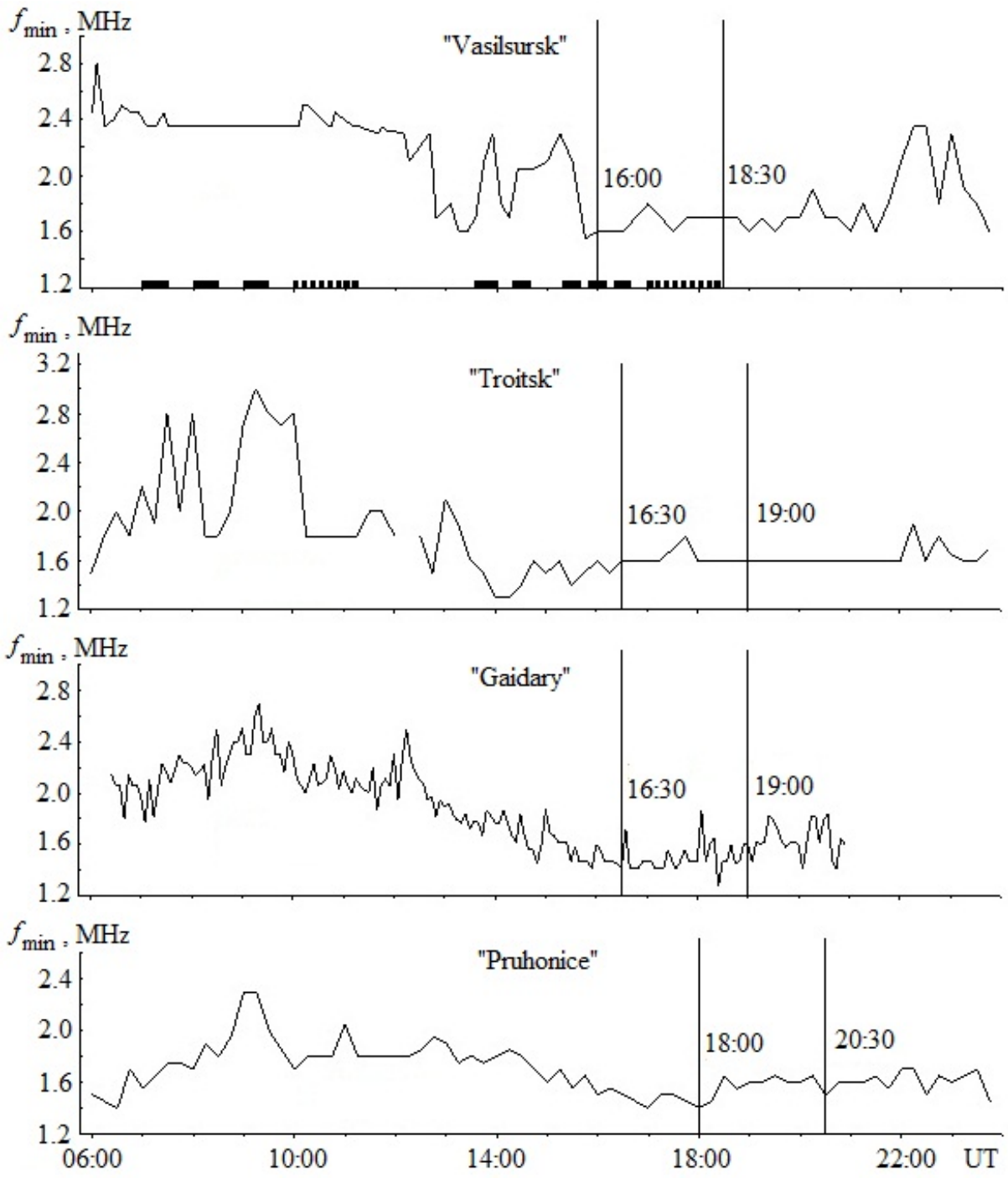

Fig. 5.7. Temporal variations in f_{min} on August 30, 2012 for four ionosondes. Vertical lines show the moments of sunset at ground level and at altitude of 400 km

On August 29, 2012, from 07:00 to 11:00, quasi-periodic variations of f_{min} with a quasi-period of $T \approx 1$ h were observed (see Fig. 5.6). The magnitude of the f_{min} bursts reached 0.4 MHz, and the value of f_{min} increased to 2.4 MHz. This behavior of the f_{min} began approximately 1 hour after the inclusion of periodic ionosphere heating in the mode [+30 min; –30 min]. On the reference day in the same time interval, the f_{min} remained at about 2.0 MHz. The frequency of bursts and their delay time in relation to the moment of turning on the stand evidence in favor of that bursts are caused by the stand operation.

On August 30, during the daytime (from 13:30 to 15:30), f_{min} bursts of up to 0.6–0.8 MHz were accompanied by the appearance of the Es-layer. From 06:00 to 10:00, the Es-layer was observed. This did not allow detecting the f_{min} increasing to 2.4 MHz (see Fig. 5.7). On the reference day August 27 (as well as August 31) f_{min} was about 2.0 MHz in the same time interval. The increase of f_{min} from 2.0 to 2.4 MHz occured during the operation of the heating stand in the mode [+30 min; –30 min].

Variations in f_{min} during the operation of the stand “Sura” in other modes and at higher frequencies did not exceed natural fluctuations.

5.5.2. Variations in f_{min} in Troitsk

Consider the variations of f_{min} on August 28, 2012. In the time interval 08:00–10:00, bursts of f_{min} values from 1.8 to 2.6 MHz were observed (see Fig. 5.5). They followed the turning on of the heating stand in the mode [+30 min; –30 min]. The bursts were repeated with a quasi-period $T = 30$ min (the first two of them merged).

A significant increase in f_{min} from 1.6 to 2.0 MHz also occurred in the time interval 14:00–15:00. At this time, the stand transmitted in the mode [+10 min; –10 min]. The f_{min} increasing ended approximately one hour before the cessation of the stand transmission.

On August 29, 2012 four activations of the heating stand in the mode [+30 min; –30 min] were accompanied by four strong f_{min} bursts from 1.8 to 2.4–3.2 MHz

(see Fig. 5.6). The delay time of these bursts in relation to the moments of turning on of the heating stand was about 1 h.

The subsequent turning on of the stand in other modes led to only insignificant f_{min} bursts (0.2–0.4 MHz). The quasi-period $T \approx 1$ h was also detected for these bursts.

On August 30, 2012 after the turning on of the heating stand in the mode [+30 min; –30 min], there were strong f_{min} bursts from 1.8 to 2.8 MHz with a quasi-period $T \approx 30$ min (see Fig. 5.7). During the time interval 08:30–10:00, a general f_{min} increasing rom $\Delta f_{min} \approx 1$ MHz was observed.

Subsequent turning on of powerful radio transmission in other modes led to slight variations in f_{min}.

5.5.3. Variations in f_{min} in Gaidary

After turning on the heating stand on August 28, 2012 in the mode [+30 min; –30 min], quasi-periodic ($T \approx 1$ h) f_{min} bursts from 1.8–2.0 MHz to 2.4 MHz were observed (see Fig. 5.5). Other turning on of the stand in other modes led to only insignificant variants of f_{min}, which were comparable to natural fluctuations. A notable f_{min} increase from 1.8 to 2.2 MHz occurred from 14:00 to 17:00. The value of the quasi-period T was ~ 1 h. The disturbance delay time was about 1 h (the stand was transmitting from 13:00 to 16:00). After 17:00, the effects caused by the movement of the evening terminator occurred.

Turning on the heating stand on August 29, 2012 in the mode [+30 min; –30 min] was accompanied by f_{min} bursts from 2.0 to 2.3–2.4 MHz (see Fig. 5.6). The delay time of the disturbances observed in the time interval 07:00–10:30, in relation to the moments of turning on the heating stand (from 06:00 to 09:30) was about 1 h. The quasi-periods of bursts were 0.5 and 1 h.

On August 30, the heating stand was turned on at 07:00, 08:00, and 09:00 for 30 min. Notable f_{min} bursts lasting about 15 min occurred at approximately 08:00, 09:00, and 10:00 (see Fig. 5.7). Their amplitude was 0.2–0.4 MHz. From 10:00 to 11:15, the stand was operated in the mode [+5 min; –5 min]. Approximately 10 min

after turning on of the stand, there were weak f_{min} bursts with an amplitude of about 0.2 MHz and a period of $T \approx 15$ min. In the time interval 12:00–14:00, f_{min} increased from 1.9 to 2.4 MHz.

Other turning on the heating stand with other modes of the transmission were accompanied by insignificant f_{min} variations which could be caused by natural sources.

5.5.4. Variations of f_{min} in Pruhonice

Variations in f_{min} on August 28, 2012 generally did not differ much from the variations on the reference day on August 27, 2012 (compare Fig. 5.4 and Fig. 5.5). Note, that on August 28, 2012, quasi-periodic f_{min} bursts were observed in the f_{min} variations in the time interval 08:45–14:00. Their amplitude reached 0.3–0.4 MHz, and the quasi-period was close to 1 h. The delay time of the disturbances was about 2.5 h, and their duration was about 5 h.

On August 29, 2012, f_{min} bursts were observed at approximately the same times as by the ionosonde in Troitsk (see Fig. 5.6). The magnitude of the bursts was 0.2–0.4 MHz. The values of f_{min} in the time interval 09:00–10:00 and 11:30–10:30 exceeded the values of f_{min} in the same time interval on the reference day by 0.3–0.4 MHz.

The variations of $f_{min}(t)$ on August 30, 2012 were generally similar to variations of the same dependence on the reference day (compare Fig. 5.4 and Fig. 5.7). However, there were some differences. In the time interval from 08:30 to 09:30, there was a surge of f_{min} from 1.8 to 2.4 MHz (see Fig. 5.7). At about the same time, f_{min} bursts were observed by the Troitsk and Gaidary ionosondes.

Two other f_{min} bursts with amplitudes of about 0.3 and 0.2 MHz were recorded at about 11:00 and 13:00.

If the first and second bursts are caused by exposure to powerful radio transmission, they are delayed relative to the time of the stand turning on (at 08:00 and 10:00) by about 1 h. The third surge most likely had a natural origin.

Thus, the turning on of a powerful stand “Sura” had little effect on the nature of the f_{min} variation registered in Vasilsursk. For the ionosonde in Troitsk, these variations were the largest, the values of Δf_{min} reached approximately 1 MHz. At the same time, for the “Gaidary” and “Pruhonice” ionosondes, they did not exceed 0.4–0.5 and 0.3–0.4 MHz, respectively. In Vasilsursk on August 29, 2012, the amplitude of quasi-periodic bursts were also about 0.4 MHz.

Significant variations in f_{min}, apparently, are caused by the increase in the probing radio wave absorption as a result of the electron density N increase. Next, we estimate the magnitude of the N perturbation in the lower ionosphere.

5.5.5. Results of Calculations

With stable parameters of ionosonde, variations in f_{min} can be caused by variations in the electron density N and the collision frequency ν in the lower ionosphere. Perturbations ν are significant within the transmission pattern of the antenna of the heating stand, where there is a significant heating of electrons. The precipitation of electrons from the magnetosphere is also accompanied by some increase in the frequency ν. However, this will be neglected when estimating the increase in the density N.

Broadband anomalous attenuation of radio waves was significant only near the resonant frequencies, but not near f_{min}. Therefore, such a weakening was also not taken into account.

It is necessary to point out the fact that the sensitivity of different ionosondes is different. This circumstance was mitigated by the fact that the information parameter used was actually the ratio f_{min}/f_{min0}, which is practically independent of the sensitivity of receiving equipment.

Under a number of simplifying assumptions, the relationship of the average altitude of the lower ionosphere in relation to increase in the electron density $n = \langle N/N_0 \rangle$ with f_{min} [9]:

$$n = n_\infty \left(1 + \frac{\ln B}{2K_0} \right), \tag{5.1}$$

where

$$n_\infty = \left(\frac{f_{\min} + f_B}{f_{\min 0} + f_B} \right)^2, \tag{5.2}$$

$$B = \frac{z_{r0}}{z_r} \left(\frac{f_{\min}}{f_{\min 0}} \right)^{1+0.5\beta}, \tag{5.3}$$

$n_\infty = n\big|_{2K_0 \to \infty}$, $f_B \approx 1.4$ MHz – electron hyrofrequency, z_{r0} and z_r – the reflection height of the probing radio wave with frequencies $f_{\min 0}$ and $f_{\min}$, $\beta \approx 2.5$ – indicator of the degree as a function of radio noise power P_n on frequency (it was assumed that $P_n \sim f^{-\beta}$), the integral absorption coefficient K_0 was estimated based on ionospheric models).

An increase of the minimum of the observed frequency from $f_{\min 0}$ to $f_{\min}$ is caused by an increase in n. The results of calculations n using relations (5.1), (5.2) and (5.3) for the four ionosondes are given in Table. 5.3.

Table 5.3. The average increase of the electron density in the lower ionosphere

Ionosonde	$f_{\min 0}$, MHz	$f_{\min}$, MHz	$n = \langle N/N_0 \rangle$	Notes
"Vasilsursk"	2.0	2.4	1.4	At the level of natural variations
"Troitsk"	1.8	3.2	3	The biggest variations
"Gaidary"	2.0	2.4	1.4	Moderate variations
"Pruhonice"	1.6	1.9	1.3	Moderate variations

It was assumed that $z_r \approx z_{r0}$. For morning and afternoon, it was assumed that K_0 was 0.5 and 0.75, respectively. The Table. 5.3 shows that the largest N changes in the lower ionosphere was in Troitsk. Above this ionosonde, the density N increased on average in height up to 3 times. This parameter over the "Gaidary" and "Pruhonice" ionosondes increased 1.4 and 1.3 times, respectively. There was an insignificant

increase in the N over the "Vasilsursk" ionosonde on August 28 and 30, 2012. At the same time, on August 29, 2012, the density N increased by 1.3–1.4 times.

The question arises, was the increase in n and, hence, in the N caused by the diurnal course of $N(t)$ or by modification of the ionosphere by powerful radio transmission? The fact is that the effect of powerful radio transmission on the ionosphere in the mode [+30 min; –30 min] occurred in the time interval from 06:00 to 09:30, i.e. during the transition from morning to daytime. It seems that both factors contributed to the increase in the density N. This is evidenced by the following arguments.

The first, when a powerful radio transmission exposed to the ionosphere at a fairly low frequency (f = 4785 kHz) in the mode [+30 min; –30 min] with an effective power $PG \approx$ 75–80 MW, the electron temperature T_e and the electron density N at the altitudes of the ionospheric dynamo region ($z \approx$ 100–150 km) increase practically by a jump (the T_e for a time of ~10^{-3}–10^{-2} s, and the N for a time of ~10–10^2 s) by 2–3 and 1.4–1.7 times, respectively.

It leads to a sharp change in the conductivity of the ionospheric plasma, and hence to the violation of the interaction between the subsystems in the system EAIM. As a result of the impact on one of the subsystems, high-energy (with energy $\varepsilon_e \sim$ 10–100 keV) electrons are redistributed at pitch angles. Some part of the electrons falls out of the magnetosphere (more precisely, from the inner radiation belt) into the D and E ionospheric regions. It leads to an increase in the absorption of the probing radio waves and to an increase in $f_{\min}$ on the ionograms.

The interaction mechanism of subsystems in the EAIM system is described in more detail in the works [1, 121]. A detailed theory of the mechanism has yet to be developed.

The second, during the operation of the heating stand in other modes (at higher frequencies), the efficiency of ionospheric plasma perturbation in the dynamo region decreased, and hence the degree of ionosphere-magnetosphere interaction decreased, which ultimately led to a decrease in n.

For the same reasons, a significant increase in the N at night is was not possible.

The third, f_{min} bursts occurred more frequently with a period of 1 h, less frequently with a period of 0.5 h (the transmission mode of the heating stand was [+30 min; –30 min]).

The fourth, the magnitude of the *N* perturbations decreased with increasing distance from the heating stand.

It remains unclear why the *N* perturbation was small or was caused only by natural drivers on August 28 and 30, 2012 in the village Vasilsursk. Probably, this is because of the development of *N* perturbations was distant from the transmission pattern of the ionosonde "Vasilsursk", with the drift of magnetospheric electrons on the geomagnetic shell and the absence (low intensity) of electron precipitation directly above the heating stand. The second reason may be an increase of *N* and ν, and hence f_{min} within the irradiated region. Against this background, the effect of electron precipitation is masked. Finally, the features of the equipment (sensitivity of the ionosonde) cannot be ruled out. In any case, this issue needs further investigation.

In conclusion, we add that these results generally confirm the results of earlier studies [108–114, 127, 128] and the results obtained by the incoherent scatter radar in Kharkiv [120]. In [120], *N* perturbations at the heights of the E region of the ionosphere were described, which were probably caused by the electron precipitation from the inner radiation belt too.

5.5.6. Estimation of Electron Flowes

Based on the method described in works [107, 120, 121], we estimate the flux density Π_e of high-energy ionizing electrons precipitated from the magnetosphere (from the inner radiation belt). Change of the ionization rate

$$\Delta q = \alpha N^2 - \alpha_0 N_0^2 \approx \alpha_0 N_0^2 \left(n^2 - 1 \right), \tag{5.4}$$

where $\alpha \approx \alpha_0 \approx 2 \cdot 10^{-13}$ $m^3 \cdot s^{-1}$ – the recombination coefficient of electrons with molecular ions, $n = \langle N/N_0 \rangle$, *N* and N_0 – the electron density in the disturbed and quiet lower ionosphere. Given the expression (5.4), we obtain the following:

$$\Pi_e = 2\frac{\varepsilon_i}{\varepsilon_e}\Delta z \Delta q = 2\frac{\varepsilon_i}{\varepsilon_e}\Delta z \alpha_0 N_0^2 \left(n^2 - 1\right), \qquad (5.5)$$

where ε_i = 35 eV – energy expended on one act of ionization, Δz – thickness of the layer with additional ionization, ε_e – electron energy.

We will assume $z \approx 90$ km, $N_0 \approx 10^{10}$ m^{-3}, $n = 2$, $\Delta z \approx 10$ km, $\varepsilon_e = 100$ keV and obtain from (5.5) that $\Pi_e \approx 6.3 \cdot 10^8$ m^{-2}s^{-1}. This flow density is not too high. For comparison the background value of Π_e in the mid-latitudes is $\sim 10^5$ m^{-2}s^{-1} [169]. During geospace storms accompanied by the precipitation of electrons from the inner radiation belt, Π_e increases by several orders of magnitude (to 10^8–10^9 m^{-2}s^{-1}) [169–171]. In this sense, the effects of powerful radio transmission can stimulate geophysical effects similar to those that occur during geospace storms. During storms, the energy flux density entering the ionosphere of high- and mid-latitudes is of the order of 10^{-4}–10^{-3} and 10^{-5}–10^{-4} J·m^{-2} s^{-1}, respectively. The flux density of powerful radio transmission of the "Sura" stand is close to 10^{-5}–10^{-4} J·m^{-2} s^{-1}. It is seen that these flows are comparable.

In general, flows of high-energy particles from the radiation belt should lead to the appearance of an artificial aurora. Estimates have shown that the change in luminosity intensity is weak, on the verge of sensitivity of existing photometers [1].

The possibility of stimulated processes in the EAIM system is also evidenced by the results of [171].

5.6. Experiment of 2013

5.6.1. Methods of Analysis

The temporal variations of the F2 layer critical frequency during the operation of the heating stand and in the reference time intervals were analyzed. As a possible response to the turn on/off of the stand, the operating modes of which are shown in Table 5.4, we considered the positive deviations (bursts) of the frequency f_oF2 relative to their background, which did not always coincide with the trend position.

At time intervals between turning on, less than 15 min, the trend smoothed the bursts, which partially masked the effect of positive bursts. Aperiodic positive deviations of f_oF2 would mean bursts of N, which would confirm the hypothesis expressed above. The trend was calculated using a fifth-degree polynomial. Increasing the degree of the polynomial did not lead to a significant change in the trend position. The amplitude of the bursts was estimated by the maximum deviation of f_oF2 values from the burst base. The delay time of the disturbances relative to the moment of turning on of the stand was determined by the difference between the moments of the beginning of the burst and the turning on of the stand. The duration of disturbances was estimated by the number of the frequency foF2 samples multiplied by the time interval of ionogram removal (5 or 15 min).

Table 5.4. Operating modes of the heating stand “Sura”

Date	Time interval	Frequency, kHz	Effective power, MW	Operating mode
August 20, 2013	07:02 – 08:00	4785	55	[+5 min; –5 min]
	08:02 – 11:00	4785	55	[+15 min; –15 min]
	11:00 – 11:45	4785	55	Безупинно
	16:27 – 17:42	5828	120	[+5 min; –5 min]
August 21, 2013	07:00 – 07:50	4785	80	[+5 min; –5 min]
	08:15 – 13:30	4785	80	[+15 min; –15 min]
	14:00 – 14:20	5828	110	[+1 min; –1 min]
	14:20 – 15:50	5828	110	[+15 min; –15 min]
	15:55 – 16:08	5828	110	Carrying
	16:08 – 16:20	5828	110	[+1 min; –1 min]
	16:40 – 17:00	5828	110	[+1 min; –1 min]
	17:00 – 18:35	5828	110	[+5 min; –5 min]
	18:40 – 19:00	5828	110	[+1 min; –1 min]
	19:10 – 01:55	4300	70	[+15 min; –15 min]
August 22, 2013	07:00 – 08:00	4785	100	[+5 min; –5 min]

	08:46 – 09:01	4785	100	Carrying
	09:46 – 10:01	4785	100	Carrying
	10:46 – 11:01	4785	100	Carrying
	11:46 – 12:01	4785	100	Carrying
	12:46 – 13:01	4785	100	Carrying
	13:16 – 13:30	4785	100	Carrying
	14:00 – 14:20	4785	100	[+1 min; –1 min]
	14:30 – 16:00	4785	100	[+6 min; –6 min]
	16:00 – 16:20	4785	45	[+1 min; –1 min]
	16:40 – 17:00	4785	45	[+1 min; –1 min]
	17:00 – 18:30	4785	45	[+3 min; –7 min]
	18:40 – 19:00	4785	45	[+1 min; –1 min]
August 23, 2013	09:21 – 13:36	5828	40	[+15 min; –15 хв]
	13:50 – 14:21	5828	40	[+1 min; –1 min]
	14:31 – 16:00	5828	100	[+6 min; –6 min]
	16:01 – 17:30	5828	100	[+1 min; –1 min]
	17:31 – 18:30	5828	100	[+3 min; –7 min]
	18:40 – 19:00	5828	45	[+1 min; –1 min]
August 25, 2013	13:46 – 14:01	5828	100	Carrying
	16:01 – 16:16	4785	90	Carrying
	16:28 – 17:03	4785	90	[+5 min; –10 min]
	18:25 – 19:15	4785	90	[+10 min; –10 min]
August 26, 2013	14:22	5405	40	[+2 min, –3 min]
	14:27	5415	40	[+2 min, –3 min]
	14:32	5425	40	[+2 min, –3 min]
	14:37	5435	40	[+2 min, –3 min]
	14:42	5445	40	[+2 min, –3 min]
	14:47	5455	40	[+2 min, –3 min]
	14:52	5465	40	[+2 min, –3 min]
	14:57	5475	40	[+2 min, –3 min]
	15:02	5485	40	[+2 min, –3 min]
	15:07	5495	40	[+2 min, –3 min]
	15:12	5495	40	[+2 min, –3 min]

	15:17	5505	40	[+2 min, –3 min]
	15:22	5405	40	[+2 min, –3 min]
	15:27	5425	40	[+2 min, –3 min]
	15:32	5445	40	[+2 min, –3 min]
	15:37	5465	40	[+2 min, –3 min]
	15:42	5485	40	[+2 min, –3 min]
	15:47	5505	40	[+2 min, –3 min]
	16:12	5395	120	[+10 min, –10 min]
	16:14	5375	120	[+10 min, –10 min]
	16:17	5395	120	[+10 min, –10 min]
	16:26 – 18:00	5435	120	[+10 min, –10 min]
August 27, 2013	07:00 – 07:46	4785	80	[+5 min; –5 min]
	08:01 – 11:46	4785	80	[+15 min; –15 min]
	12:00 – 12:15	4785	85	Carrying
	13:00 – 13:15	4785	85	Carrying
	14:00 – 14:15	4785	85	Carrying
	14:39	5395	110	[+2 min; –2 min]
	14:43	5415	110	[+2 min; –2 min]
	14:47	5435	110	[+2 min; –2 min]
	14:51	5455	110	[+2 min; –2 min]
	14:55	5475	110	[+2 min; –2 min]
	14:59	5495	110	[+2 min; –2 min]
	15:03	5515	110	[+2 min; –2 min]
	15:07	5535	110	[+2 min; –2 min]
	15:11	5395	110	[+2 min; –2 min]
	15:15	5415	110	[+2 min; –2 min]
	15:19	5435	110	[+2 min; –2 min]
	15:23	5455	110	[+2 min; –2 min]
August 27, 2013	15:27	5475	110	[+2 min; –2 min]
	15:31	5495	110	[+2 min; –2 min]
	15:35 – 16:03	5515	110	[+2 min; –2 min]
	16:10 – 16:50	5455	110	[+10 min; –10 min]
August 28, 2013	06:00 – 11:15	4785	85	[+15 min; –15 min]

	12:00 – 12:15	4785	85	Carrying
	13:00 – 13:15	4785	85	Carrying
	13:39	5365	110	[+2 min; –2 min]
	13:43	5385	110	[+2 min; –2 min]
	13:47	5405	110	[+2 min –2 min]
	13:51	5425	110	[+2 min; –2 min]
	13:55	5445	110	[+2 min; –2 min]
	13:59	5465	110	[+2 min; –2 min]
	14:03	5465	110	[+2 min; –2 min]
	14:07	5485	110	[+2 min; –2 min]
	14:11	5505	110	[+2 min; –2 min]
	14:15	5525	110	[+2 min; –2 min]
	14:19	5545	110	[+2 min; –2 min]
	14:23	5365	110	[+2 min; –2 min]
	14:27	5405	110	[+2 min; –2 min]
	14:31	5445	110	[+2 min; –2 min]
	14:35	5485	110	[+2 min; –2 min]
	14:39	5525	110	[+2 min; –2 min]
	15:09 – 19:19	4544	70	[+10 min; –10 min]

5.6.2. Space Weather Conditions

On August 20, 21, and 27, 2013, there was a sharp increase of of the density n_{sw} of the solar wind approximately an order of magnitude for about 10 hours (Fig. 5.8*a*, 5.8*b*). The temperature variations T_{sw} reached $3 \cdot 10^5$ K. The increase in n_{sw} and T_{sw} led to bursts of the solar wind pressure, energy ε_A, inputed to the Earth's magnetosphere, and changes in the values of the indices AE, K_p, and D_{st} (see Fig. 5.8*a*, 5.8*b*).

The first magnetic storm began around 12:00 on August 20, 2013. Its sudden onset lasted until 02:00 on August 21, 2013. In the time interval 02:00–05:00, the main phase of the storm took place, for which $B_{z\ \min} \approx -9$ nT, $\varepsilon_{A\max} \approx 10$ GJ/s, $AE_{\max} \approx 600$ nT, $K_p = 4+$, $D_{st\ \min} = -45$ nT. Then, the storm recovery phase was recorded.

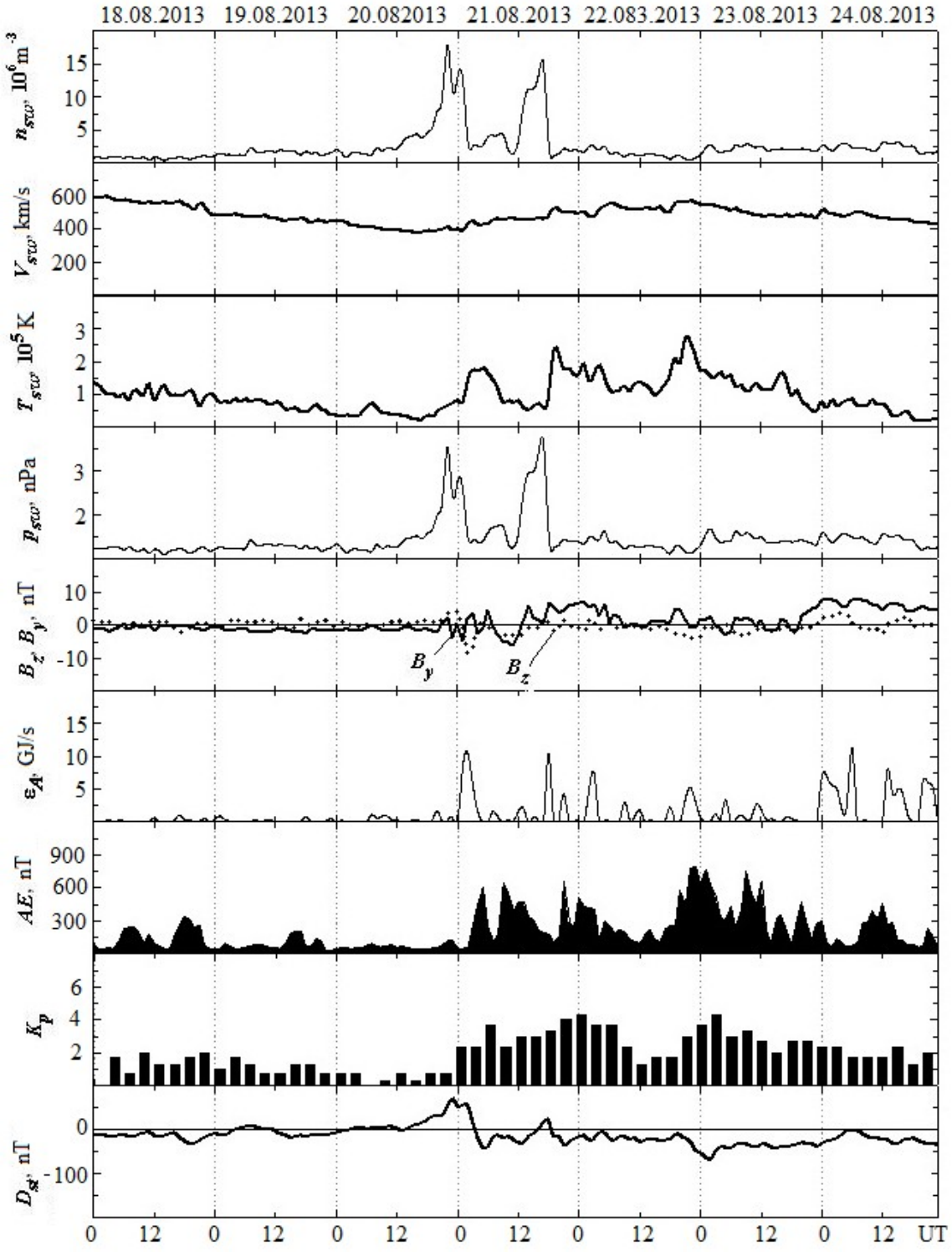

Fig. 5.8*a*. Temporal variations of solar wind parameters: density n_{sw}, radial speed V_{sw}, temperature T_{sw}, dynamic pressure p_{sw}, B_y and B_z-components (line and points) of IMF, calculated values of energy ε_A, transferred from solar wind in the magnetosphere per second, AE, K_p and D_{st} indeces during August 18–24, 2013 (data are available at the site http://wdc.kugi.kyoto-u.ac.jp)

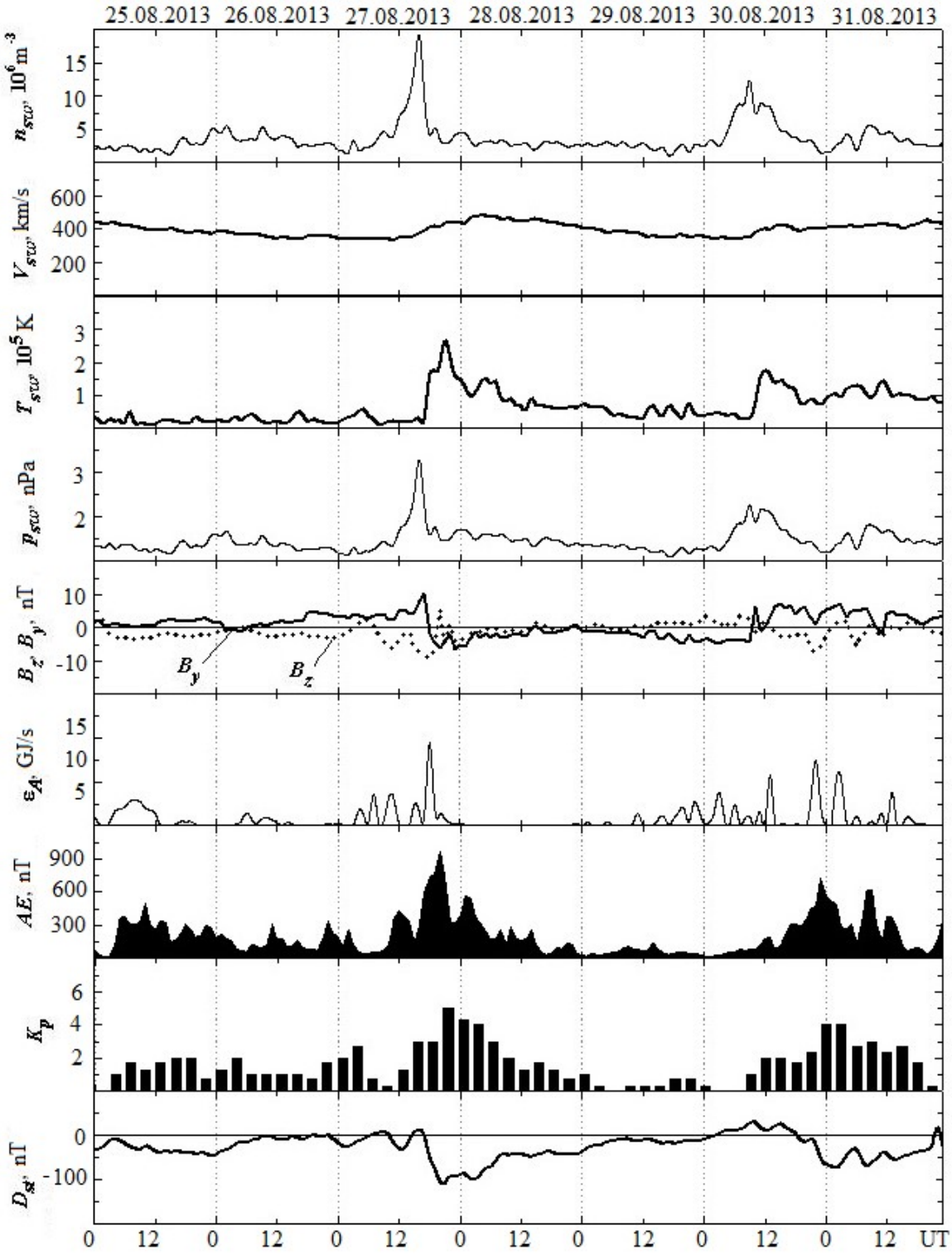

Fig. 5.8*b*. Temporal variations of solar wind parameters: density n_{sw}, radial speed V_{sw}, temperature T_{sw}, dynamic pressure p_{sw}, B_y and B_z-components (line and points) of IMF, calculated values of energy ε_A, transferred from solar wind in the magnetosphere per second, AE, K_p and D_{st} indeces during August 25–31, 2013 (data are available at the site http://wdc.kugi.kyoto-u.ac.jp)

The main phase of the next magnetic storm was observed in the interval from 18:00 on August 22, 2013 to 03:00 on August 23, 2013. Thus, $B_{z\ \min} \approx -5$ nT, $\varepsilon_{A\max} \approx 5$ GJ/s, $AE_{\max} \approx 750$ nT, $K_p = 4+$, $D_{st\ \min} = -70$ nT. The recovery phase lasted until the middle of the day on August 26, 2013.

The main phase of the third magnetic storm began at 16:00 and ended at 20:00 on August 27, 2013. For this storm, $B_{z\ \min} \approx -10$ nT, $\varepsilon_{A\max} \approx 10$ GJ/s, $AE_{\max} \approx 920$ nT, $K_{p\ \max} = 5$, $D_{st\ \min} = -110$ nT. The recovery phase lasted until 09:00 on August 29, 2013.

It is advisable to estimate the energy of magnetic storms according to the following equation[172]:

$$E_{st} = \frac{3}{2} E_m \frac{\left| D^*_{st\,\min} \right|}{B_0},$$

where $E_m = 8 \cdot 10^{17}$ J is energy of the dipole magnetic field of Earth, $B_0 \approx 3 \cdot 10^{-5}$ nT is the value of the induction of the geomagnetic field at the equator. Adjusted value

$$D^*_{st\,\min} = D_{st\,\min} - b p_{sw}^{1/2} + c\,.$$

Here $b = 5 \cdot 10^5$ nT/Pa$^{1/2}$, $c = 20$ nT, p_{sw} is the solar wind pressure in Pa. The power of the magnetic storm with the duration of the main phase ΔT is given by the obvious ratio:

$$P = E_{st}/\Delta T.$$

The main parameters describing the magnetic storm energy are given in Table 5.5 which shows that the energy of all the storms was about 10^{15} J, and power was 10^{11} W. Such storms, according to the classification [158], are moderate. On the one hand, they are able to bring the subsystems in the system Earth – atmosphere – ionosphere – magnetosphere in a metastable state. On the other hand, that is possible when the ionosphere is not very disturbed. All those circumstances create favorable conditions for studying the peculiarities of the interaction between the subsystems of the EAIM when the ionosphere is heated by the powerful radio transmission.

The most important parameter that characterizes geospace storms is the Akasofu energy function ε_A. It describes the amount of energy coming from the solar wind into

the EAIM system. During the analyzed storms, the values of ε_A did not exceed 10 GJ/s. This means that geospace storms were moderate [31, 158].

Table 5.5. Parameters of magnetic storms in August 2013

Parameter	August 21	August 22–23	August 27
$D_{st\,\min}$, nT	–45	–70	–110
p_{sw}, nPa	2.5	2.7	4.4
$D^*_{st\,\min}$, nT	–53	–76	–123
E, J	$2\cdot10^{12}$	$3\cdot10^{12}$	$5\cdot10^{12}$
Δt, h	3.5	6	4
P, W	$1.6\cdot10^{11}$	$1.4\cdot10^{11}$	$3.5\cdot10^{11}$

During the measurement campaign, both positive (PIS) and negative (NIS) ionospheric storms took place (Table 5.6). For the PIS, the values of the critical frequency f_oF2 and the electron density N in the maximum of the F2 layer increased in comparison with the values on the reference day August 25, 2013, and f_oF2 and N decreased for NIS. The increase in N did not exceed 50%, and its decrease did not exceed 40% (see Table 5.6). Most storms were minor in accordance with the classification [31, 158], and three of them were moderate (see Table 5.6).

5.6.3. Temporal Variations in the Critical Frequency Near Gaidary Village

On August 20, 2013, an increase in the critical frequency from 6.3 to 8 MHz was initially observed (Fig. 5.9*a*). After 07:30, there was a decrease of approximately 1 MHz which was followed by the increase in the time interval 09:30–15:00. After 16:00, there was a fairly rapid increase in f_oF2 by about 1.5 MHz. Slow variations of the critical frequency were accompanied by bursts of 0.15–0.28 MHz with duration of 5–10 min.

Table 5.6. The main parameters of ionospheric storms in August 2013

Date	Time interval	Storm type	Δf_oF2_{max}, MHz	N/N_0	Ionospheric index
August 21	09:00 – 10:00	PIS (Minor)	1.3	1.4	1.4
August 21	10:00 – 12:00	PIS (Minor)	1.6	1.5	1.7
August 21	12:00 – 15:00	NIS (Minor)	–1	0.8	1.1
August 22	08:00 – 20:00	NIS (Moderate)	–2.1	0.6	2.5
August 23	11:00 – 15:00	NIS (Minor)	–0.8	0.8	0.9
August 26	08:00 – 20:00	NIS (Moderate)	–2	0.6	2.4
August 27	08:00 – 18:00	NIS (Minor)	–0.8	0.8	0.9
August 28	10:00 – 15:00	NIS (Moderate)	–0.7	0.7	1.5

On August 21, 2013, a gradual increase in f_oF2 from 5.5 to 8.7 MHz was observed in the time interval 03:00–06:30. It was followed by a half-hour decrease in f_oF2 to 8.8 MHz (see Fig. 5.9*b*). Then, a rapid drop in f_oF2 to 7.2–7.3 MHz was registered. This value was observed from 10:00 to 15:00. There was an increase in f_oF2 values by more than 1 MHz from 15:00 to 18:00, and then, it decreased to the nighttime values. Both before and during the operation of the heating stand, bursts of f_oF2 from 0.10 to 0.30 MHz were observed. From approximately 14:40 to 16:10, quasi-periodic variations of f_oF2 with a period of T = 10 min and an amplitude of 0.10–0.12 MHz were recorded.

On the morning of August 22, 2013, a strong Es layer was observed, which shielded the F region of the ionosphere almost all the time (see Fig. 5.9*c*). In the time interval 06:00–15:00, the regular variations of f_oF2 did not exceed 0.6 MHz. f_oF2 bursts of 0.10–0.15 MHz with a duration of 10–15 min were superimposed on them.

On August 23, 2013, from 08:00 to 12:00, a decrease in f_oF2 by 0.8 MHz was observed (see Fig. 5.9*d*). In the time interval from 09:30 to 10:30, there was a burst of f_oF2 from 7.0 to 7.5 MHz. Slow variations of f_oF2 were superimposed by bursts of 0.15–0.23 MHz with a duration of 10–15 min.

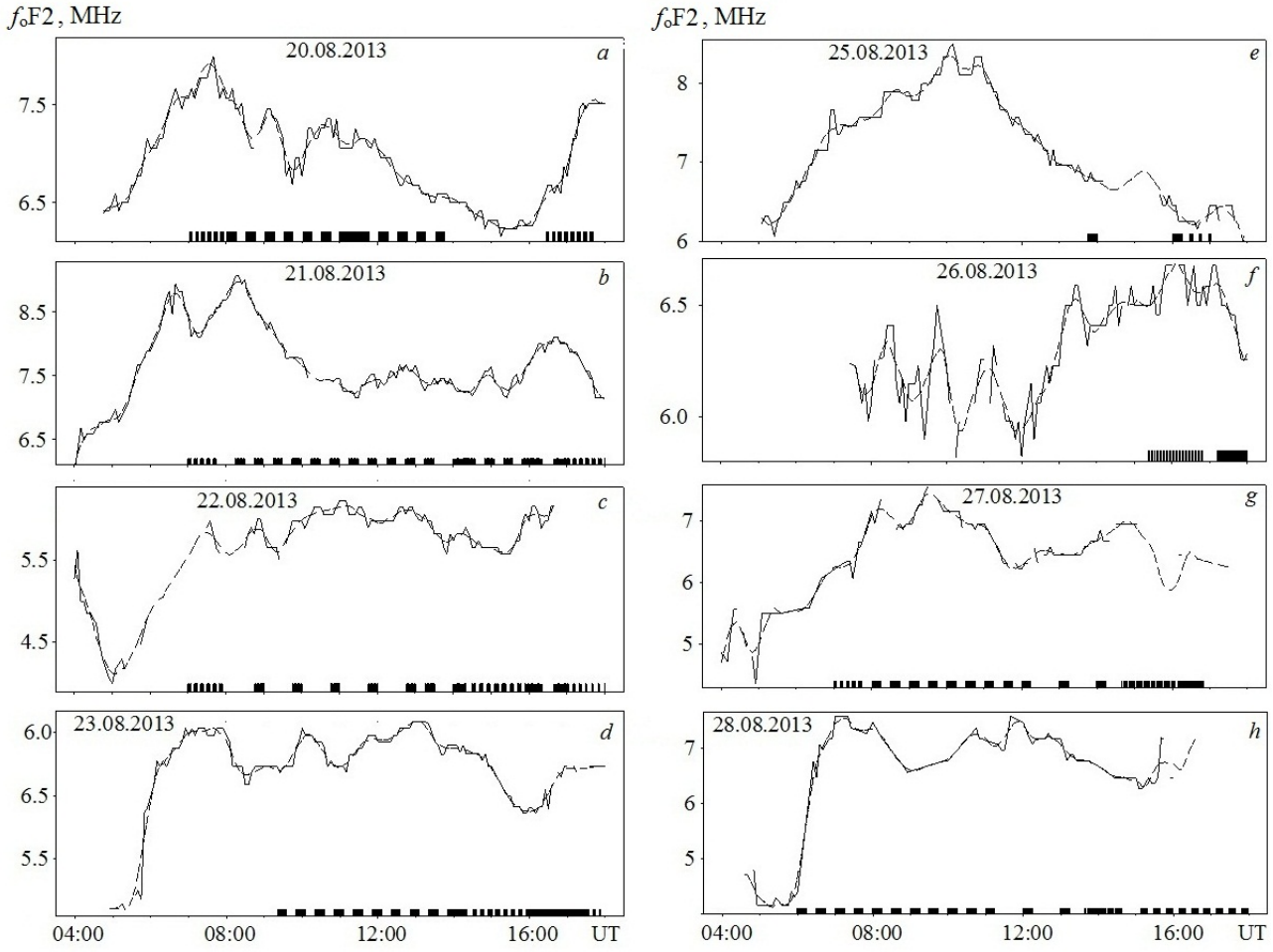

Fig. 5.9. Temporal variations of the critical frequency of the ionosphere F2 layer near Gaidary village. Here and below, rectangles on the time axis show the operation of the "Sura" stand

The day of August 25, 2013 was magnetically quiet. The heating stand was turned on from 13:46 to 14:01 and from 16:01 to 16:16 in the transmission mode with carrier frequencies of 5828 and 4785 kHz and an effective power of 100 and 90 MW, respectively. Approximately from 14:00 to 15:30, the Es-layer was registered. The behavior of f_oF2(t) was typical for undisturbed conditions (see Fig. 5.9*e*): by 10:00, there was an increase in f_oF2 values to 8.3 MHz. Then, gradual decrease in f_oF2 occurred. The magnitude of f_oF2 bursts varied in the range of 0.06–0.30 MHz, and their duration was 5–30 min.

On August 26, 2013, the f_oF2 values fluctuated near 6 MHz (see Fig. 5.9*e*) from 05:00 to 17:00. Occasionally, there was the Es layer which shielded the F region of the ionosphere.

The day of August 27, 2013 was magnetically quiet until 12:00–13:00, after which the ionosphere began to be affected by the geospace storm. Observations of the F region were sometimes interrupted due to the presence of the Es-layer (see Fig. 5.9*g*). Regular diurnal variations of f_oF2 were superimposed on f_oF2 bursts. During the operation of the heating stand from 08:00 to 11:46, there were f_oF2 bursts of 0.15–0.38 MHz.

On August 28, 2013, in the time interval 07:00–09:00, a decrease in f_oF2 was observed compared to the reference day by approximately 0.7 MHz. Slow variations of f_oF2 were superimposed by bursts of 0.15–0.30 MHz (see Fig. 5.9*h*). From 00:00 to 05:00, there was a powerful Es-layer that shielded the ionosphere layers located above. Es-layer cutoff frequency decreased to approximately 3.5–4.0 MHz from 05:00 to 14:30. After 15:00, the Es layer began to shield the F region of the ionosphere again.

On August 29 and 30, 2013, the Es layer existed almost all day, which made it impossible to measure the F2-layer critical frequency, and hence the use of these days as the reference (the heating stand was not operated during these days).

5.6.4. Temporal Variations in the Critical Frequency Near Troitsk

On August 20, 2013, the f_oF2 increased from 5.3 to 7.5 MHz from 04:00 to 08:00. Then, gradual decrease of f_oF2 to 6.2 MHz occurred at about 14:00 (Fig. 5.10*a*). After a short decrease in f_oF2 by approximately 0.5 MHz in the time interval 14:00–16:00, a slight increase in f_oF2 was observed until 18:00.

The first burst of f_oF2 of approximately 0.5 MHz occurred in the time interval 06:30–07:15 (see Fig. 5.10*a*). From 08:00 to 14:00, f_oF2 bursts of 0.17–0.26 MHz with duration of 15–45 min were also recorded.

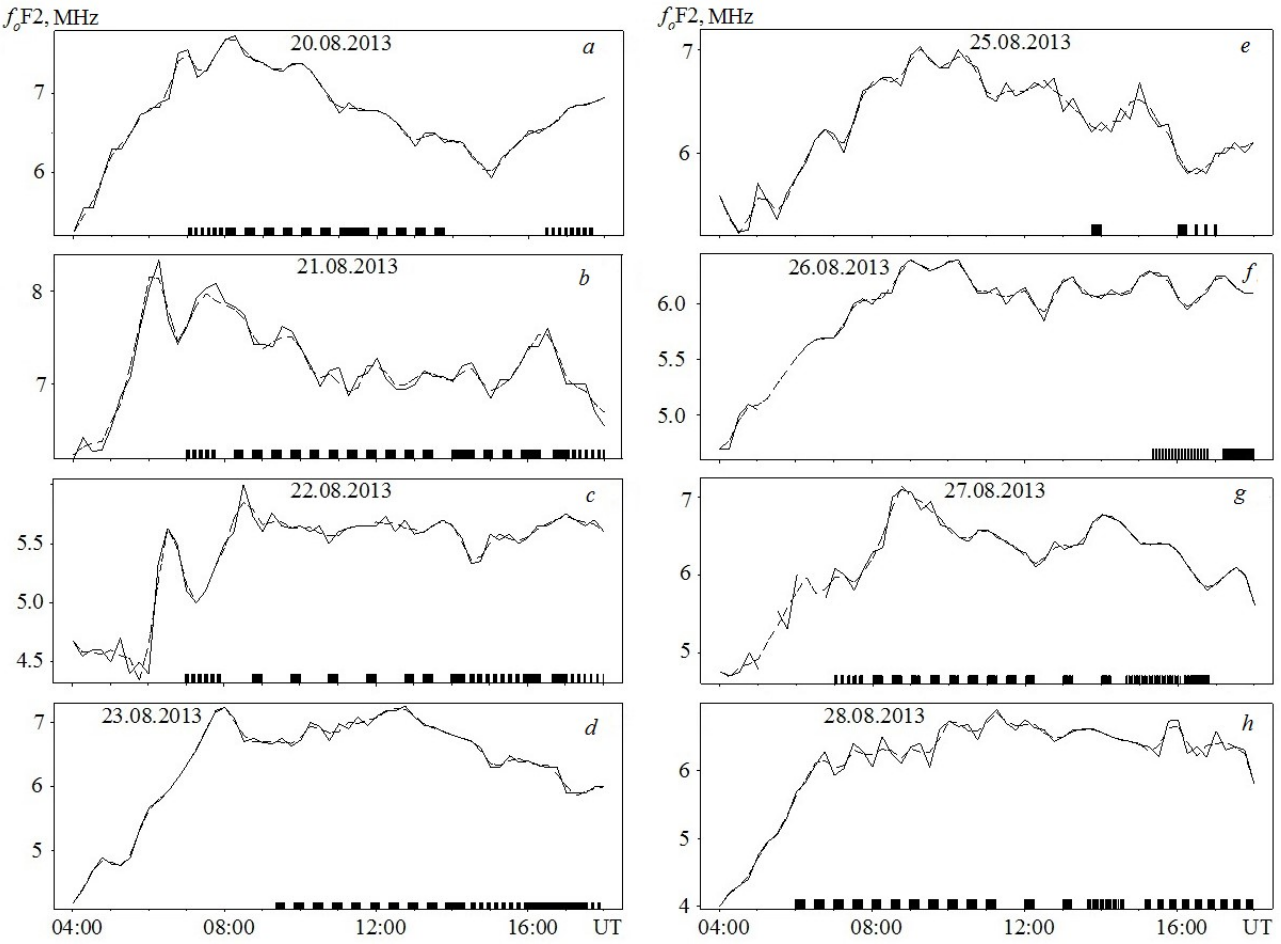

Fig. 5.10. Temporal variations in the F2-layer critical frequency near Troitsk

On August 21, 2013, the increase in f_oF2 of approximately 1 MHz was observed in the time interval 05:00–07:00 (see Fig. 5.10*b*). From 07:00 to 16:00, gradual decrease in the critical frequency of 0.17–0.26 MHz occurred which was superimposed on bursts lasting from 15 to 30 min.

On August 22, 2013, f_oF2 increase from 4.6 to 5.7 MHz was observed from 06:00 to 07:30 (see Fig. 5.10*c*). In the interval 07:30–08:00, f_oF2 was about 5 MHz. Then, there was a sharp increase in the critical frequency from 5 to 5.9 MHz. From 09:00 to 18:00, the smoothed f_oF2 values changed slightly. The bursts of 0.12–0.18 MHz lasting about 15 min were superimposed on the monotonic changes of f_oF2.

On August 23, 2013, the frequency f_oF2 increased from 4 to 7.2 MHz fluctuating slightly from 04:00 to 08:00. Then, for half an hour, f_oF2 decreased by approximately 0.5 MHz (see Fig. 5.10*g*). Then, the average value of f_oF2 increased from 6.7 to 7.2 MHz. After 12:45, there was a predominant decrease in f_oF2 values. f_oF2 bursts were superimposed on the smooth course of f_oF2, which were well expressed in the time interval 09:30–17:00. The magnitude of the bursts was 0.1–0.3 MHz and their duration was 15–60 min.

On August 25, 2013, the critical frequency initially increased on average from 5.5 to 7 MHz, and after 09:30 it gradually decreased from 7 to 6.5 MHz (see Fig. 5.10*d*). Slow variations of f_oF2 were superimposed by bursts of 0.08–0.16 MHz with the duration of 15 min or more.

On August 26, 2013, a gradual increase in f_oF2 was observed from approximately 4.7 to 6.3 MHz from 04:00 to 09:00 (see Fig. 5.10*e*). Then, for 9 hours, the f_oF2 values fluctuated around 6 MHz. Slow variations of f_oF2 were accompanied by quasi-periodic oscillations with $T \sim 1$ h and an amplitude of 0.1–0.15 MHz.

On August 27, 2013, the critical frequency increased on average from 4.8 to 7.1 MHz from 04:00 to 09:00. Then, f_oF2 slowly decreased to 6 MHz at 12:30 and then increased approximately to 0.7 MHz at 14:00. Then, f_oF2 gradually decreased (see Fig. 5.10*g*). Slow variations in f_oF2 were superimposed on bursts of 0.15–0.30 MHz lasting about 15–30 min.

On August 28, 2013, the increase in f_oF2 from 4.0 to 6.2 MHz was observed from 04:00 to 08:00. Then, the critical frequency changed slightly until 17:30 (see Fig. 5.10*h*). On average, f_oF2 bursts with a magnitude of 0.33–0.41 MHz and a duration of 15–30 min were superimposed on the monotonic course. The bursts were significantly amplified by the transmision of the stand in the modes [+15 min; –15 min] and [+10 min; –10 min] (see Fig. 5.9*h*). At the same time, they were weakly expressed at [+2 min; –2 min] (see Fig. 5.9*h*).

5.6.5. Temporal Variations in the Critical Frequency Near Pruhonice

On August 20, 2013, there was an increase in the smoothed values of the critical frequency from 4.5 to 7.1 MHz during 04:00–10:30 (Fig. 5.11*a*). In the time intervals 09:30–12:00 and 12:30–15:00, f_oF2 increased by approximately 0.5 MHz. From 16:00, there was an evening increase in f_oF2. Slow variations in the critical frequency were superimposed on its bursts of 0.09–0.14 MHz lasting about 15–30 min.

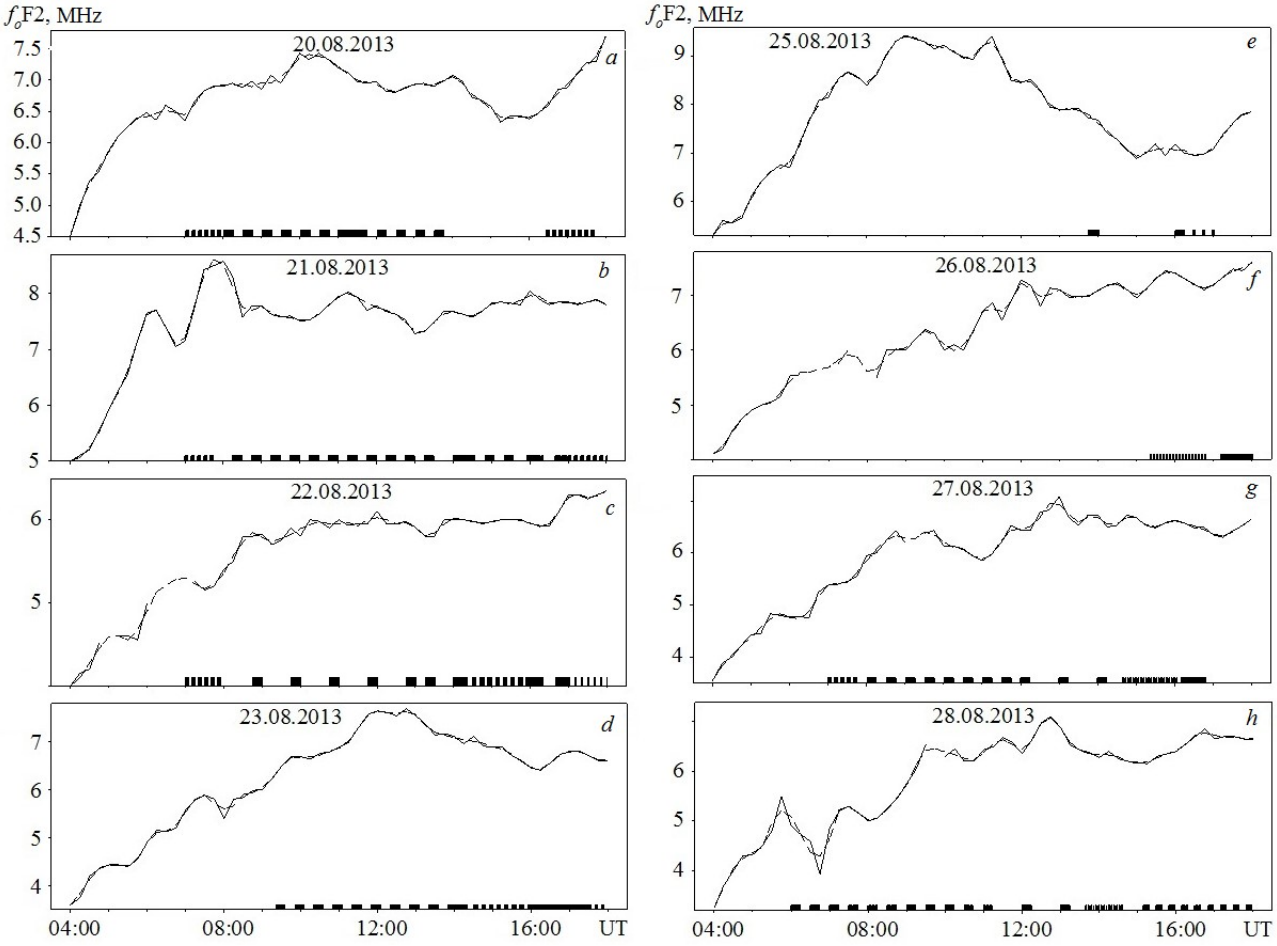

Fig. 5.11. Temporal variations in the F2-layer critical frequency near Pruhonice

On August 21, 2013, the f_oF2 value increased by 0.7 and 1.5 MHz in the time intervals 05:30–06:45 and 07:00–08:30, respectively (see Fig. 5.11*b*). From 08:30 to 17:00, variations of the smoothed f_oF2 values were insignificant. Bursts of

0.11–0.22 MHz with duration of about 15–30 min were superimposed on the regular course of the critical frequency.

On August 22, 2013, there was an increase in the critical frequency by 0.3, 0.5, and 0.3 MHz from 04:30 to 05:45, from 05:45 to 07:45, and from 08:00 to 09:30, respectively (see Fig. 5.11*c*). From approximately 09:30 to 18:00, the smoothed f_oF2 values remained almost unchanged and were close to 6.0 MHz. Slow variations of f_oF2 were accompanied by bursts of 0.12–0.18 MHz with a duration of about 15–30 min.

On August 23, 2013, the critical frequency first increased from 4.3 to 7.3 MHz in the time interval 05:20–12:15. Then, it decreased to 6.7 MHz from 12:15 to 16:00. In the time interval 16:00–18:00, the f_oF2 frequency burst of about 0.3 MHz was observed (see Fig. 5.11*d*). During the operation of the heating stand, f_oF2 bursts of 0.22–0.33 MHz with a duration of 15–30 min were recorded.

On the reference day August 25, 2013, the smoothed f_oF2 values increased from 5.5 to 9.2 MHz from 05:00 to 09:00 (see Fig. 5.11*d*). A decrease in the critical frequency from 9.2 to 7 MHz was observed in the time interval 09:00–16:00. Slow changes in f_oF2 were accompanied by bursts of 0.1–0.6 MHz with a duration of 30–60 min.

On August 26, 2013, there was a gradual increase in the f_oF2 variation from 4 to 7.5 MHz from 04:00 to 18:00. That increase was superimposed on quasi-periodic variations of f_oF2 with a period of $T \sim 1$ h and an amplitude of 0.2–0.3 MHz (see Fig. 5.11*e*).

On August 27, 2013, the smoothed f_oF2 values increased from 3.5 to 6.2 MHz from 04:00 to 08:45 and decreased by approximately 0.5 MHz from 09:00 to 11:00. They increased again by 1.2 MHz from 11:00 to 13:00 (see Fig. 5.11*g*). In the time interval 13:00–18:00, the variations in the critical frequency were insignificant. As on other days, slow changes in f_oF2 were accompanied by bursts of 0.15–0.25 MHz with a duration of about 15 min.

On August 28, 2013, the average time dependence of f_oF2 was nonmonotonic (see Fig. 5.11*h*). Slow variations with a characteristic time of 1.5–2 h were

superimposed on f_oF2 bursts with a magnitude of 0.15–0.25 MHz and a duration of 15 min or more.

5.6.6. Occurrence Frequency of f_oF2 Bursts

As can be seen from Fig. 5.9–5.11, f_oF2 bursts of several tenths of a megahertz were observed both before and after the heating stand was turned on as well as during reference time intervals. The f_oF2 bursts' duration varied from 10 to 60 min. Obviously, during the reference time intervals, the bursts were of natural origin. In some cases, when variations in f_oF2 were quasi-periodic, it makes sense to associate the bursts with the passage of internal gravitational waves (IGW) in the atmosphere. In cases with aperiodic increases in electron density in the F region of the ionosphere, the bursts are probably caused by processes accompanying geospace storm.

To prove that f_oF2 bursts occurred during the operation of the heating stand were caused by the operation, it is expedient to compare the frequency of the bursts occurrence during the stand operation and during the reference day. To do this, the time intervals from 04:00 to the time of turning on of the heating stand on August 25 and 26, 2013 (considered as the reference intervals) were divided into 30-minute intervals that simulates the operation of the heating stand [+15 min; –15 min]. The relative frequency of aperiodic f_oF2 bursts and their duration were estimated. The occurrence frequency for the reference intervals was 50, 58, and 58% for the "Gaidary", "Troitsk", and "Pruhonice" ionosondes, respectively (Table 5.7). The law of distribution of burst durations in the interval [0; 30 min] was close to uniform. These indicate that the occurrence of "bursts" and their absence have almost equal probability.

For the "Gaidary" ionosonde, the relative frequency of the bursts occurrence after the turning on of the stand was 76% during the first 15 minutes. For the "Troitsk" and "Pruhonice" ionosondes, it was 68%. The lower value of the relative frequency for the last two ionosondes may be explained by the lower frequency of the ionogram registration (one ionogram per 15 min).

Table 5.7. Relative frequency of f_oF2 bursts occurrence (the estimates for the reference intervals shown in parenthesesis)

Ionosonde	Relative frequency, %
“Gaidary”	76 (50)
“Troitsk”	68 (58)
“Pruhonice”	68 (58)

5.6.7. Time Delay and Duration of f_oF2 Bursts

The next parameters that allow separating the f_oF2 bursts of from natural and artificial origin are the time delay and the duration of the bursts. According to the “Gaidary” ionosonde data (1 ionogram per 5 min), the bursts were observed after each turning on the stand with the time delay of 5 min, rarely up to 10 min. The bursts lasted about 10–15 min.

On the refernce day, the duration of the bursts varied from 5 to 30 min, the time delay varied from 5 to 30 min. The latter means that the time delay is distributed according to the uniform law on 30 min interval.

The time delay at Troitsk and Pruhonice did not exceed 15 min. It is impossible to determine the delay more precisely because of the lagrer time interval between the adjacent ionograms (15 min). The duration of the bursts was typically close to 15 min.

5.6.8. Amplitudes of Critical Frequency and Electron Density Bursts

The ranges of change in the magnitude of the f_oF2 bursts are given in Table 5.8–5.10. It is seen that the δf_oF2 values were typically a few tenths of a megahertz. The values were almost the same on the reference day. More precisely, the standard deviation of f_oF2 fluctuations during the operation of the heating stand was $\sigma = 0.15–0.25$ MHz while $\sigma_n = 0.11–0.19$ MHz in the reference intervals. This means that the

signal-to-noise ratio $q = (\sigma/\sigma_n)^2 \approx 1.86–1.73$. Knowing $\delta f_o F2$, we can calculate the value of the relative perturbations of the electron density $\delta N \approx 2\delta f_o F2/f_o F2$.

Table 5.8. Parameters of disturbances in August 2013 (“Gaidary” ionosonde)

Date	Number of turn on (off)	Number of bursts $f_o F2$	$\delta f_o F2$, MHz	δ_N, %	Notes
August 20	12	9	0.15–0.23	4.3–6.6	Mode [+5 min; –5 min]. *PG* = 55 MW
August 21	15	11	0.10–0.30	2.5–7.5	Mode [+15 min; –15 min]. *PG* = 80 MW
August 22	6 (6)	10	0.10–0.15	3.3–5.0	Carrier mode [+15 min; –45 min]. *PG* = 100 MW
August 23	9	7	0.15–0.23	4.3–6.4	Mode [+15 min; –15 min]. *PG* = 40 MW
August 25, 26	18	9	0.06–0.30	1.7–7.5	Reference day
August 27	7	4	0.15–0.38	4.3–10.8	Mode [+15 min; –15 min]. *PG* = 85 MW
August 28	6	5	0.15–0.30	4.3–8.6	Mode [+15 min; –15 min]. *PG* = 85 MW

Estimates of δ_N are shown in the Tables 5.8–5.10. The δ_N values varied typically from 3–4 to 10–13% during the operation of the heating stand. On the reference days, these values were slightly lower – from 1.7 to 7.5%.

The largest (5.7–8.4%, but not higher than 10–13%) values of δ_N during the stand operation occurred in Troitsk. The smallest values (4.2–6.8%) were detebted in Pruhonice. In Gaidary, the δ_N values ranged from to 3.8–7.5%.

5.6.9. Arguments in Favor of the Transmission Effects in the Ionosphere

There are four arguments in favor the hypothesys on the $f_o F2$ bursts causation by the influence of powerful radio transmission on the ionosphere. First, the relative

frequency of bursts occurrence after turning on the heating stand was quite high (76, 68 and 68%) for all three ionosondes. On the reference day, this frequency was 50, 58 and 58%, respectively (see Table 5.7). Second, the disturbance delay values were very close. Of course, the accuracy of their assessment depended on the frequency of ionogram registration. The duration of the bursts also changed slightly. The bursts not related to the operation of the stand followed one another with random law. Third, in the pauses between the turning on the stand, the value of δf_oF2 decreased, which indicated a relaxation of the electron density. Fourth, the σ values were larger during the stand operation.

Table 5.9. Parameters of disturbances in August 2013 ("Troitsk" ionosonde)

Date	Number of turn on (off)	Number of bursts f_oF2	δf_oF2, MHz	δ_N, %	Notes
August 20	12	6	0.17–0.26	4.9–7.3	Mode [+5 min; –5 min]. *PG* = 55 MW
August 21	14	10	0.17–0.26	4.9–7.3	Mode [+15 min; –15 min]. *PG* =80 MW
August 22	6 (6)	7	0.12–0.18	4.2–6.3	Carrier mode [+15 min; –45 min]. *PG* = 100 MW
August 23	9	7	0.17–0.26	4.9–7.3	Mode [+15 min; –15 min]. *PG* = 40 MW
August 25, 26	12	7	0.08–0.16	2.5–5.0	Reference day
August 27	11	9	0.15–0.30	4.6–9.2	Mode [+15 min; –15 min]. *PG* = 85 MW
August 28	11	8	0.33–0.41	10.5–13.0	Mode [+15 min; –15 min]. *PG* = 85 MW

Note that the parameters of the ionospheric disturbances depended on the mode of the heating stand operation, space weather conditions, and the presence of natural disturbances.

Table 5.10. Parameters of disturbances in August 2013 (“Pruhonice” ionosonde)

Date	Number of turn on (off)	Number of bursts f_oF2	δf_oF2, MHz	δ_N, %	Notes
August 20	12	8	0.07–0.12	2.4–4.9	Mode [+5 min; –5 min]. *PG* = 55 MW
August 21	14	9	0.11–0.22	2.9–5.8	Mode [+15 min; –15 min]. *PG* = 80 MW
August 22	6 (6)	7	0.12–0.18	4.0–6.0	Carrier mode [+15 min; –45 min]. *PG* = 100 MW
August 23	9	5	0.22–0.33	6.3–9.4	Mode [+15 min; –15 min]. *PG* = 40 MW
August 25, 26	12	7	0.11–0.22	2.4–4.9	Reference day
August 27	11	10	0.15–0.25	4.6–7.7	Mode [+15 min; –15 min]. *PG* = 85 MW
August 28	11	8	0.15–0.25	5.0–7.1	Mode [+15 min; –15 min]. *PG* = 85 MW

More experiments and additional research facilities are required to confirm the effects of powerful transmission on the ionosphere.

5.7. Dependence on the Mode of the Heating Stand Operation

Aperiodic disturbances had a time delay of 5–10 min and, apparently, did not exceed 15 min. Therefore, the optimal duration of the heating is close to 15 min. The relaxation time of the electron density near the maximum of ionization is about 10–20 min during the day [146]. Therefore, the pause in heating modes should be close to this value. Thus, convenient modes for generating f_oF2 bursts are the following: [+15 min; –15 min] and [+15 min; –45 min]. The last mode was used on August 22, 2013. A good correlation (correlation coefficient is 0.75) of bursts with turning on the

stand on this day was obtained (see Fig. 5.9*c*). Good correlation (correlation coefficient is 0.83) also found for August 28, 2013 (see Fig. 5.10*h*).

Bursts of the critical frequency f_oF2 also occurred during the stand operation in the mode [+5 min; –5 min]. In this case, the *N* perturbations did not have enough time to relax, and there was an "accumulation effect" of perturbations. This effect was observed on August 20, 2013 in the time intervals 07:30–07:45, 16:37–16:52 and on August 27, 2013 in the time intervals 07:00–07:20 (see Fig. 5.9). The "accumulation effect" also apparently took place on August 28, 2013 during the stand operation in the mode [+10 min; –10 min] (see Fig. 5.10*h*).

5.7.1. The Nature of the Disturbances

In some cases, the critical frequency bursts were masked by quasi-periodic (wave) disturbances which could also be generated by powerful periodic radio transmission. Examples of such wave disturbances are the disturbances observed on August 20, 2013 in the time intervals 07:50–08:30 and 16:45–17:40, as well as on August 21, 2013 from 17:30 to 19:00. The time delay of quasi-periodic disturbances was close to 30 and 50 min at night and during the day, respectively. At $R \approx 960$ km, the velocity of the disturbances v was close to 530 and 320 m/s, and their amplitude was $\delta_{Na} \approx 3$–5%, i.e., approximately the same as for δ_N. The excess of the nighttime v values over the daytime values is explained by the fact that the height of the layer F2 maximum at night is approximately 100 km higher than during the day. At the same time, with increasing altitude, the neutral temperature T_n increases. Since v is proportional to $T_n^{1/2}$, larger heights and T_n correspond to larger v values.

The nature of such quasi-periodic disturbances is clear: they are associated with the generation and propagation of travelling ionospheric disturbances (TIDs). These disturbances were studied in the detail in [107, 119, 173–278]. In these works, the velocity of quasi-periodic disturbances was estimated. Depending on the time and

altitude, it was equal to 300–500 m/s. The very close values of the propagation velocities suggests that the wave disturbances in some cases are of artificial origin.

5.7.2. The mechanism of Aperiodic Disturbances

There is no doubt that aperiodic bursts of critical frequency, which correlate with the turning on of the heating stand, are caused by the bursts of electron density. The only reasonable mechanism for N increasing at the altitudes of the ionospheric F region may be additional ionization of neutrals by flows of high-energy electrons precipitating from the Earth's radiation belt. It is well known that during periods of geospace storms, the radiation belt is replenished with high-energy particles. Thus, the geospace storm acts as an accumulator of particles, which are then released under the influence of powerful radio transmission. This mechanism was proposed in [107, 173]. It is important to note that the eruption of electrons with energies ε_e = 102 keV stimulated by the radio transmission of the "Sura" stand, was observed by DEMETER satellite [179, 180].

The equation of the balance of the electron density in the F region of the ionosphere without taking into account the transfer processes is as follows (see, for example, [1]):

$$\frac{dN}{dt} = q - \beta N ,$$

where q is the electron production rate, β is a linear recombination coefficient. In the quasi-stationary case $q \approx \beta N$. Then, when q is increased by Δq, we obtain

$$\Delta q \approx \beta \Delta N = \beta N_0 \delta_N ,$$

where N_0 is an undisturbed N value. In this case, the energy flux density spent on the ionization of neutrals (see, for example, [31]) is the following:

$$\Pi = 2\varepsilon_i \Delta z \Delta q = 2\varepsilon_i \Delta z \beta N_0 \delta_N ,$$

Where Δz is the thickness of the ionization layer, $\varepsilon_i \approx 35$ eV is the ionization energy of one molecule by the precipitating electrons. Electron flux density with energy ε_e is

$$\Pi_e = \frac{\Pi}{\varepsilon_e} = 2\Delta z \beta N_0 \delta_N \frac{\varepsilon_i}{\varepsilon_e}.$$

With δ_N = 1–10%, Δz = 50 km, $N_0 = 5 \cdot 10^{11}$ m^{-3}, $\beta = 10^{-3}$ s^{-1} [165], $\varepsilon_e = 10^2$ keV we obtain $\Pi_e \approx 1.8 \cdot 10^8$–$1.8 \cdot 10^9$ m^{-2}s^{-1}, $\Pi \approx 2.8 \cdot 10^{-6}$–$2.8 \cdot 10^{-5}$ J·m^{-2}s^{-1}.

Note that during the measurements of 2010–2012 [174–176] which were carried out under quiet geomagnetic conditions, similar f_oF2 bursts were not detected after the turning on the heating stand. This implies that the precipitation of high-energy electrons requires their accumulation in the radiation belt for some time prior to the heating. Geospace storms should occur during the preciding period for that.

Similar electron flux densities were observed by the authors during moderate magnetic storms [170].

With a radius of the disturbed region $R \approx 2200$ km (distance from the heating stand to the ionosonde “Pruhonice”), the area covered by the precipitation of electrons $S \approx 1.5 \cdot 10^{13}$ m^2. This value is a lower bound. The actual spatial scale can be more than 2200 km. Then, the total electron flux power spent on the ionization is $P_e = \Pi S = 4.2 \cdot 10^7$–$4.2 \cdot 10^8$ W. With the duration of the precipitation process $\Delta T = 10^3$ s, its energy is close to $4.2 \cdot 10^{10}$–$4.2 \cdot 10^{11}$ J. Given that the power of three radio transmitters is $P \approx 5 \cdot 10^5$ W, the trigger factor is$K_{tr} = P_e/P \approx$ 84–840. For larger values of the area S, the value K_{tr} is even larger.

It is important that $K_{tr} >> 1$, i.e. there is a trigger effect with stimulated precipitation of particles. This is one of the manifestations of the interaction of subsystems in the EAIM system.

Note that the emission of electrons stimulated by powerful radio transmission can be observed only when the magnetic traps of the radiation belt are filled with electrons of corresponding energies, i.e. under a certain space weather conditions when the whole system is in a metastable state.

It is known that magnetic traps can remain filled for two weeks after the onset of the main phase of severe magnetic storm. For moderate magnetic storms, this may last for several days.

Thus, the processes stimulated by powerful radio transmission in the EAIM system were most likely possible because of weak and moderate geospace storms that took place in the last decade of August 2013.

In [179], the precipitation of the electrons was observed at distances up to 300 km from the ionosonde. The problem of the disturbanse propagation over long distances (~2000–3000 km) requires special consideration. Presumably, the expansion may be facilitated by the generation of polarization fields that occur when electrons precipitate initially only within a magnetic flux tube with the base in the ionosphere region irradiated by the powerful radio transmission. The initial transverse size of the tube is about 80 km [180]. The role of polarization fields is considered in more detail in [180, 181].

Interaction of subsystems in the EAIM system is discussed in more detail in [121, 178]. The bursts of the frequency $f_{\min}$ which are described in [121, 178] and ones of the f_{o}F2 which are analyzed in this paper, have a single nature associated with an additional ionization of the atmosphere. The difference may be in the energy of the fluxes of the precipitating electrons. Additional ionization in the lower ionosphere is observed at $\varepsilon_e \sim 10^2$ keV, and in the F region it can occur at $\varepsilon_e \sim 1$–10 keV.

Thus, there is reason to believe that the relatively weak flux of high-power transmission can act as a trigger for a number of processes in the EAIM system which is in a metastable state. Naturally, this statement requires further verification by independent methods of the disturbances diagnostic.

REFERENCES

1. Chernogor L.F. Physics of powerful radio emission in geospace: Monograph. Kharkiv: V.N.Karazin Kharkiv National University, 2014. 448 p. (in Russian)

2. Alpert Ya.L. Propagation of electromagnetic waves and the ionosphere. Moscow: Nauka, 1972. 564 p. (in Russian)

3. Kravtsov Yu.A., Feizulin Z.I, Vinogradov A.G. Passing of radio waves through the Earth's atmosphere. Moscow: Radio and Communication, 1983. 224 p. (in Russian)

4. Davies K. Ionospheric radio. London: Peter Peregrinus Ltd, 1990. 580 p.

5. Yakovlev O.N. Space Radiophysics. Moscow: Scientific book, 1998. 432 p. (in Russian)

6. Yakovlev O.N. et al. Propagation of radio waves. Moscow: LENAND, 2009. 496 p. (in Russian)

7. Dikiy L.A. Theory of oscillations of the Earth's atmosphere. Leningrad: Gidrometeoizdat, 1969. 196 p. (in Russian)

8. Yen K. S., Liu C. H. Theory of ionospheric waves. London: Academic Press, 1972. 464 p.

9. Beer T. Atmospheric waves. N.Y., Toronto, 1974. 315 p.

10. Gershman B.N. Dynamics of ionospheric plasma. Moscow: Nauka, 1974. 256 p. (in Russian)

11. Gossard E.E., Hook W.H. Waves in the atmosphere. Moscow: Mir, 1978. 532 p. (in Russian)

12. Avakyan S.V. et al. Waves and radiation of the upper atmosphere. Alma-Ata: Nauka, 1981. 167 p. (in Russian)

13. Sorokin V.M., Fedorovich G.V. Physics of slow MHD waves in ionospheric plasma. Moscow: Energoizdat, 1982. 136 p. (in Russian)

14. Wave disturbances in the ionosphere / Ed. V. I. Drobzheva. – Alma-Ata: Nauka, 1987. 172 p. (in Russian)

15. Hines C.O. Internal gravity waves at ionospheric hights. *Can. J. Phys.* 1960. V. 38, P. 1441–1481.

16. Tolstoy I. Long-Period Gravity Waves in the Atmosphere. *J. Geophys. Res.* 1967. V. 72, № 18. P. 4605–4622.

17. Chimonas G. Observations of Waves in the Ionosphere. *Planet and Space Sci.* 1970. V. 18, № 4. P. 591–605.

18. Yen K.C., Liu C.H. Acoustic gravity waves in the upper atmosphere. *Rev. Geophys. Space Phys.* 1974. V. 12, P. 193–216.

19. Francis S.H. A Theory of medium-scale travelling ionospheric disturbances. *J. Geophys. Res.* 1974. V. 79, № 34. P. 5245–5260.

20. Francis S.H. Global propagation of atmospheric gravity waves: a review. *J. Atmos. Terr. Phys.* 1975. V. 37. P. 1011–1054.

21. Grigoriev G.S., Chunchuzov E.P. Acoustic-gravitation waves in the atmosphere. In the book: Polar lights and glow of the night sky. Moscow: Nauka. 1975. № 23, p. 5–21. (in Russian)

22. Ponomarev E.A., Eruschenkov A.I. Infrasonic waves in the Earth's atmosphere (Review). Izv. universities. Radiophysics. 1977. V. 20, № 12. P. 1773–1789. (in Russian)

23. Williams P.J.S. Tides, atmospheric gravity waves and travelling disturbances in the ionosphere. *Modern ionospheric science.* A collection of articles published on the occasion of the anniversary: "50 years of ionospheric research in Lindau". 1996. P. 136–180.

24. Grigoriev G.I. Acoustic-gravitation waves in the Earth's atmosphere. *Izv. universities. Radiophysics.* 1999. V. 42, № 1. P. 3–25. (in Russian)

25. Litvinenko L.N., Yampolsky Yu.M. Electromagnetic manifestations of geophysical effects in Antarctica. Kharkiv: RINAS, 2005. 331 p. (in Russian)

26. Burmaka V.P., Taran V.I., Chernogor L.F. Investigation results of wave disturbances in the ionosphere by the method of incoherent scattering. *Advances in modern radio electronics.* 2005. № 3. P. 4–35. (in Russian)

27. Burmaka V.P., Taran V.I., Chernogor L.F. Wave-Like Processes in the Ionosphere under Quiet and Disturbed Conditions. 1. Kharkov Incoherent Scatter Radar Observations. *Geomagnetism and Aeronomy.* 2006. V. 46, № 2. P. 193–208. (in Russian)

28. Burmaka V.P., Taran V.I., Chernogor L.F. Wave-Like Processes in the Ionosphere under Quiet and Disturbed Conditions. 2. Analysis of Observations and Simulation. *Geomagnetism and Aeronomy.* 2006. V. 46, № 2. P. 209–218. (in Russian)

29. URSI Guidelines for the Interpretation and Processing of Ionograms. Moscow: Nauka, 1987. 342 p. (in Russian)

30. Grudinskaya G.P. Propagation of radio waves / Textbook. manual for radio engineering. specialist. universities. Ed. 2nd, rev. and add. Moscow: “Higher School”, 1975. 280 p. (in Russian)

31. Domnin I.F., Chernogor L.F. Physics of geocosmic storms: monograph. Kharkiv: V.N. Karazin KhNU, 2014. 408 p. (in Russian)

32. Danilov A.D., Morozova L.D. Ionospheric storms in the F2 region. Morphology and Physics (Review). *Geomagnetism and Aeronomy*. 1985. V. 25, № 5. P. 705–721 (in Russian)

33. Chernogor L.F. Physical effects of solar eclipses in the atmosphere and geospace: Monograph. Kharkiv: Karazin V.N. Kharkiv National University, 2013. 480 p. (in Russian)

34. Eccles W. H. Effect of the eclipse on wireless telegraphic signals. *Electrician*. 1912. V. 69. P. 109–117.

35. Vasiliev K.N., Veleshin A.S., Kosenkov A.R. Ionospheric effect of the solar eclipse on February 15, 1961 according to observations in Moscow. *Geomagnetism and Aeronomy*. 1961. V. 1, № 2. P. 277–278. (in Russian)

36. Danilkin N.P., Kochenova N.A., Svechnikov A.M. State of the ionosphere over Rostov-on-Don during the solar eclipse on February 15, 1961. *Geomagnetism and aeronomy*. 1961. V. 1, № 4. P. 612–615. (in Russian)

37. Shapiro B.S., Shashunkina V.M. Motions in the F region of the ionosphere over Tbilisi during the eclipse on February 15, 1961. *Geomagnetism and aeronomy*. 1961. V. 1, № 5. P. 760–765. (in Russian)

38. Shashunkina V.M., Turbin R.I. Preliminary observation results of the ionospheric effect of the solar eclipse on February 15, 1961. *Geomagnetism and aeronomy*. 1961. V. 1, № 5. P. 835–838. (in Russian)

39. Sukhanova R.D. Ionospheric effect of the solar eclipse on February 15, 1961 according to observations in Solekhard. *Geomagnetism and Aeronomy*. 1961. V. 1, № 6. P. 1066–1067. (in Russian)

40. Grishkevich L.V., Vasin V.A. About the effects in the ionosphere observed during the periods of solar eclipses on 02.12.1956 and 15.02.1961 in Gorky. *Geomagnetism and Aeronomy*. 1961. V. 1, № 6. P. 949–954. (in Russian)

41. Klobuchar J.A., Whitney H.E. Ionospheric electron content measurements during a solar Eclipse. *J. Geophys. Res.* 1965. V. 70, № 5. P. 1254–1257.

42. Hunter A.N. et al. Faraday rotation studies in Africa during the solar eclipse of June 30, 1973. *Nature*. 1974. V. 250. P. 205–206.

43. Cohen E. A. The study of the effect of solar eclipses on the ionosphere based on satellite beacon observations. *Radio Sci*. 1984. V. 19, № 3. P. 769–777.

44. Ionospheric effects of the solar eclipse of March 9, 1997, as deduced from GPS data / E. L. Afraimovich et al. *Geophys. Res. Lett.* 1998. V. 25, № 4. P. 465–468.

45. Afraimovich E.L., Voeykov S.V., Perevalova N.P. et al. Ionospheric Effects of the March 29, 2006, Solar Eclipse over Kazakhstan. *Geomagnetism and Aeronomy*. 2007. V. 47. № 4. P. 491–500. (in Russian)

46. Evans J. V. An F region eclipse. *J. Geophys. Res.* 1965. V. 70. P. 131–142.

47. Observations of the May 30, 1984, annular solar eclipse at Millstone Hill / J. E. Salah et al. *J. Geophys. Res.* 1986. V. 91 № A2. P. 1651–1660.

48. Akimov L.A. et al. Complex radiophysical and optical studies of dynamic processes in the atmosphere and geospace caused by the solar eclipse on August 11, 1999. *Foreign radio electronics. Advances in modern radio electronics*. 2002. № 2. P. 25–63. (in Russian)

49. Akimov L.A. et al. Features of atmospheric-ionospheric effects of the solar eclipse on May 31, 2003: the results of optical and radiophysical observations in Kharkov. *Foreign radio electronics. Advances in modern radio electronics*. 2005. № 3. P. 55–70. (in Russian)

50. L. A. Akimov et al. Atmospheric-ionospheric effects of the solar eclipse of May 31, 2003, in Kharkov. *Geomagnetism and Aeronomy*. 2005. V. 45, № 4. P. 494–518.

51. Burmak V.P. et al. Atmospheric and ionospheric effects of a private solar eclipse on October 3, 2005 in Kharkov. 1. Observation results. *Space science and technology*. 2007. V. 13, № 6. P. 74–86. (in Russian)

52. Grigorenko E.I., Lyashenko M.V., Chernogor L.F. Effects of solar eclipse of March 29, 2006, in the ionosphere and atmosphere. *Geomagnetism and Aeronomy*. 2008. V. 48, № 3. P. 337–351.

53. Domnin I.F., Emelyanov L.Ya., Chernogor L.F. Dynamics of ionospheric plasma over Kharkov during the solar eclipse on January 4, 2011. *Radiophysics and radio astronomy.* 2012. V. 17, № 2. P. 132–145. (in Russian)

54. Bertin F., Hughes K. A., Kersley L. Atmospheric waves induced by the solar eclipse of 30 June 1973. *J. Atmos. Terr. Phys.* V. 39(4). P. 457–461.

55. Sen Gurta A., Goel G. K., Mathur B. S. Effect of the 16 February 1980 solar eclipse on VLF propagation. *J. Atmos. Terr. Phys.* 1980. V. 42. № 11/12. P. 907–909.

56. Cheng K., Huang Y.-N., Chen S.-W. Ionospheric effects of the solar eclipse of September 23. 1987, around the equatorial anomaly crest region. *J. Geophys. Res.* 1992. V. 97, № A1. P. 103–111.

57. A study of tomographically reconstructed ionospheric images during a solar eclipse / C. R. Huang et al. *J. Geophys. Res*. 1999. V. 104, № A1. P. 79–94.

58. Borisov B.B., Egorov D.A., Egorov N.E. et al. A Comprehensive Experimental Study of the Ionospheric Response to the Solar Eclipse of March 9, 1997. *Geomagnetism and Aeronomy*.. 2000. V. 40, № 3. P. 94–103. (in Russian)

59. Uryadov V.P., Leonov A.M., Ponyatov A.A. On variations in the characteristics of the HF signal along the oblique sounding path during the solar eclipse on August 11, 1999. *Izv. universities. Radiophysics*. 2000. V. 43, № 8. P. 682–686. (in Russian)

60. Gokov A.M., Chernogor L.F. Observation Results of processes in the lower ionosphere accompanying the eclipse of the Sun on August 11, 1999. *Radiophysics and radio astronomy.* 2000. V. 5, № 4. P. 348–360. (in Russian)

61. Farges T. et al. Disturbances of the western European ionosphere during the total solar eclipse of 11 August 1999 measured by a wide ionosonde and radar network. *J. Atmos. Sol. Terr. Phys*. 2001. V. 63. P. 915–924.

62. Cheng K., Huang Y. N., Chen S.W. Ionospheric effects of the solar eclipse of September 23, 1987, around the equatorial anomaly crest region. *J. Geophys. Res.* 1992. V. 97, № A1. P. 103–111.

63. Atmos J. Special Eclipse Issue (The eclipse of 7 March 1970). *Terr. Phys*. 1972. V. 34, P. 559–739.

64. Effects of the total solar eclipse of 16 February 1980 on TEC at low latitudes / M. R. Deshpande et al. *Proc. Indian. Nat. Acad. Sci*. 1982. V. A48, № 3. P. 427–433.

65. Bezrodny V.G. et al. Fluctuations of ultra-long radio waves in the Earth–ionosphere waveguide. Moscow: Nauka, 1984. 144 p. (in Russian)

66. TEC observations at Waltair during the total solar eclipse of 16 Februrary 1980 / P. V. S. Rama Rao et al. *Proc. Indian Nat. Acad. Sci.* 1982. V. 48, № 3. P. 434–438.

67. Roble R. G., Emery B. A., Ridley E. C. Ionospheric and thermospheric response over Millstone Hill to the May 30, 1984, annual solar eclipse. *J. Geophys. Res.* 1986. V. 91, № A2. P. 1661–1670.

68. The Chelyabinsk meteorite fall: electronic resource // Wikipedia. http://ru.wikipedia.org/wiki/Падение_метеорита_Челябинск

69. Bronstein V.A. Physics of meteoric phenomena. Monograph. Moscow: Nauka, 1981. 416 p. (in Russian)

70. 69. Kruchinenko V.G. Mathematical-physical analysis of meteoric manifestation: Monograph. Kiev: Naukova Dumka, 2012. 294 p. (in Ukrainian)

71. Comet-asteroid hazard, truth and fiction / K.I. Churyumov et al. Kiev-Baku, 2012. 178 p. (in Russian)

72. Asteroid-comet hazard: yesterday, today, tomorrow / Ed. Shustova B.M., Rykhlova L.V. Moscow: FIZMATLIT, 2010. 384 p. (in Russian)

73. Catastrophic Effects of Space Bodies / Ed. Adushkin V.V. and Nemchinov I.V. Moscow: ICC ”Akademkniga”, 2005. 310 p. (in Russian)

74. Stulov V.P., Mirsky V.N., Visly A.I. Aerodynamics of bolides. Moscow: Science. Fizmatlit, 1995. 240 p. (in Russian)

75. Chernogor L.F. Physics and ecology of catastrophes. Monograph. Kharkiv: V.N. Karazin Kharkiv National University, 2012. 556 p. (in Russian)

76. Chernogor L.F. Plasma, electromagnetic and acoustic effects of the Chelyabinsk meteorite. *Engineering physics*. 2013. № 8. Pp. 23–40. (in Russian)

77. Chernogor L.F. Electrical, magnetic, electromagnetic and plasma effects of the Chelyabinsk meteorite. *Global electrical circuit*. Materials of the All-Russian conference. Borok, October 28, November 1, 2013 Yaroslavl, 2013. Pp. 112–113. (in Russian)

78. 77. Chernogor L.F. Physical effects of the passage of the Chelyabinsk meteorite. *Additional information of the National Academy of Sciences of Ukraine*. 2013. № 10. Pp. 97–104. (in Russian)

79. Chernogor L. F., Rozumenko V. T. The physical effects associated with Chelyabinsk meteorite's passage. *Problems of Atomic Science and Technology*. 2013. Vol. 86, № 4. P. 136–139.

80. Chernogor L.F. Large-scale disturbances of the Earth's magnetic field accompanying the fall of the Chelyabinsk meteoroid. *Radio physics and electronics*. 2013. V. 4 (18), № 3. P. 47–54. (in Russian)

81. Chernogor L.F., Garmash K.P. Perturbations in the geospace accompanying the fall of the Chelyabinsk meteorite. *Radiophysics and Radio Astronomy.* 2013. V. 18, № 3. P. 231–243. (in Russian)

82. Geophysical conditions during the explosion of the Chelyabinsk (Chebarkul) meteoroid on February 15, 2013 / V.V. Alpatov, et al. Moscow: FGBU "IPG", 2013. 37 p. (in Russian)

83. Geochemistry. 2013. T. 51, N. 7. (Thematic issue). (in Russian)

84. Astronomical Herald. 2013. V. 47, N. 4. (Thematic issue) (in Russian)

85. Brown P.G. et al. 500-kilotone airburst over Chelyabinsk and an enhanced hazard from small impactors. *Nature*. 2013. V. 503. P. 238–241.

86. Popova O.P. et. al. Chelyabinsk airburst, damage assessment, meteorite, and characterization. *Science*. 2013. V. 342. P. 1069–1073.

87. Popova O. P. et al. Supplementary material for Chelyabinsk airburst, damage assessment, meteorite recovery, and characterization. *Science*. 2013. V. 342. 146 p.

88. Geophysical effects of the fall of the Chelyabinsk meteoroid. Dynamic processes in geospheres, collection of scientific articles and works. IDG RAS. Issue 5.Special edition. Moscow: GEOS, 2014. 160 p. (in Russian)

89. Chernogor L.F. Chelyabinsk meteorite: the biggest impact from space in the last 100 years. *Universitates*. 2013. № 2. P. 59–63. (in Russian)

90. Chernogor L.F. Chelyabinsk meteorite – a harbinger of space punishment. Part 1. *Science and technology*. 2013. № 6. P. 2–6. (in Russian)

91. Chernogor L.F. Chelyabinsk meteorite – a harbinger of space punishment. Part 2. *Science and technology.* 2013. № 7. P. 5–11. (in Russian)

92. Chornogor L.F. Life on a tiny and vulnerable planet: what reminded us of the Chelyabinsk meteorite. *Outlook*. 2013. № 3. P. 66–69. (in Ukrainian)

93. Chernogor L.F. et al. Satellite observations of ionospheric disturbances that followed the fall of the Chelyabinsk meteorite. *Space science and technology*. 2013. V. 19, № 6. P.38–46. (in Russian)

94. Chernogor L. F. Geomagnetic field effects of the Chelyabinsk meteoroid. *Geomagnetism and Aeronomy*. 2014. V. 54, N. 5. P. 613–624.

95. Chernogor L. F. Radar detection of mini-asteroids. *Radioelectronics and communications systems*. 2013. V. 56, № 11. P. 544–551.

96. Chernogor L.F. Main effects of the meteorite fall Chelyabinsk: results of physical and mathematical modeling. *Materials of the All-Russian scientific conference "Meteorite Chelyabinsk – a year on Earth"*. Chelyabinsk. 2014. P. 229–265. (in Russian)

97. Chernogor L. F. Ionospheric effects of the Chelyabinsk meteoroid. *Geomagnetism and Aeronomy*. 2015. V. 55, №. 3. P. 353–368.

98. Chernogor L.F., Shevelev N.B. Parameters of infrasound effects generated by the Chelyabinsk meteoroid on February 15, 2013. *Bulletin of the Kharkiv National University of the Name of V. N. Karazin. Radio physics and electronics*. 2016. V. 25. P. 70–73. (in Russian)

99. Chernogor L.F., Liashchuk O.I. The parameters of infrasonic waves generated by Chelyabinsk meteoroid 15 February 2013. *Kinematics and Physics of Celestial Bodies*. 2017. V. 33, № 4. P. 196–206.

100. Lazorenko O.V., Chernogor L.F. System spectral analysis of the infrasonic signal generated by the Chelyabinsk meteoroid. *Proceedings of universities. Radio electronics*. 2017. V. 60, № 8. P. 427–436. (in Russian)

101. Chernogor L.F., Lazorenko O.V. System Spectral Analysis of Infrasound Signal Generated by Chelyabinsk Meteoroid. *Radioelectronics and communications systems.* 2017. Vol. 56, № 11. P. 544–551.

102. Chernogor L.F. Acoustic effects of the Chelyabinsk meteoroid. *Radiophysics and Radio Astronomy.* 2017. V. 22, № 1. P. 53–66. (in Russian)

103. Chernogor L.F. Atmospheric-seismic effect of the Chelyabinsk meteoroid. *Radiophysics and Radio Astronomy.* 2017. V. 22, № 2. P. 123–137. (in Russian)

104. Chernogor L.F. Atmospheric effects of the gas-dust trace of the Chelyabinsk meteoroid. *Izvestia RAN. Physics of the atmosphere and ocean*. 2017. V. 53, № 3. P. 296–306. (in Russian)

105. Chernogor L.F. Perturbations in the lower ionosphere accompanying the fall of the Chelyabinsk space body. *Space exploration*. 2017. V. 55, № 5. P. 342–352. (in Russian)

106. Chernogor L.F. Magnetospheric Effects during the Approach of the Chelyabinsk Meteoroid. *Geomagnetism and Aeronomy*. 2018. V. 58, № 2. P. 267–280. (in Russian)

107. Chernogor L.F. Phase variations of kilometer radio waves accompanying the effect of powerful radio emission on the ionosphere. *Radiophysics and Radio Astronomy.* 2009. V. 14, № 4. P. 377–389. (in Russian)

108. Pakhomova O.V., Chernogor L.F. Study by the method of vertical sounding of the reaction of the ionosphere to the effect of powerful radio emission. *Bulletin of Kharkov University. Ser. Radiophysics and Electronics*. 1988. № 318. P. 29–30. (in Russian)

109. Chernogor L.F. Statistical characteristics of large-scale disturbances in the ionosphere, initiated by the action of powerful non-stationary radiation. *Geomagnetism and Aeronomy*. 1989. V. 29, № 3. P. 513–515. (in Russian)

110. Garmash K.P., Chernogor L.F., Shvartsburg A.B. The emergence of large-scale disturbances in the ionosphere, initiated by powerful non-stationary radio emission. *Computer optics*. 1989. V. 6. P. 62–71. (in Russian)

111. Kostrov L.S., Chernogor L.F. Doppler radio sounding of large-scale wave disturbances in the ionosphere generated by powerful radio emission. *Geomagnetism and Aeronomy*. 1990. V. 30, № 1. P. 159–161. (in Russian)

112. Garmash K.P., Chernogor L.F. Electron-Density Profiles in the *D* Region of the Ionosphere Under Quiet and Disturbed Conditions from Partial Reflections. *Geomagnetism and Aeronomy*. 1996. V. 36, № 2. P. 75–81. (in Russian)

113. Garmash K.P., Chernogor L.F. Effects in near-Earth plasma stimulated by the action of powerful radio emission. *The successes of modern radio electronics*. 1998. № 6. P. 17–40. (in Russian)

114. Garmash K.P., Chernogor L.F. Electromagnetic and geophysical effects in near-earth plasma stimulated by the influence of powerful radio emission. *Electromagnetic phenomena*. 1998. V. 1, № 1. P. 90–110. (in Russian)

115. Burmaka V.P. et al. Variations in the parameters of scattered signals and the ionosphere accompanying the effect of powerful radio emission on plasma. *Izv. universities. Radiophysics*. 2009. V. 52, № 11. P. 859–880. (in Russian)

116. Chernogor L.F. et al.Variations in the spectrum of ionospheric wave disturbances during periodic heating of plasma by powerful high-frequency radio emission. *Izv. universities. Radiophysics*. 2011. V. 54, № 2. P. 81–96. (in Russian)

117. Chernogor L.F., Frolov V.L. Traveling ionospheric disturbances generated by periodic heating of plasma by powerful high-frequency radio emission. *Izv. universities. Radiophysics*. 2012. V. 55, № 1–2. P. 14–36. (in Russian)

118. Chernogor L.F., Frolov V.L., Pushin V.F. Oscillations of the infrasonic range in the ionosphere when exposed to powerful radio emission. *Izv. universities. Radiophysics*. 2012. V. 55, № 5. P. 327–340. (in Russian)

119. Chernogor L.F. Generation mechanisms of infrasonic range oscillations in the upper atmosphere under the influence of powerful periodic radio emission. *Radiophysics and Radio Astronomy.* 2012. V. 17, № 3. P. 240–253. (in Russian)

120. Chernogor L.F., Domnin I.F., Panasenko S.V., Uryadov V.P. Aperiodic large-scale disturbances in the E region of the ionosphere stimulated by powerful radio emission. *Izv. universities. Radiophysics*. 2012. V. 55, № 3. P. 173–185. (in Russian)

121. Chernogor L.F. Large-scale disturbances in the lower ionosphere caused by powerful non-stationary radio emission. *Radiophysics and Radio Astronomy.* 2013. V. 18, № 1. P. 49–64. (in Russian)

122. Mendillo M., Hawkins G.S., Klobuchar J.A. A sudden vanishing of the ionospheric F-region due to the launch of Skylab. *J. Geophys. Res.* 1975. V. 80, № 16. P. 2217–2228.

123. Zasov G.F. et al. Observation of disturbances in the lower ionosphere during experiments under the Soyuz – Apollon program. *Geomagnetism and aeronomy*. 1977. V. 17, № 2. P. 346–348. (in Russian)

124. Karlov V.D., Kozlov S.I., Tkachev G.N. Large-scale disturbances in the ionosphere arising during the flight of a rocket with a running engine (Review). *Space Reasearch*. 1980. V. 18, № 2. P. 266–277. (in Russian)

125. Karlov V.D. et al. About one type of large-scale disturbances in the ionosphere. *Geomagnetism and Aeronomy*. 1984. V. 24, №2. P. 319–322. (in Russian)

126. Misyura V.A. et al. On the possibility of studying episodic short-term disturbances in the lower ionosphere using the method of vertical sounding. *Geomagnetism and Aeronomy*. 1987. V. 27, № 4. P. 677–679. (in Russian)

127. Misyura V.A., Pakhomova O.V., Chernogor L.F. Study of global and large-scale disturbances in the ionosphere using a network of ionosondes. *Space science and technology*. Kiev: Naukova Dumka. 1989. V. 4. P. 72–75. (in Russian)

128. Pakhomova O.V., Chernogor L.F. Apparent velocities of propagation of disturbances in near-earth space. *Space science and technology*. Kiev: Naukova Dumka. 1990. V. 5. P. 71–74. (in Russian)

129. Chernogor L.F. Radiophysical and geomagnetic effects of rocket launches: Monograph. Kharkiv: V.N.Karazin Kharkiv National University, 2009. 386 p. (in Russian)

130. Zhivolup T.G., Chernogor L.F. Ionospheric effects during the flight of the “Proton” rocket: results of vertical sounding. *Space science and technology*. 2010. V. 16, № 3. P. 25–31. (in Russian)

131. Zhivolup T.G., Chernogor L.F. Ionospheric effects during flights of the “Soyuz” rocket during quiet and magnetically disturbed conditions. *Space science and technology*. 2010. V. 16, № 3. P. 32–41. (in Russian)

132. Garmash K.P., Kostrov L.S., Rozumenko V.T. et al. Global Ionospheric Disturbances Caused by a Rocket Launch against a Background of a Magnetic Storm. *Geomagnetism and Aeronomy*. 1999. V. 39, № 1. P. 72–78. (in Russian)

133. Burmaka V.P., Kostrov L.S., Chernogor L.F. Statistical characteristics of Doppler HF radar signals during sounding of the middle ionosphere disturbed by rocket launches and solar terminator. *Radiophysics and Radio Astronomy*. 2003. V. 8, №2. P. 143–162. (in Russian)

134. Burmaka V.P., Taran V.I., Chernogor L.F. Results of complex radiophysical observations of wave disturbances in the geocosmos accompanying missile launches and flights. *Space science and technology*. ADDITIONER. 2003. V. 9, № 2. P. 57–61. (in Russian)

135. Burmaka V.P., Chernogor L.F., Chernyak Yu.V. Wave disturbances in the geospace accompanying the launches and flights of the “Soyuz” and “Proton” rockets. *Radiophysics and Radio Astronomy.* 2005. V. 10, № 3. P. 254–272. (in Russian)

136. Chernogor L. F., Blaunstein N. Radiophysical and geomagnetic effects of rocket burn and launch in the near-the-earth environment. Boca Raton, London, New York: CRC Press. Taylor & Francis Group, 2013. 542 p.

137. Adushkin V.V. et al. Environmental problems and risks of impacts of rocket and space technology on the environment. Ankil Moscow, 2000. 640 p. (in Russian)

138. The impact of rocket and space technology on the environment / edited by Adushkin V.V., Kozlov S.I., Silnikov M.V. Moscow: GEOS, 2016. 795 p. (in Russian)

139. Lazorenko O.V., Panasenko S.V., Chernogor L.F. Adaptive Fourier transform. *Electromagnetic waves and electronic systems*. 2005. V. 10, № 10. P. 39–50. (in Russian)

140. Panasenko S.V., Chernogor L.F. Radiophysical studies results of wave disturbances in the lower ionosphere. *The successes of modern radio electronics.* 2005. № 7. P. 38–56. (in Russian)

141. Lazorenko O.V., Lazorenko S.V., Chernogor L.F. Wavelet analysis of nonlinear wave processes. *Advances in modern radio electronics*. 2005. № 10. P. 3–21. (in Russian)

142. Chernogor L.F. Advanced Methods of Spectral Analysis of Quasiperiodic Wave‐Like Processes in the Ionosphere: Specific Features and Experimental Results. *Geomagnetism and Aeronomy*. 2008. V. 48, №5. P. 681–702. (in Russian)

143. Lazorenko O.V., Chernogor L.F. Ultra-wideband signals and processes. Monograph. Kharkiv: V.N.Karazin Kharkiv National University, 2009. 576 p. (in Russian)

144. Emelyanov L.Ya., Sklyarov I.B., Chernogor L.F. Ionospheric response to the solar eclipse of August 1, 2008: results of vertical sounding. *Space science and technology*. 2009. V. 15, № 4. P. 12–21. (in Russian)

145. Shakina N.P. Hydrodynamic instability in the atmosphere. Leningrad: Gidrometeoizdat, 1990. 310 p. (in Russian)

146. Brunelli B.E., Namgaladze A.A. Physics of the ionosphere. Moscow: Nauka, 1988. 27 p. (in Russian)

147. Physics of the upper atmosphere / Ed. J.A. Ratcliffe. Moscow: State. Publishing House of Phys.-Math. lit., 1963. 504 p. (in Russian)

148. Chernogor L.F. Wave Response of the Ionosphere to the Partial Solar Eclipse of August 1, 2008 *Geomagnetism and Aeronomy*. 2010. V. 50, № 3. P. 361–376. (in Russian)

149. Chernogor L.F. Electron precipitation from the magnetosphere stimulated by the eclipse of the Sun. *Radiophysics and Radio Astronomy.* 2000. V. 5, № 4. P. 371–375. (in Russian)

150. Schunk R.W., Nagy A.F. Ionospheres: physics, plasma physics, and chemistry. Cambridge atmhttp://umlcar.uml.edu/stationlist.html

151. ospheric and space scince series, 2000. 555p.

152. http://wdc.kugi.kyoto-u.ac.jp/wdc/Sec3.html

153. Barabash V.V., Chernogor L.F. Effects of the solar eclipse on January 4, 2011, observed with an ionosonde. *Remote radio sounding of the ionosphere*: collection of abstracts of the conference of young scientists. (Kharkov, April 12–15, 2011). Kharkov, 2011. P. 52. (in Russian)

154. Andreeva E.S. et al. Radiotomographic registration of ionospheric disturbances from ground explosions. *Space Research*. 2001. V. 39, № 1. P. 13–17. (in Russian)

155. Kunitsyn V.E., Tereshchenko E.D., Andreeva E.S. Radiotomography of the ionosphere. Moscow: Fizmatlit, 2007. 336 p. (in Russian)

156. Obukhov A.M. On the question of geostrophic wind. Izv. Academy of Sciences of the USSR. *Ser. geogr. and geophysis*. 1949. V. 13, № 4. P. 281–289 (in Russian)

157. Gokhberg M.B., Shalimov S.L. Impact of earthquakes and explosions on the ionosphere. Moscow: Nauka, 2008. 295 p. (in Russian)

158. Chernogor L.F. Physics of the Earth, atmosphere and geosapce in the light of the systemic paradigm. *Radiophysics and Radio Astronomy.* 2003. V. 8, № 1. P. 59–106. (in Russian)

159. Chernogor L.F. On nonlinearity in nature and science: monograph. Kharkiv: V.N. Karazin Kharkiv National University, 2008. 528 p. (in Russian)

160. Golitsyn G.S., Grigoriev G.I., Dokuchaev V.P. Radiation of acoustic-gravitational waves during the movement of meteors in the atmosphere. *Izv. Academy of Sciences of the USSR. Physics of the atmosphere and ocean*. 1977. V. 13, № 9. P. 926–935. (in Russian)

161. Chernogor L.F. Earth – atmosphere – ionosphere – magnetosphere as an open dynamic nonlinear physical system (part 1). *Non-linear world*. 2006. V. 4, № 12. P. 655–697. (in Russian)

162. Chernogor L.F. Earth – atmosphere – ionosphere – magnetosphere as an open dynamic nonlinear physical system (part 2). *Non-linear world*. 2007. V. 5, № 4. P. 198–231. (in Russian)

163. Chernogor L.F., Rozumenko V.T. Earth – atmosphere – geospace as an. open nonlinear dynamical system. *Radio Physics and Radio Astronomy*. 2008. V. 13, № 2. P. 120–137.

164. Chernogor L.F. The Earth-atmosphere-geospace system: main properties and processes. *International Journal of Remote Sensing*. 2011. V. 32, № 11. P. 3199–3218.

165. Gurevich A.V., Shvartsburg A.B. Nonlinear theory of radio wave propagation in the ionosphere. Moscow: Nauka, 1973. 272 p. (in Russian)

166. Gurevich A.V. Nonlinear Phenomena in the Ionosphere. Springer – Verlag, New York, Heildelberg, Berlin, 1978. 372 p.

167. Mityakov N.A., Grach S.M., Mityakov S.N. Perturbation of the ionosphere by powerful radio waves. Results of Science and Technology. Ser. “Geomagnetism and high layers of the atmosphere“, V. 9. Moscow: VINITI, 1989. 138 p. (in Russian)

168. Frolov V.L. Artificial turbulence of the mid-latitude ionosphere. Nizhny Novgorod: Publishing House of the Nizhny Novgorod University. Lobachevsky N.I., 2017. 468 p. (in Russian)

169. Wratt D.S. Ionization enhancement in the middle latitude D-region due to precipitating high energy electrons. *J. Atmos. Terr. Phys*. 1976. V. 38, №. 5. P. 511–516.

170. Tadokoro H. et al. Electron flux enhancement in the inner radiation belt during moderate magnetic storms. *Ann. Geophys*. 2007. V. 25, №. 6. P. 1359–1364.

171. Sokolov S.N. Magnetic Storms and Their Effects in the Lower Ionosphere: Differences in Storms of Various Types. *Geomagnetism and Aeronomy.* 2011. V. 51, № 6. P. 757–768. (in Russian)

172. Buonsanto M.J. Ionospheric storms: A Review. *Space Sci. Rev*. 1999. Vol. 88. P. 563–601.

173. Burmaka V.P. et al. Variations in the parameters of scattered signals and the ionosphere connected with plasma modification by high-power radio waves / *Radiophysics and Quantum Electronics*. 2009. V. 52, № 11. P. 774–795.

174. Chernogor L.F. et al. Variations in the ionospheric wave perturbation spectrum during periodic heating of the plasma by high-power high-frequency radio waves / *Radiophysics and Quantum Electronics*. 2011. V. 54, № 2. P. 75–88.

175. Chernogor L.F., Frolov V.L., Pushin V.F. Infrasound oscillations in the ionosphere affected by high-power radio waves. *Radiophysics and Quantun Electronics*. 2012b. V. 55, № 5. P. 296–308.

176. Chernogor L.F., Frolov V.L. Traveling ionospheric disturbances generated due to periodic plasma heating by high-power high-frequency radiation. *Radiophysics and Quantum Electronics*. 2012c. V. 55, № 1, 2. P. 13–32.

177. Chernogor L.F., Frolov V.L. Features of propagation of the acoustic-gravity waves generated by high-power periodic radiation. *Radiophysics and Quantum Electronics.* 2013a. V. 56, №. 4. P. 197–215.

178. Chernogor L.F., Frolov V.L. Features of the wave disturbances in the ionosphere during periodic heating of the plasma by the “Sura” radiation. *Radiophysics and Quantum Electronics*. 2013b. V. 56, № 5. P. 276–289.

179. Belov A.S. et al. Excitation of guided ELF-VLF waves through modification of the F2 ionospheric layer by high-power radio waves. *Plasma Phys. Rep*. 2012. V. 38**,** №. 3. P. 219–224.

180. Markov G.A. et al. Excitation of a magnetospheric maser through modification of the Earth's ionosphere by high-power HF radio emission from a ground-based transmitter. *Zh. Eksper. Teoret. Fiz*. 2012. V. 111, № 6. P. 916–920.

181. Cole K.D. Formation of field-aligned irregularities in the magnetosphere. *J. Atmos. and Terr. Phys*. 1971. V. 33. P. 741–750.

S C I E N T I F I C E D I T I O N

Bogomaz Oleksandr
Ph.D., Head of the Department of Researcher of Institute of Ionosphere

Chernogor Leonid
D.Sc., Prof., Head of the Department of Space Radiophysics,
V.N. Karazin Kharkiv National University

Barabash Volodymyr
Ph.D., Researcher of Institute of Ionosphere

Katsko Sofiia
Ph.D., Researcher of Institute of Ionosphere

APERIODIC AND WAVE DISTURBANCES IN THE IONOSPHERE: THE RESULTS OF VERTICAL SOUNDING

MONOGRAPH

English

Published (PDF): 13.06.2021. Signed for printing: 15.06.2021.
Format 60×84/16. Offset Paper. Digital printing.
The headset is Times New Roman. Conventionally printed sheets 9,3.
Circulation: 150 copies. Order № 22511.

Printed from the finished original layout.

Compilers:

Institute of Ionosphere of NAS and MES of Ukraine
61001, Ukraine, Kharkiv, Kyrpychova str., 16

NGO European Scientific Platform
21037, Ukraine, Vinnytsia, Zodchykh str. 18/81
Tel.: +38 098 1948380; +38 098 1956755
E-mail: info@ukrlogos.in.ua | URL: www.ukrlogos.in.ua

Publisher [ISBN]: Primedia E-launch LLC.
TX 75001, United States, Texas, Dallas.
E-mail: info@primediaelaunch.com | URL: www.primediaelaunch.com

Publisher [printed copies]: Sole proprietorship - Gulyaeva V.M.
08700, Ukraine, Obuhiv, Malyshka str. 5. E-mail: 5894939@gmail.com
Certificate of the subject of the publishing business: ДК No 6205 of 30.05.2018 p.